Asset Pricing with Climate Risks and Heterogeneous Beliefs

Von der Fakultät für Wirtschaftswissenschaften der
Rheinisch-Westfälischen Technischen Hochschule Aachen
zur Erlangung des akademischen Grades eines Doktors der
Wirtschafts- und Sozialwissenschaften genehmigte Dissertation

vorgelegt von

Marco Simon Thalhammer

Berichter: Herr Univ.-Prof. Dr. sc. pol. Thomas S. Lontzek
Berichter: Herr Univ.-Prof. Dr. oec. Ole Wilms

Tag der mündlichen Prüfung: 20.10.2023

Acknowledgements

I am indebted and sincerely grateful to my supervisors Thomas Lontzek and Ole Wilms. Furthermore, I am thankful to Arthur Enders, Karl Schmedders, and Walter Pohl for our cooperation on research projects and many valuable discussions we've had on the subject. I am very grateful to all my colleagues at RWTH Aachen for being supportive during my whole stay.
Finally, I would like to give special thanks to my parents for their enduring support.

Abstract

This thesis analyzes how climate risks are priced on financial markets. We show that climate tipping thresholds, disagreement about climate risks, and preferences that price in long-run risks are crucial to an understanding of the impact of climate change on asset prices. Our model simultaneously explains several findings that have been established in the empirical literature on climate finance: (i) news about climate change can be hedged in financial markets, (ii) the share of green investors has significantly increased over the past decade, (iii) investors require a positive, although small, climate risk premium for holding "brown" assets, and (iv) "green" stocks outperformed "brown" stocks in the period 2011–2021. The model can also explain why investments in mitigating climate change have been small in the past. Finally, the model predicts a strong, non-linear increase in the marginal gain from carbon-reducing investments as well as in the carbon premium if global temperatures continue to rise.

This thesis also presents an adapted numerical solution approach based on projection methods and Gauss-Hermite quadrature to solve long-run risk asset-pricing models with disasters and heterogeneous agents, where closed-form solutions are unavailable. We demonstrate an effective approach for handling nonlinearities, such as a tipping threshold. The proposed approach demonstrates sufficient accuracy in solving the equilibrium conditions, making it computationally efficient even for models involving multiple states and agents.

Contents

List of Figures

List of Tables

1 Introduction

A rapidly growing literature in climate science has identified specific temperature thresholds beyond which we can expect to see significant and potentially irreversible changes to the planet's ecosystems and the services they provide, such as food production, water resources, and natural habitats. For example, the Intergovernmental Panel on Climate Change (IPCC) has highlighted the importance of limiting global warming to 1.5°C above preindustrial levels to avoid the most severe impacts of climate change. There is, however, an ongoing scientific debate over the uncertainty surrounding the precise magnitude and timing of these thresholds and the exact impacts that will result from exceeding them.

While natural scientists debate the likelihood and magnitude of climate disasters linked to temperature thresholds, there remains a widespread and often contentious public debate about climate change and its risks. This disagreement is reflected in the diverse range of views and opinions evident among policymakers regarding the appropriate response to climate change, with positions ranging from inaction to drastic carbon-reduction policies. This ongoing debate has generated uncertainty about the potential economic impact of policy responses to climate change, affecting asset values and investment decisions.

In this paper, we provide a novel framework to analyze how climate risks are priced on financial markets. For this, we integrate temperature thresholds and divergent beliefs about climate change and policy responses into an asset-pricing model with long-run risks (Bansal and Yaron 2004) and two types of investors (Pohl et al. 2021). The persistent global average temperature anomaly, reflecting the degree of warming above preindustrial levels, creates long-run risk in the model. The two investor types—"green" and "brown"—hold opposing views on the extent to which changes in global temperature impact consumption disaster probabilities. While both groups have identical Epstein–Zin preferences with a preference for the early resolution of risk, green investors believe that climate change has a larger effect on disaster probabilities, whereas brown investors believe in a smaller impact. We use our asset-pricing model to examine the pricing of assets with different exposures to climate risks. "Green" assets have a relatively smaller exposure to such risks than "brown" assets.

We show that the interplay of temperature thresholds, disagreement about climate change, and Epstein–Zin preferences provides several insights into how climate-related risks are priced on financial markets. First, the model reveals a new channel for risk sharing: not only is climate risk itself priced, but the risk of receiving bad news today about the future climate is also priced. Brown investors implicitly sell insurance against this climate news risk to green investors. Importantly, climate news risk is only priced if agents care about long-run risks (Epstein–Zin preferences). In contrast, under expected utility, this insurance on climate change news is not traded by investors. Second, bad news about the climate, such as an unexpected acceleration of the global temperature increase, increases the market share of

green investors because they benefit from buying insurance against such news shocks. Third, brown stocks carry a larger risk premium ("carbon premium") compared to green stocks, as increasing climate risks are followed by governmental responses to slow down climate change (for example in the form of higher carbon taxes), which affect brown stocks more than green stocks.[1] Fourth, if the temperature threshold to trigger disaster events is sufficiently far away from the current temperature anomaly, then the corresponding carbon premium is small in the short run, and large in the long run. (For expected utility, the carbon premium is zero below that threshold.) In such a scenario, the news-channel effect dominates the carbon-premium effect, and the model shows an outperformance of green over brown stocks in response to bad climate news over the short run.

Our asset-pricing model provides a simultaneous explanation for several findings on the impact of climate risks on financial markets. Notably, the model delivers the following stylized facts, which have been established[2] in recent empirical studies: (i) news about climate change can be hedged in financial markets (Engle et al. 2020; Ardia et al. 2023); (ii) the market share of green investors has increased significantly over the past years (Global Sustainable Investment Alliance 2020; van der Beck 2022); (iii) investors require a premium for holding assets that are exposed to climate change risk, implying a positive carbon, or more generally, climate risk premium (Bolton and Kacperczyk 2021; 2022; Bansal et al. 2021; Hsu et al. 2023); (iv) in contrast, the past decade has shown a strong outperformance of green over brown stocks (Huij et al. 2021, Pástor et al. 2022).

The model analysis also highlights the significance of temperature thresholds in shaping the impact of climate investments. In the absence of such thresholds, where disasters can occur at any time and temperature, the marginal gain from investments to slow down climate change would initially be large but decrease as climate risks rise. By contrast, if disasters can only occur after a temperature threshold has been crossed, the marginal gain from investments is small for low temperatures as the likelihood of crossing the threshold in the (near) future is low. As temperatures rise and approach the threshold, however, the marginal gains from such investments increase significantly and become very large. The model predicts that the market share of green investors, the carbon premium, and the gains from climate investments will significantly increase if climate risks continue to rise over time, highlighting the importance of temperature thresholds in shaping market outcomes.

Climate financial risks are a direct consequence of two broad types of risk associated with climate change. Physical risks arise because climate change can potentially trigger large-scale catastrophic events. Such events have the potential to cause major disruptions in our

[1] This essentially implies a positive correlation between physical and transitional climate risks which seems plausible since governmental responses to slow down climate change should be a consequence of increased physical climate risks.

[2] Recent years have seen a surge in research examining the impact of climate financial risks on asset prices; see Giglio et al. (2021a) for an overview of this literature.

ecosystem leading to severe weather events such as global droughts, floods, heatwaves, or hurricanes, which may damage assets and infrastructure, impair productive assets, and disrupt supply chains and business operations (IPCC 2014). The economy also faces transition risk as a consequence of policy measures, technological changes, and reputational concerns. The introduction of new regulations, laws, carbon costs, or other policies related to climate change can have a dramatic impact on companies' operations and cash flows. As the world transitions toward renewable energy sources and other sustainable technologies, companies that fail to adapt or adopt these technologies may face increased costs or declining market share. Companies that are perceived as not taking climate change seriously may face reputational damage, leading to a loss of customers, partners, or employees.

In this paper, we use the term climate financial risks to describe the financial risks stemming from both physical and transition risk. If a severe climate disaster materializes, there are likely also going to be strong governmental responses. In the past, governments have often been reluctant to introduce effective policies to slow down climate change, such as a large, globally binding carbon tax or outright restrictions on energy consumption. However, the actual experience of a climate disaster is likely going to lead to immediate action to slow down climate change.[3] We argue that due to such strong governmental responses, brown firms with high carbon emissions should also be more exposed to climate risks. In our model, we provide a new channel through which news about long-term climate risks affect the differential pricing of brown and green stocks today.

Our asset-pricing model builds on previous finance literature that incorporates climate risks into financial models. The global temperature anomaly[4] is modeled as a highly persistent long-run risk process as in Bansal and Yaron (2004). Bansal et al. (2021) provide evidence that long-run temperature changes are reflected in equity valuations. Climate financial risks depend

[3]For example, throughout the twentieth century, Australia experienced destructive wildfires. But only following the devastating bushfires ("Black Summer") of July 2019 to March 2020 did the Australian Government announce a broad plan aimed at addressing the impacts of climate change and reducing the risk of future wildfires—the "Australian Bushfire & Climate Plan" of July 2020; see `https://emergencyleadersforclimateaction.org.au/australian-bushfire-climate-plan/`, last accessed April 7, 2023. Another instance of a strong policy response following physical damage related to climate change occurred in the United States in the spring of 2023, when the Pacific Fishery Management Council unanimously approved the closure of fall-run (Chinook) salmon fishing from northern Oregon to the California–Mexico border. (Limited recreational salmon fishing was allowed off southern Oregon in the fall of 2023.) Clearly, some overfishing may have contributed to the problem, but essentially a long drought in California (made worse by climate change) and reckless water usage (due to a policy of the previous federal administration) resulted in physical environmental damage—namely, the huge decline in the population of Chinook. In response to this physical damage, the regulatory body closed an entire branch of the local fishing industry; see `https://www.nbcbayarea.com/news/local/salmon-fishing-ban-west-coast/3200108/`, last accessed April 10, 2023. This policy will not mitigate climate change, but aims to reduce the damage to the fish population.

[4]Climate scientists examine a wide range of natural processes to describe climate change. These include greenhouse gas concentrations, atmospheric circulation patterns, ocean currents, and changes in solar radiation, and many others. In public discourse, however, climate change is often simply described by the increase in the global temperature compared to its value in the preindustrial era.

on the global temperature anomaly and are modeled as catastrophic events as in Barro (2006), Gabaix (2012), and Wachter (2013). Since climate change poses significant financial risks to households, businesses, and investors due to the increased likelihood of catastrophic events that have the potential to cause significant economic damage, using a standard approach, one would expect that such low-probability large-impact events should command a large risk premium (Rietz 1988; Barro 2006). Recent studies, however, have yielded mixed results on the pricing of climate risks on financial markets. The key difference between our paper and the standard approaches to modeling catastrophic events in asset pricing is our inclusion of climate tipping points, which we show is crucial to an understanding of how climate risks are priced on financial markets. Giglio et al. (2021b) use real estate data to estimate discount rates for the valuation of investments in climate change abatement. In their model, they do not include a temperature process but instead use a persistent process for an endogenous climate disaster probability. They show that the term structure of discount rates for climate-hedging investments is upward sloping, but bounded above by the risk-free rate.

Our model also builds on the existing literature that analyzes the impact of disagreement on financial markets with Epstein–Zin investors. Borovička (2020) analyzes the incentives to trade risks for models with recursive utility when agents disagree about the expected growth rate of consumption. He shows that optimistic investors with fundamentally wrong beliefs can survive in the long run so that the classical market selection hypothesis no longer holds for models with recursive utility. Pohl et al. (2021) show that even small belief differences have large effects in models with long-run risks and recursive preferences and that the disagreement can help to explain several asset-pricing puzzles. Chen et al. (2012) and Branger et al. (2020) analyze the impact of disagreement about disaster risks on financial markets. While the former show that disagreement about disaster risk generates strong risk sharing motives such that even a small share of optimists is sufficient to significantly reduce the disaster risk premium, the latter analyze how market incompleteness affects risk sharing incentives.

The significance of news as a separate source of priced risk for Epstein-Zin investors was first identified by Ai and Bansal (2018). In that setting, Epstein-Zin investors demand an additional premium around macroeconomic announcements, a premium that is absent for CRRA investors.

Pástor et al. (2021) provide an alternative explanation how the outperformance of green over brown stocks in the past decade can be reconciled with a positive carbon risk premium. Their premise is that investors enjoy holding green assets. When bad news about the climate arrives, the tastes of investors and hence their portfolio weights shift to holding a larger fraction of green assets. This drives up the prices, and hence the returns of green investments. Heeb et al. (2022) provide evidence that investors are willing to pay more for green assets, however the willingness does not increase with the greenness of the asset in contrast to the

assumption in Pástor et al. (2021).

Our explanation in turn is solely based on differences in beliefs about the impact of climate change. Ardia et al. (2023) construct a climate concern index based on newspaper articles on climate risks and show that bad news about the climate increases the value of green firms and decreases the value of brown firms. Moreover, their climate index allows them to analyze whether climate news affects the valuations of green and brown assets through changes in expectations about the future cash flows of the firms or through changes in investors' preferences. They find that returns are affected via both channels and hence provide evidence for both theories, the one presented in this paper as well as the model in Pástor et al. (2021).

Integrating recursive preferences into asset-pricing models can offer valuable insights into the pricing of climate risks on financial markets. However, this enhanced model complexity typically does not allow for analytical solutions and demands higher computational power to accurately solve the model. Daniel et al. (2016) tackle their 'EZ-Climate model' using a discrete-time binomial tree model. In contrast, we opt for numerical methods as demonstrated in Pohl et al. (2018), employing a global collocation projection approach to solve our model framework. This numerical approach proves to be more suitable for our analysis, providing precise solutions for our research objectives.

The remainder of this paper is organized as follows. Section 2 documents empirical findings on the impact of climate risks on financial markets as well as the key underlying assumptions for our climate economy. In Section 3 we present our model, as well as the key mechanism via which climate risks are traded in response to belief differences. Section 4 discusses the outcomes of our model and relates them to the data. Section 5 provides details about the numerical solution methods used to solve the model and accuracy of the results. Section 6 concludes.

2 Climate Change: Selected Empirical Findings

Our asset-pricing model draws upon established insights from the climate change literature that have not yet received much attention in finance. In Section 2.1 we provide a brief review of the pertinent literature. Our model produces testable implications for the pricing of climate risks, which we contrast with empirical evidence from the finance literature, in Section 4. For this purpose, we document several stylized facts from financial markets, in Section 2.2.

2.1 Temperature Thresholds and Differences of Opinion

Our asset-pricing model relies on two fundamental assumptions derived from the climate change literature. First, we include a temperature threshold beyond which climate-induced consumption disasters can occur. Second, we model two distinct groups of investors that have divergent views on the probability of occurrence of those disasters.

Climate scientists use the term *climate system tipping point* to refer to a critical threshold in crucial components of the Earth's climate system—the *tipping elements*—beyond which rapid and irreversible changes can occur (Lenton et al. 2008). For example, Arctic sea ice has been shrinking rapidly in recent decades due to global warming. As the ice cover reduces, more sunlight is absorbed by the ocean, leading to further warming and the melting of the remaining ice. This positive feedback loop could eventually lead to the Arctic becoming ice-free in the summer, which would have significant consequences for the climate, ecosystems, and human societies in the region and beyond. Other potential tipping elements in the climate system include the collapse of the West Antarctic Ice Sheet, the slowdown of the Atlantic meridional overturning circulation (AMOC), and the release of methane from thawing permafrost and clathrates in the ocean.

Several works in climate economics have developed models incorporating climate system tipping points; see, for example, Lemoine and Traeger (2014), Lontzek et al. (2015), van der Ploeg and de Zeeuw (2018), and the discussion in Cai (2021). Typically these models address a specific tipping element or an ensemble of tipping elements. Cai et al. (2017) and Cai and Lontzek (2019) in turn assume a representative tipping element, whose nature is stochastically evolving. Consequently, these models embed for each tipping element a distinct tipping point. Recently, Armstrong McKay et al. (2022) presented an updated assessment of the location of tipping points for major tipping elements, considering both regional and global tipping elements. While a few tipping elements may be triggered within the 1.5°C–2°C range, most tipping points are expected to be located beyond 2°C, with a considerable range of uncertainty regarding the location of that critical internal threshold. Building on this literature, our asset-pricing model also integrates the concept of a critical threshold. However, in contrast to the abovementioned studies we define a temperature threshold beyond which catastrophic events

can be triggered. We do not model any particular tipping element but rather the direct adverse impacts on the economy resulting from catastrophic events. Thus, our temperature threshold can be viewed as a generic tipping point, and in the subsequent discussion we will use the term "tipping point" in that sense. Since the likelihood of a climate-induced consumption disaster is zero as long as the global temperature anomaly remains below this tipping point temperature, we are assuming a safe operating space in that temperature range. Once the global average temperature exceeds its tipping point level, the risk of a disaster occurring increases significantly. The existence of tipping points with regard to climate disasters distinguishes our model from the conventional approach to modeling consumption disasters in asset pricing, which allows potential disasters to occur at any time; see, for example, Barro (2009), Gabaix (2012) and Wachter (2013). We demonstrate that this difference has significant consequences for the pricing of assets that are vulnerable to climate risks.

Models with tipping points have previously been proposed in the asset-pricing literature. Bansal et al. (2016) set a temperature threshold of 2°C for a tipping point, after which a quadratic loss function (in temperature) describes the expected disaster size, and the probability of disaster increases linearly with temperature. Daniel et al. (2016) introduce a model with a positive probability of a tipping point, leading to a large negative shock to consumption as soon as the temperature rises above its 2015 level; in our model, this approach corresponds to an immediate disaster risk.

The scientific consensus on climate change is that it is real, primarily caused by human activities, and poses a significant threat to planet Earth and its inhabitants. This consensus is shared by an overwhelming majority of climate scientists and scientific organizations. However, some individuals and organizations, often those with significant political and financial influence, reject this scientific evidence and consensus, often for ideological or economic reasons. Therefore, despite the emergence of a scientific consensus in recent years there is still considerable debate regarding the potential impact of global warming on the real economy, as documented by an extensive literature.

In his book *Why We Disagree about Climate Change*, Hulme (2009) sheds light on the factors that contribute to such disagreement, arguing that while climate change is a physical phenomenon, it has also taken on social, cultural, and political dimensions. These additional dimensions have resulted in varying beliefs and attitudes to climate change, as reflected in public surveys such as that of Howe et al. (2015) and Saad (2017). Despite an increase in the proportion of Americans who express concern over climate change and acknowledge its anthropogenic causes, a significant portion of the US population still does not share these concerns or recognize the consequences of climate change. For example, according to the survey by Howe et al. (2015), in 2014 only 58% of the respondents believed that climate change will significantly harm future generations.

For a wide range of tipping elements Armstrong McKay et al. (2022) show that the probability of exceeding climate tipping points rises with higher temperature levels. There is, however, a high degree of uncertainty regarding future emission paths and thus regarding future climate change. This uncertainty in turn affects the likelihood of climate-induced disasters. Using the expert elicitation study of Kriegler et al. (2009), Lontzek et al. (2015) develop a method to compute contemporaneous, temperature-dependent hazard rates of triggering various tipping points. Cai et al. (2016) use this method to compute cumulative probabilities of triggering major global tipping points. With 2.8°C in 2100 the likelihood of having crossed at least one of five major tipping points is 46.3 percent. In another scenario with 4.7°C in 2100 that likelihood is 87.11 percent. Yet in a very optimistic scenario with 1.5°C in 2100 that likelihood is only 11.49 percent. These findings reveal considerable disagreement about the probability of a climate-induced disaster, particularly as global temperatures rise.

Bernstein et al. (2022) provide insights into differences in beliefs regarding the impact of climate change, based on real estate market data. Through a comparison of individual properties in the same US zip code, the authors find that houses with higher exposure to sea level rise due to climate change are more likely to be owned by Republicans than by Democrats. This suggests that Republicans are less concerned about climate risks, and therefore more willing to hold assets that are exposed to high climate risk. In a similar vein, Baldauf et al. (2020) use an equilibrium model of housing choice to demonstrate that house prices reflect heterogeneity in beliefs regarding long-term climate change risks.

Given the existence of varying beliefs regarding the severity and future scenarios of climate change, it is reasonable to assume that investors may hold different beliefs about the associated risks. In our asset-pricing model, we account for this fact by explicitly allowing for heterogeneous beliefs among two groups of investors.

2.2 Empirical Findings on Financial Markets

In recent years there has been a notable growth in the literature exploring the impact of climate-related financial risks on the pricing of financial assets. For an overview of this rapidly growing research area, see Giglio et al. (2021a). In the following we limit our focus to a review of the most pertinent literature that directly relates to the research presented in the present paper. In particular, we discuss four stylized facts.

First, news about climate change can be hedged on financial markets. Engle et al. (2020) show how to construct portfolios that provide a hedge against news about climate change. They measure the "greenness" of a stock by its environmental score from environmental, social, and governance (ESG) ratings and show that green stocks are less exposed to climate news compared to brown stocks. Using a mimicking portfolio approach to construct portfolios, Engle et al. (2020) show that a portfolio that is long in green stocks and short in brown stocks

can efficiently hedge climate change news. Furthermore, to test the theory of Pástor et al. (2021), Ardia et al. (2023) construct a climate change concern index based on newspaper articles and show that brown stocks are more exposed to climate concern shocks than green stocks are. Hence, a portfolio long in green and short in brown stocks can be used to hedge climate news. Moreover, the authors' climate index allows them to analyze whether climate news affects the valuations of green and of brown assets through changes in expectations regarding the future cash flows of the firms or through changes in investor preferences as suggested by Pástor et al. (2021). They find that returns are affected via both channels.

Second, the market share of green investors has increased significantly over the past decade. The Global Sustainable Investment Alliance (2020) reports that the market share of sustainable investments increased by 8% from 2016 to 2020. While 27.9% of global assets under management were sustainable investments back in 2016, this figure had increased to 35.9% by 2020. Figure 1 from the Alliance's Review (2020) shows the share of investments in sustainable assets for different countries.[5] From 2014 to 2021, the market share of sustainable investments increased in Canada, the United States, Australia/New Zealand, and Japan. Europe is the only exception, the share of green investing having decreased over the years.[6]

Asset managers' willingness to invest in sustainable investments has experienced a significant upswing in recent years. Figure 2, sourced from Principles of Responsible Investment (2021), highlights the rise in the number of Principles of Responsible Investment (PRI) investor signatories and the collective assets under management from 2006 to 2021. The number of signatories has consistently grown in the past decade, with the collective assets under management represented by all 3,826 PRI signatories (comprising 3,404 investors and 422 service providers as of 2021) amounting to approximately US $121 trillion as of March 31, 2021. It is, however, important to note that these commitments do not automatically translate into better ESG scores for signatory companies everywhere. This is demonstrated by Gibson Brandon et al. (2022), who find that such a translation only applies to institutions outside the US. In the US, meanwhile, there is a disconnect between what institutional investors claim to do and what they actually do, which could be interpreted as a form of "greenwashing" by US PRI signatories. The increase in the fraction of people who see climate change as a threat is also visible in the survey by Howe et al. (2015). While in 2014 only 58% of the respondents said that they believe climate change will significantly harm future generations, this number has increased to 64% in 2021.[7]

[5]Note that sustainable assets here contain all ESG classifications. However, given the rising climate concerns of the past decade, it seems plausible to assume that these results are not purely driven by increases in investments in assets with high S and G scores.

[6]EU regulation resulted in the declassification of previously sustainable investment as no longer sustainable, which explains the downward trend in Europe; see *Regulation (EU) 2019/2088 of the European Parliament and of the Council* of 27 November 2019, `https://eur-lex.europa.eu/legal-content/EN/TXT/HTML/?uri=CELEX:32019R2088&from=EN#d1e1107-1-1`.

[7]We thank the authors for making their survey data publicly available.

Figure 1: Share of Sustainable Investments

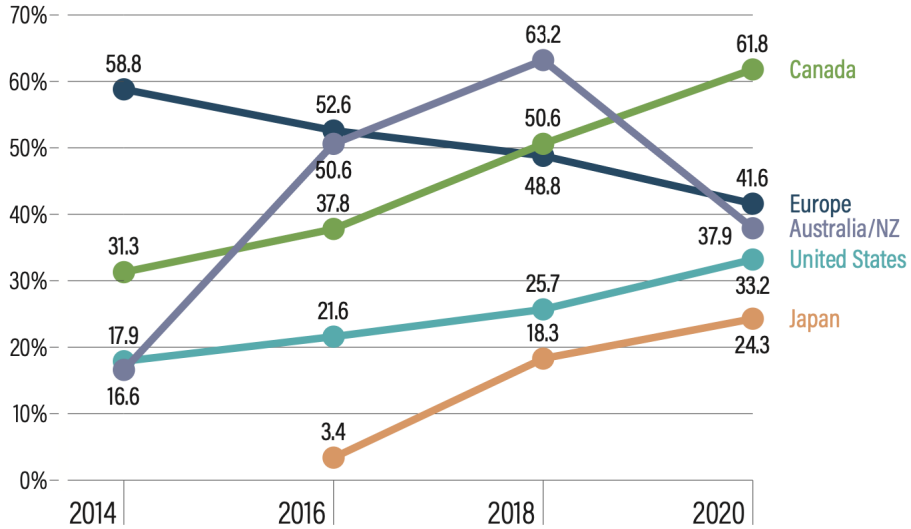

The figure plots the share of investments in sustainable assets for different countries. Source: Global Sustainable Investment Alliance (2020).

Figure 2: PRI Investor Signatories

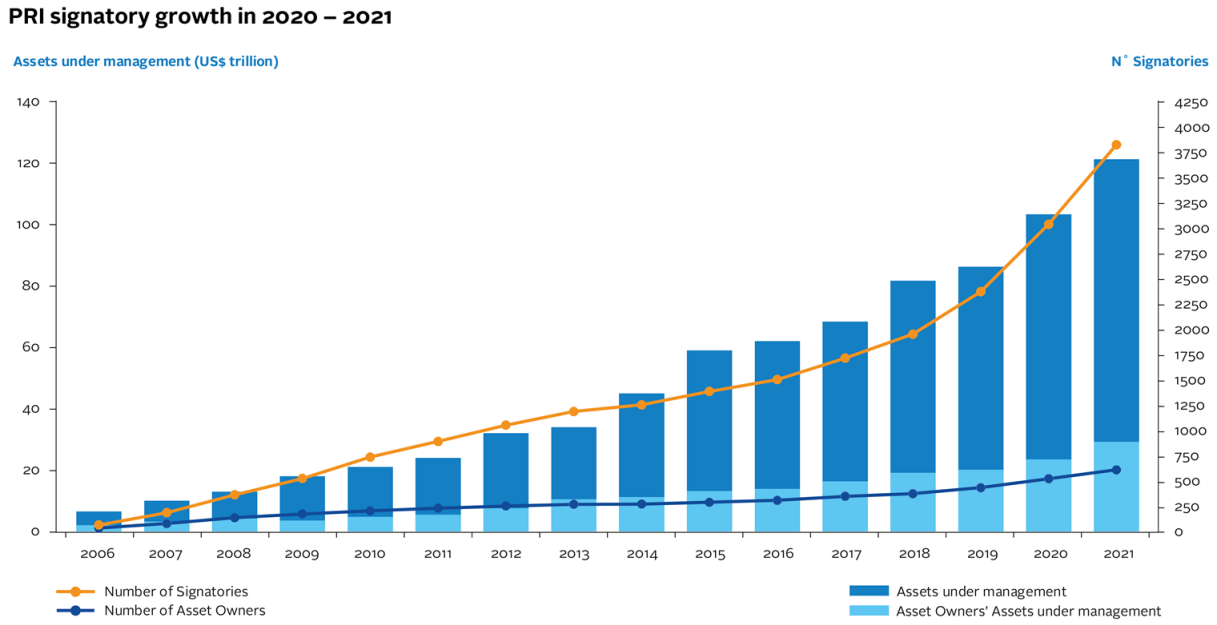

The figure plots the development of the number of PRI investor signatories and collective assets under management from 2006 to 2021. Source: Principles of Responsible Investment (2021).

Third, investors demand a premium for holding assets that are exposed to climate change, either due to higher carbon emissions or to greater sensitivity to long-term temperature changes, indicating a positive carbon—or more generally—climate risk premium (Bolton and Kacperczyk 2021, 2022; Bansal et al. 2021). Fischer and Lundtofte (2021) show in a long-horizon asset-pricing model that stocks with a sufficiently adverse impact on the climate should yield a positive alpha relative to the CAPM. However, the observed magnitude of the climate risk premium has been limited in the past decade, and some alternative studies (Aswani et al. 2023; Bauer et al. 2022; Enders et al. 2023) have failed to identify a positive climate risk premium.Sautner et al. (2023a) use earning call announcements to derive detailed firm-level exposures to various climate risks and Sautner et al. (2023b) find that the unconditional risk premium of firm-level climate change exposures among S&P 500 stocks has been insignificant (after controlling for realized returns). While most studies analyze the carbon premium using realized, ex post returns, Pástor et al. (2022) also try to estimate the carbon premium using expected returns. They do this by using the difference in implied costs of capital and by controlling for surprises to either climate concerns or earnings of green versus brown stocks. This results in a slightly positive carbon premium. As we explain below, our model offers an explanation for why climate risk premia have remained relatively small in the past but are likely to increase significantly in the future.

Fourth, green stocks outperformed brown stocks during the decade prior to the COVID-19 pandemic. This finding is robust to either using environmental scores from ESG ratings as a measure of greenness, as used by Pástor et al. (2022), or directly using emissions data to assess the carbon footprint of a company, as employed by Huij et al. (2021). Both studies report an outperformance of a portfolio of green stocks over a portfolio of brown stocks, of 59% and 45% from 2010 until 2021, respectively.[8] van der Beck (2022) provides evidence of significant fund flows toward sustainable funds and shows that the temporary outperformance of green over brown stocks can be explained by the price pressure arising from these fund flows.

We return to these four stylized facts in the discussion of the key implications of our asset-pricing model in Section 4. In addition, our model has further implications. Investments and policies aimed at curbing global carbon emissions have been insufficiently effective in significantly slowing down climate change, rendering a climate catastrophe increasingly probable according to numerous climate experts. While we recognize that there may be various reasons, particularly political ones, for the tardy response to climate change that we do not consider in our model, it provides a partial, market-based rationale for the historically low levels of investment in carbon-reducing technologies in financial markets. Furthermore, our model predicts that the marginal benefit of mitigating climate change is set to rise exponentially as the average global temperature (anomaly) approaches the climate tipping point.

[8]We would like to thank the authors for providing us with their portfolio return series.

3 The Economy

We consider an endowment economy where changes in global temperature can potentially trigger climate-induced disasters. Log consumption growth $\Delta c_{t+1} \equiv \log\left(\frac{C_{t+1}}{C_t}\right)$ is given by

$$\Delta c_{t+1} = \mu_c + \sigma_\eta \eta_{t+1} + D_{t+1}, \tag{1}$$

where $\eta_{t+1} \sim i.i.d.\ N(0,1)$ and D_{t+1} are climate-induced consumption disasters. Similar specifications to model the impact of climate change on the economy have also been used in Bansal et al. (2021), Karydas and Xepapadeas (2019), Giglio et al. (2021b), and Giglio et al. (2021a). As in Wachter (2013), we assume that

$$D_{t+1} = N_{t+1} d, \tag{2}$$

where d is the disaster-induced decline in consumption growth and N_{t+1} is a Poisson counting process with time-varying intensity π_t. In line with the climate economics literature (see, for example, Lontzek et al. (2015)), we assume that disaster probabilities depend on climate change:

$$\pi_t = g(T_t), \tag{3}$$

where T_t denotes the global temperature anomaly measured in degrees Celsius—so, temperature rise above preindustrial levels. Note that the true temperature process is irrelevant for asset prices but that what matters are the beliefs of investors about climate risks. For example, Choi et al. (2020) show that investors update their beliefs about climate change in response to abnormally hot weather and Acharya et al. (2022) provide direct evidence that physical climate risk in the form of heat stress affects asset prices. The latter argue that this effect could be driven either by increased physical risk itself or by increased investor awareness of these kinds of risks, in line with our interpretation of climate risks.

So, T_t can be viewed more broadly as what investors believe about the global temperature anomaly. Hence, events such as extremely high temperatures or climate events such as the Paris Agreement are likely to shift the attention of investors and affect their beliefs about climate change. We do not adopt a specific stance on how investors form their expectations, but simply assume that climate change news is subsumed in the innovations to T_t.

The true function $g(T_t)$ is unknown and there are two groups of investors, $h \in \{G, B\}$, who disagree over how much changes in global temperature affect the probability of a consumption disaster. We assume that the green investor, G, believes that climate change has a large impact on disaster probabilities while the brown investor, B, believes in a smaller impact:

$$g^G(T_t) \geq g^B(T_t), \tag{4}$$

where $g^h(T_t) = \pi_t^h$ denotes the beliefs of agent h about the probability of a climate-induced disaster. We assume that

$$g^h(T_t) = \begin{cases} 0, & \text{if } T_t < T_{tipp} \\ l^h T_t, & \text{otherwise,} \end{cases} \tag{5}$$

where $l^G > l^B$. T_{tipp} denotes the threshold temperature above which climate-induced disasters can occur. Hence, as long as global temperature, T_t, is below the tipping point T_{tipp}, the climate-induced disaster probability is zero.[9] Only if the tipping point is crossed do disaster probabilities increase proportionally to temperature. Investors disagree on the magnitude of this effect.

As argued in Section 2.1, climate experts disagree significantly regarding the probability of climate-induced disasters and their impacts on the economy. Furthermore, also in line with our model assumptions, that disagreement is growing with rising temperature levels.

We assume that global temperature, T_t—or, more precisely, what investors believe about the dynamics of global temperature—follows an AR(1) process and is given by

$$T_{t+1} = \mu_T(1-\nu) + \nu T_t + \sigma_\zeta \zeta_{t+1}, \tag{6}$$

where $\zeta_{t+1} \sim i.i.d.\ N(0,1)$. As argued above, from an investor perspective the shocks ζ_{t+1} can be viewed as news about climate change. Note that in the climate economics literature it is common practice to model emissions, which then affect global temperature, and that emissions might themselves be a function of consumption growth. To demonstrate our main findings, we abstract from such feedback loops in our model, although they do constitute an interesting avenue for future research. In Appendix E we provide an illustrative examination of the relationshop between consumption growth, emissions and temperature, as presented in Bansal et al. (2021). We also discuss how this can be linked to the AR(1) process for temperature within our model framework.

We consider the pricing of two different assets: a green and a brown stock. We argue that brown stocks should be more exposed to climate financial risks for the following reason: Assume that a climate disaster such as a significant increase in sea level that causes large-scale flooding materializes. Such an event will put pressure on governments to take immediate actions to slow down climate change. So even though policymakers might have in the past been reluctant to put stringent climate policies in place, they are likely to do so if severe damage due to climate change materializes. Hence, brown stocks will not only be exposed to the physical disaster itself, but additionally their future cash flows should decrease due to

[9] We acknowledge that, in general, threshold temperature levels are unknown and today's temperature level might lie beyond a safe operating space. In fact, we assume a positive but negligible probability if $T_t < T_{tipp}$. A state with 0 probability is not possible as the subjective distribution $dP^B_{t,t+1}$ in (15) would no longer be absolutely continuous with respect to $dP^G_{t,t+1}$.

more stringent climate policies.

Hence, we assume that the log dividend growth, $\Delta d^i_{t+1} \equiv \log\left(\frac{D^i_{t+1}}{D^i_t}\right)$, of asset i is given by

$$\Delta d^i_{t+1} = \mu_d + \Phi\sigma_\eta\eta_{t+1} + k^i D_{t+1}, \tag{7}$$

where the market portfolio has a climate exposure of $k^i = 1$, brown stocks are more exposed to climate disaster risks with $k^i > 1$, and green stocks have $k^i < 1$. Mean log dividend growth is represented by μ_d and Φ denotes the leverage parameter to account for the excess volatility of dividend growth over consumption growth.

3.1 Investors

We assume that there are two groups of investors, $h \in \{G, B\}$, with Epstein–Zin preferences (see Epstein and Zin (1989) and Weil (1989)). We argue below that this is crucial to obtaining risk sharing dynamics in line with the empirical evidence on the hedging of climate risks. By having two different parameters to account for agents' willingness to substitute consumption across (uncertain) states of nature and across time, Epstein–Zin preferences allow for simultaneously having a high risk aversion and low risk-free rate, consistent with the equity-premium puzzle. Let V^h_t denote agent h's continuation utility in period t:

$$V^h_t = \left[(1-\delta)\left(C^h_t\right)^{1-\frac{1}{\psi}} + \delta E^h_t\left(\left(V^h_{t+1}\right)^{1-\gamma}\right)^{\frac{1-\frac{1}{\psi}}{1-\gamma}}\right]^{\frac{1}{1-\frac{1}{\psi}}}, \tag{8}$$

where C^h_t is the individual consumption of agent h. We normalize this function by aggregate consumption, $v^h_t = V^h_t/C_t$, so that

$$v^h_t = \left[(1-\delta)(s^h_t)^\rho + \delta R^h_t\left(v^h_{t+1}\cdot e^{\Delta c_{t+1}}\right)^\rho\right]^{\frac{1}{\rho}}, \quad h \in \{G, B\}, \tag{9}$$

with $s^h_t = \frac{C^h_t}{C_t}$, and $R^h_t(x) = \left(E^h_t\left(x^\alpha\right)\right)^{\frac{1}{\alpha}}$ being the certainty equivalent operator. $E^h_t(.)$ denotes the expectation of agent h conditional on information at time t. While agents have different beliefs, they share the same preference parameters.[10] The subjective discount factor is denoted by δ, $\rho = 1 - \frac{1}{\psi}$ determines the elasticity of intertemporal substitution ψ, and $\alpha = 1 - \gamma$ determines the relative risk aversion, γ, of the agents. By setting $\alpha = \rho$ we obtain the special case of CRRA preferences.

[10] This assumption could be relaxed, as, for example, shown in Pohl et al. (2021).

3.2 Equilibrium

We solve for the equilibrium consumption shares using the numerical procedure proposed by Pohl et al. (2021).[11] The social planner maximizes the weighted sum of the individual agents' utilities where λ_t^h denotes the optimal weights (also called Negishi weights) that are determined in equilibrium. The endogenous state variable λ_t^h captures the time-varying weights of the two agents in the social planner's problem.[12] The Negishi weights are linked to the individual consumption shares s_t^h via the following first-order optimality condition for the individual consumption decisions:

$$\lambda_t^G(1-\delta)(s_t^G)^{\rho-1} = \lambda_t^B(1-\delta)(s_t^B)^{\rho-1}, \tag{10}$$

subject to the market-clearing condition

$$s_t^G + s_t^B = 1. \tag{11}$$

By reformulationg 10, the Negishi weights are linked to the individual consumption shares s_t^h via

$$\frac{\lambda_t^G}{\lambda_t^B} = \left(\frac{s_t^G}{s_t^B}\right)^{\frac{1}{\psi}}. \tag{12}$$

Note that the weights are monotone in s_t, and hence that an increase in λ_t^h implies an increase in s_t^h. Agents with an increasing consumption share over time will therefore also have an increasing weight in the optimization problem. The dynamics of the Negishi weights are given by the following equation:

$$\lambda_{t+1}^B = \frac{\lambda_t^B \Pi_{t+1}^B}{\lambda_t^G \Pi_{t+1}^G + \lambda_t^B \Pi_{t+1}^B}, \tag{13}$$

with

$$\Pi_{t+1}^h = \delta e^{\rho \Delta c_{t+1}} \frac{dP_{t,t+1}^h}{dP_{t,t+1}} \frac{(v_{t+1}^h e^{\Delta c_{t+1}})^{\alpha-\rho}}{R_t^h (v_{t+1}^h e^{\Delta c_{t+1}})^{\alpha-\rho}}, h \in \{B, G\}. \tag{14}$$

By plugging in equation 14 into equation 13, the dynamics of the Negishi weights in equilibrium are given by

$$\frac{\lambda_{t+1}^B}{\lambda_{t+1}^G} = \frac{\lambda_t^B}{\lambda_t^G} \frac{dP_{t,t+1}^B}{dP_{t,t+1}^G} \left(\frac{(v_{t+1}^B)}{R_t^B (v_{t+1}^B e^{\Delta c_{t+1}})} \frac{R_t^G (v_{t+1}^G e^{\Delta c_{t+1}})}{(v_{t+1}^G)} \right)^{\frac{1}{\psi}-\gamma}, \tag{15}$$

where $P_{t,t+1}^h$ denotes the subjective distribution of the state at $t+1$ conditional on time t

[11] To obtain sufficient accuracy of our numerical solution, we require that Euler errors are less than 10^{-4}. More importantly, we double check that there are no changes in the economic outcomes of the model, such as the carbon premium or the welfare cost of carbon, if the accuracy is increased. Put differently, further increasing the accuracy has only a negligible effect on equilibrium outcomes. Details are provided in Section 5.

[12] The Negishi weights can be normalized in a way that the following condition has to hold: $\lambda^G + \lambda^B = 1$. In the reminder of this paper, we will always refer to the normalized Negishi weights.

information. The term $dP^B_{t,t+1}/dP^G_{t,t+1}$ is the Radon–Nikodym derivative of $P^B_{t,t+1}$ with respect to $P^G_{t,t+1}$. Knowing the true conditional distribution $P_{t,t+1}$, given the information at time t, we can rewrite each agent's subjective expectations $P^h_{t,t+1}$ about the state of the economy in the next period in terms of the true distribution:

$$E^h_t[x] = E_t\left[x\frac{dP^h_{t,t+1}}{dP_{t,t+1}}\right], \tag{16}$$

for some measurable function $dP^h_{t,t+1}/dP_{t,t+1}$.

Note that in our model investors disagree about climate disaster probabilities, which depend on the state of the economy T_t. However, they agree on the dynamics of temperature itself as well as on the normal shocks to consumption. Hence, the only relevant elements (non unit elements) in $dP^B_{t,t+1}/dP^G_{t,t+1}$ arise from the disagreement about D_{t+1}. The subjective distribution for the disaster term is given by

$$P^h(N_{t+1} = x|\pi^h_t > 0) = \frac{(\pi^h_t)^x}{x!}e^{-\pi^h_t}. \tag{17}$$

In the special case $\pi^h_t = 0$, before reaching the tipping threshold, it trivially holds that $P^h(N_{t+1} = 0|\pi^h_t = 0) = 1$ and $P^h(N_{t+1} = x|\pi^h_t = 0) = 0$ for $x > 0$. It follows that

$$\frac{dP^B_{t,t+1}}{dP^G_{t,t+1}} = \begin{cases} \left(\frac{\pi^B_t}{\pi^G_t}\right)^x e^{-\pi^B_t+\pi^G_t} & \pi^B_t, \pi^G_t > 0 \\ 1 & \pi^B_t = \pi^G_t = 0. \end{cases} \tag{18}$$

In Appendix D we show the corresponding probability ratios when we assume a binary, i.e. 0/1 disaster process instead of a Poisson counting disaster process.

3.3 Climate Risk Sharing

In the following we explain how investors with Epstein–Zin utility share risks—that is, both shocks to news about climate change modeled by changes in global temperature and climate disaster risks depending on the climate tipping point. In particular, we show that, in line with the financial market data, investors share temperature risks, while climate disaster risks are only traded once the tipping point is crossed. Furthermore, we argue below that these risk sharing dynamics can explain the empirical findings on the performance of brown and of green assets and the shares of brown and of green investors.

For this, we first consider the special case of CRRA preferences. In this case, equation (15) simplifies to

$$\frac{\lambda^B_{t+1}}{\lambda^G_{t+1}} = \frac{\lambda^B_t}{\lambda^G_t}\frac{dP^B_{t,t+1}}{dP^G_{t,t+1}}.$$

Hence, for CRRA preferences all that matters for the next period's consumption shares is the disagreement about the state in the subsequent period. Assume that $T_t < T_{tipp}$. In this case $\pi_t^B = \pi_t^G = 0$ and hence $\lambda_{t+1}^h = \lambda_t^h$. So investors have no incentive to trade with one another as they agree on the subsequent state of the economy. Hence, the wealth shares of brown and green investors would stay constant under these assumptions. In contrast, if $T_t \geq T_{tipp}$, investors disagree about the probability of a climate disaster and we obtain

$$\frac{dP_{t,t+1}^B}{dP_{t,t+1}^G} = \left(\frac{l^B}{l^G}\right)^x e^{(l^G - l^B)T_t}.$$

As $l^G > l^B$, it follows that $\lambda_{t+1}^B > \lambda_t^B$ if $x = 0$. Intuitively, the brown investor believes in a lower probability of disaster. Hence, he is willing to speculate that no disaster occurs in the subsequent period. If in fact no disaster materializes, his consumption share will increase. In contrast, $\lambda_{t+1}^B < \lambda_t^B$ if $x > 0$. The green investor believes in a larger disaster probability and hence her consumption share will increase if a disaster materializes. This is the speculation motive highlighted in Borovička (2020) and Pohl et al. (2021). This has interesting implications for the market shares of investors. It implies that as long as no disaster occurs, the share of brown investors must either stay constant or increase over time, which contrasts with recent evidence on the increasing market shares of green investors; see Section 2.2.

For Epstein–Zin preferences, there arises an additional risk sharing motive in equation (15), captured by the term

$$\left(\frac{(v_{t+1}^B)}{R_t^B(v_{t+1}^B e^{\Delta c_{t+1}})} \frac{R_t^G(v_{t+1}^G e^{\Delta c_{t+1}})}{(v_{t+1}^G)}\right)^{\frac{1}{\psi}-\gamma}.$$

We focus on the case where $\gamma > \frac{1}{\psi}$, which implies that investors have a preference for the early resolution of risks—a common assumption in modern asset-pricing models (see, for example, Bansal and Yaron (2004) and Wachter (2013)). Suppose that a state materializes that the green investor particularly dislikes, i.e. such that

$$\frac{(v_{t+1}^B)}{R_t^B(v_{t+1}^B e^{\Delta c_{t+1}})} > \frac{(v_{t+1}^G)}{R_t^G(v_{t+1}^G e^{\Delta c_{t+1}})}.$$

This implies

$$\left(\frac{(v_{t+1}^B)}{R_t^B(v_{t+1}^B e^{\Delta c_{t+1}})} \frac{R_t^G(v_{t+1}^G e^{\Delta c_{t+1}})}{(v_{t+1}^G)}\right)^{\frac{1}{\psi}-\gamma} < 1$$

so that the consumption share of the brown investor decreases and, in turn, the share of the green investor increases. In this case investors essentially trade insurance against states that they particularly dislike based on their beliefs. This is what Borovička (2020) and Pohl et al. (2021) call the risk sharing motive. In our model, green investors particularly dislike

increases in temperature as these increase the probability of a climate disaster. Hence, the green investor can buy insurance against these increases from the brown investor, such that she gets compensated by a larger consumption share when the bad temperature state materializes. Thus, for Epstein–Zin preferences (unexpected) increases in temperature lead to an increase in the consumption share of the green investor. This effect is present even if $T_t < T_{tipp}$ as long-term changes in T_t are priced in by Epstein–Zin investors. In Section 4 we show that this effect is quantitatively large for common calibrations of the model and can explain the outperformance of green stocks.

3.4 Wealth Shares and Asset Prices

In this brief section, we discuss the relation between the consumption shares of the investors and their respective wealth shares or market shares (we use the two terms interchangeably in the following) and show how to price any asset in our modeling framework.

The wealth share, w_t^h, of investor h is given by

$$w_t^h = \frac{W_t^h}{W_t},$$

where W^h and W_t denote the wealth of investor h and total wealth, respectively. We compute w_t^h using the identity

$$w_t^h = s_t^h \cdot \frac{W_t^h}{C_t^h} \cdot \left(\frac{W_t}{C_t}\right)^{-1}.$$

The aggregate wealth–consumption ratio $\frac{W_t}{C_t}$ follows from the standard asset-pricing equation

$$E_t^h(M_{t+1}^h R_{t+1}^i) = 1,$$

where M_{t+1}^h denotes the stochastic discount factor:

$$M_{t+1}^h = \delta \cdot \frac{\frac{\partial v_t^h}{\partial C_{t+1}^h}}{\frac{\partial v_t^h}{\partial C_t^h}}.$$

Hence, the stochastic discount factor (SDF) depends on the ratio of the partial derivative of continuation utility with respect to future consumption to the partial derivative of continuation utility with respect to today's consumption. The SDF is a fundamental concept in asset pricing theory and helps to explain why some assets have a higher expected return than other assets. In general, the SDF provides the appropriate discount rate for valuing payoffs in a specific time-period and state of the world. These states of the world are typically linked to different consumption levels.

For Epstein–Zin preferences, M^h_{t+1} is given by

$$M^h_{t+1} = \delta \cdot \left(\frac{s^h_{t+1}}{s^h_t}\right)^{-\frac{1}{\psi}} \left(e^{\Delta c_{t+1}}\right)^{-\gamma} \cdot \left(\frac{v^h_{t+1}}{R^h_t(v^h_{t+1}e^{\Delta c_{t+1}})}\right)^{\frac{1}{\psi}-\gamma},$$

and the wealth–consumption ratio of investor h satisfies

$$\frac{W^h_t}{C^h_t} = \frac{1}{1-\delta} \cdot \left(\frac{v^h}{s^h}\right)^{1-\frac{1}{\psi}}. \tag{19}$$

As explained in Cochrane (2017), in models with recursive preferences and long-run risk, people are afraid of assets that go down when there is bad news about long-run future consumption growth. This can explain the risk premiums between different assets. While some may view this as a limitation of the model, as there is not always a constant stream of news about long-run consumption growth, global warming could naturally act as a source of long-run risk which introduces uncertainty about future states of the world. In our model, investors demand a risk premium for holding stocks that go down when unexpected positive shocks to temperature occur. This is why the model produces a positive carbon premium even in the distant tipping point case.

We are using the equations from above to solve the wealth–consumption ratio and price–dividend ratios in our model, which are discussed in detail in Section 4. Figure 31 in Appendix A plots the consumption share of the green investor against her wealth share for the calibration of our economy presented in Section 4. We find that there is almost a one-to-one mapping between the two. So, changes in consumption shares imply equivalent changes in wealth shares, and we use the two terms interchangeably.

4 Results and Discussion

In the following we present the predictions of our climate finance economy and show that it can match the climate risk sharing dynamics on financial markets, the market shares of green and of brown investors, and the pricing of green and of brown stocks. Furthermore, our model makes important predictions regarding welfare gains from climate mitigating policies as well as the carbon premium when global temperatures continue to increase. We calibrate the model using key insights from both the climate economics literature and the asset-pricing literature. Note that even though we provide evidence for the specific choices of all model parameters, we are less concerned about finding the best calibration for our model, but rather are interested in the qualitative predictions our model makes and what we can learn from it about the pricing of climate-exposed assets as well as the benefits of climate mitigating policies.

4.1 Calibration

As formulated in equation (6), our modeling framework allows us to include investors' beliefs about global average temperature as a state variable that dynamically evolves around its long-run average. For the expected long-run mean global surface temperature above the preindustrial level we assume $E(T_t) = \mu_T = 2°\text{C}$, which according to Nauels et al. (2017) falls between the expected 2300 levels for the RCP2.6 and RCP4.5 paths. The "true" long-run temperature level is unknown and will depend on our future emissions and policy efforts to curb carbon emissions. The latest IPCC report presents five illustrative emission scenarios. Even under the intermediate greenhouse gas emissions scenario, warming of 2°C would very likely be exceeded by the end of the century. Another reason for choosing 2°C is that in the form of the Paris Climate Agreement (COP 21) there is a legally binding international treaty on climate change that, adopted by 196 parties in 2015, introduces the goal of limiting global warming to significantly less than 2°C, or preferably 1.5°C (UNFCCC (2015)). We argue that this agreement also serves as a reference point for investors' beliefs. As noted earlier, we do not incorporate a measure of atmospheric carbon content into our model. Nevertheless, the persistence component of our temperature process can at least in part capture the positive relationship between global average temperature and cumulative emissions as shown in Matthews et al. (2009). In our benchmark calibration we assume that the persistence of temperature is given by $\nu = 0.995$. The implied half-life or doubling time is about 140 years, which falls within the range of uncertainty currently used in the literature (see Folini et al. (2021) or Smith et al. (2018)). This implies that, assuming no exogenous shocks to temperature, global temperature will increase from 1.2°C today to 1.5°C degree by 2100. Hence, we assume that investors believe in more moderate global warming compared to current average

projections. The volatility of the unexpected shocks to temperature is set to $\sigma_\zeta = 0.1$, which implies that there is a 25% probability that global temperature exceeds 2°C by 2100 in line with the predictions by many climate experts (see IPCC (2022). In Section 4.8 we show that our results are robust with regard to changes in the calibration of the climate processes. For example using $E(T_t) = \mu_T = 2.5$°C instead of $\mu_T = 2$°C, which implies that global temperature will increase from 1.2°C today to 1.64°C degree by 2100 on average, and there is a 32% probability that temperature exceeds 2°C by 2100, has negligible impact on equilibrium outcomes.

For the calibration of our consumption and dividend process, we stick to the related literature as closely as possible: in line with the literature on long-run consumption risks (see Bansal and Yaron (2004) and Bansal et al. (2012)), we set $\psi = 1.5$, $\gamma = 8$, $\delta = 0.9763$, $\mu_c = \mu_d = 0.02$, $\sigma_\eta = 0.02$, and $\Phi = 2.6$. The notations μ_c, μ_d, σ_η, and Φ are used to match the mean and volatility of consumption and dividend growth. For example, Bansal and Yaron (2004) use $\mu_c = \mu_d = 0.0180$ to match the average consumption and dividend growth rate of about 2% per year in the United States. Wachter (2013) gives us $\sigma_\eta = 0.02$ and $\Phi = 2.6$ to match the volatility of consumption and dividend growth of about 1.5% and 6.5% per year, respectively. We seek to calibrate our model such that the implied annual asset-pricing moments are in line with empirical findings (see Table 3 in Section 4.5). Furthermore, $\gamma > 1/\psi$ is crucial to matching the moments of asset prices as well as to obtaining climate risk sharing dynamics in line with the data.

We calibrate disaster probability and size to approximately match the findings in Cai et al. (2016).[13] While we prefer to focus on our qualitative results, we take the findings in Cai et al. (2016) as a proxy and assume that in the case of a disaster, the log consumption growth drops by 20% ($d = -0.2$). We assume the subjective temperature-induced disaster probability to be twice as high for the green investor with $l^G = 0.03$ (3% per 1°C of temperature increase) compared to for the brown investor with $l^B = 0.015$ (1.5% per 1°C of temperature increase).[14] This implies a disaster probability of 4.2% (8.4%) per year under the beliefs of the brown (green) investor once the tipping threshold is passed ($T_t = 2.8$°C).

We assume a climate exposure for the green stock of $k^G = 0.75$ and for the brown stock of $k^B = 3.0$. Barro (2006) reports that severe disasters have, in the past, destroyed up 50% of GDP while mild disasters have led to a decrease of 15–20%. Our exposures imply that dividends of brown stocks drop by 45% while dividends of green stocks drop by 15%. Note that our results are robust to variations in the climate exposures and all we require for our qualitative findings to hold is that $k^G < k^B$. We demonstrate the robustness of our findings

[13] Cai et al. (2016) formulate a stochastic model with interactive climate tipping points. They compute that for approximately $T_t = 3$°C the annual average damage caused by disastrous climate change events amounts to a roughly 1.8 percent loss of global GDP.

[14] Here we adopt the findings of Lontzek et al. (2015), who derive hazard rates for optimistic and pessimistic experts based on the elicitation study in Kriegler et al. (2009).

in Section 4.8. The full calibration of our model is summarized in Table 1.

Table 1: Baseline Calibration

Parameter	**Value**	**Interpretation**
γ	8	risk aversion
ψ	1.5	intertemporal elasticity of substitution
δ	0.9763	time discount factor
μ_c	0.02	average consumption growth rate
σ_c	0.02	volatility of i.i.d. normal consumption shock
μ_d	0.02	average dividend growth rate
Φ	2.6	dividend leverage
d	-0.2	disaster size
μ_T	2	long-run mean temperature
ν	0.995	persistence of temperature
σ_ζ	0.1	volatility of i.i.d. normal temperature shock
l^G	0.03	belief parameter green investor
l^B	0.015	belief parameter brown investor
T_{Tipp}	2.8	temperature tipping threshold
k^B	3	climate risk exposure brown stocks
k^G	0.75	climate risk exposure green stocks
k^M	1	climate risk exposure market portfolio

To demonstrate the key mechanisms of our model, we present two sets of results. Our main results include the distant tipping point with $T_{tipp} = 2.8$°C. We call this model the *Tipping Point* case. Second, we consider a model with immediate climate disaster risks where disasters could occur as of today as has been assumed in many climate finance models; see, for example, Giglio et al. (2021b,a) and Bansal et al. (2021). This is equivalent to setting $T_{tipp} = 0$°C so that disaster risks can occur as of today. We call this model the *Immediate Disaster Risk* case.

4.2 Hedging Climate News and Climate Disaster Risk

In the following, we show how the different beliefs about the impact of climate change on the real economy affect the hedging incentives of the green and the brown investor. For this, we first present, in Figure 3, the subjective climate disaster probabilities π_t^h as a function of temperature, T_t, for the green investor ($h = G$) as well as for the brown investor ($h = B$). Solid lines show results for the tipping point case. As long as $T_t < T_{tipp}$, both agents agree that the probability of a climate disaster hitting today is zero. In contrast, once the tipping point is crossed, both agents believe in a positive probability of disaster. Green investors, who believe more strongly in climate change, believe in a larger climate disaster probability so that $\pi_t^G > \pi_t^B$. In line with Zickfeld et al. (2007), this difference increases with T_t. In

Figure 3: Subjective Disaster Probabilities

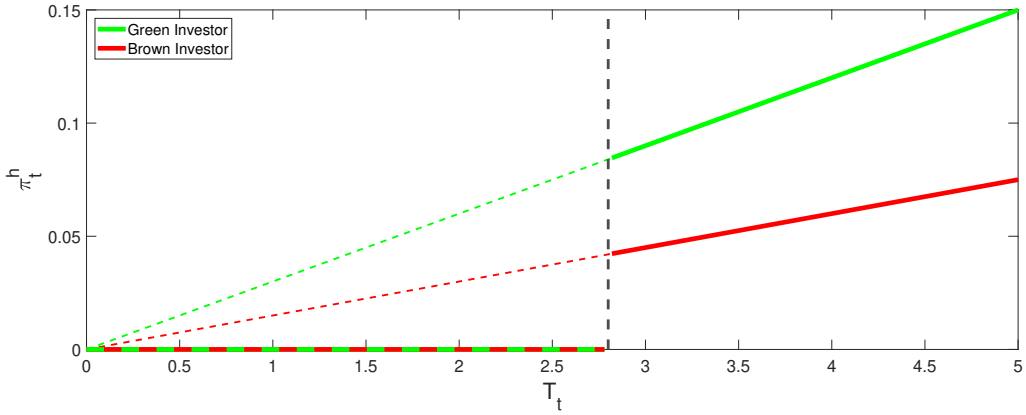

The figure plots subjective climate disaster probabilities π_t^h as a function of temperature, T_t, for the green investor as well as for the brown investor. Solid lines show results with the distant tipping threshold ($T_{tipp} = 2.8$°C, marked by the vertical line) and dashed lines results with immediate disaster risk ($T_{tipp} = 0$°C).

the case of immediate climate disaster risks (dashed lines), disaster probabilities π_t^h are a continuous function of T_t and the difference $\pi_t^G - \pi_t^B$ increases with temperature (assuming $T_t > 0$). Hence, investors disagree even if temperatures are low, which induces strong risk sharing incentives as we show below.

Figure 4 shows changes in the consumption share of the green investor, $s_{t+1}^G - s_t^G$, as a function of temperature, T_t, for different shocks in period $t+1$. The left panel shows results for CRRA utility where $\gamma = 1/\psi$ and the right panel for Epstein–Zin utility with $\gamma = 8$ and $\psi = 1.5$. Red lines depict the case where a disaster hits in $t+1$ and blue lines the case with no disaster in $t+1$. Lines with circles show the case of a positive shock in T_{t+1} ($T_{t+1} - E_t(T_{t+1}) = +0.0816$°C), lines with triangles that of a negative shock in T_{t+1} ($T_{t+1} - E_t(T_{t+1}) = -0.0816$°C), and the plain solid lines the average change in the consumption share. Results are shown for $s_t^G = 0.5$.

First, consider the immediate disaster risk case with CRRA utility. As shown in Section 3.3, investors only trade based on their beliefs about the probability of a disaster in the next period. However, they do not hedge climate news risk. Hence, independent of the shock to T_{t+1}, the consumption share of the green investor decreases as long as no disaster hits. Only if a disaster materializes does the wealth share of the green investor increase. Hence, in such a model, as long as no climate disaster materializes the wealth shares of brown investors persistently increase over time. In contrast to the empirical evidence in Engle et al. (2020), climate news risk (shocks to temperature in our model) is not traded by the investors in the CRRA case as investors agree on the distribution of global temperature.

Figure 4: Risk Sharing

(a) Immediate Disaster Risk

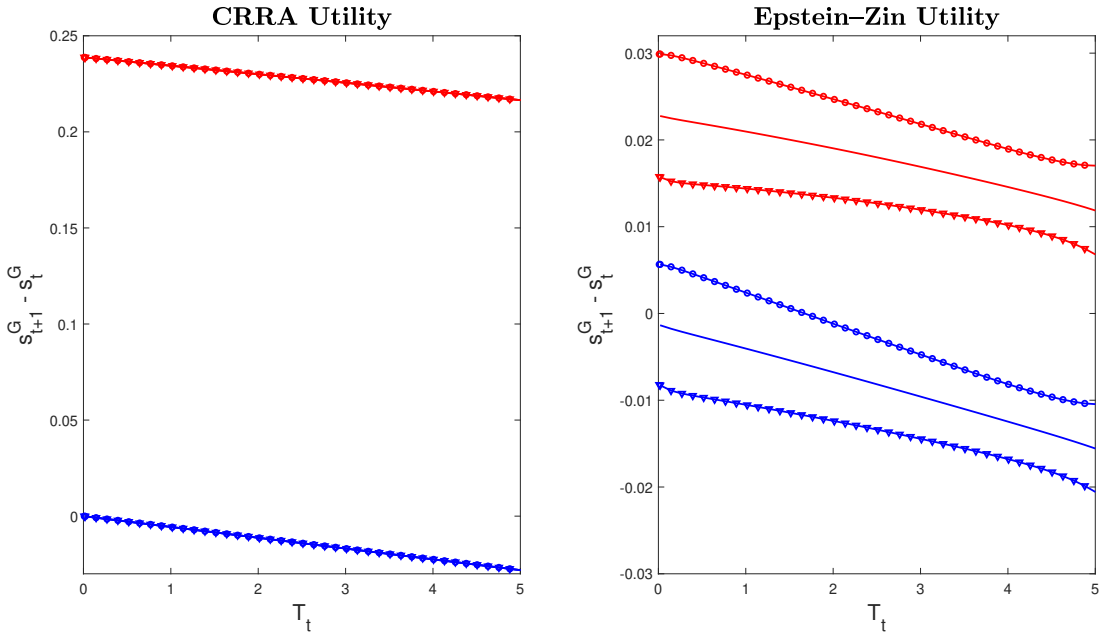

(b) Distant Tipping Threshold ($T_{tipp} = 2.8$°C)

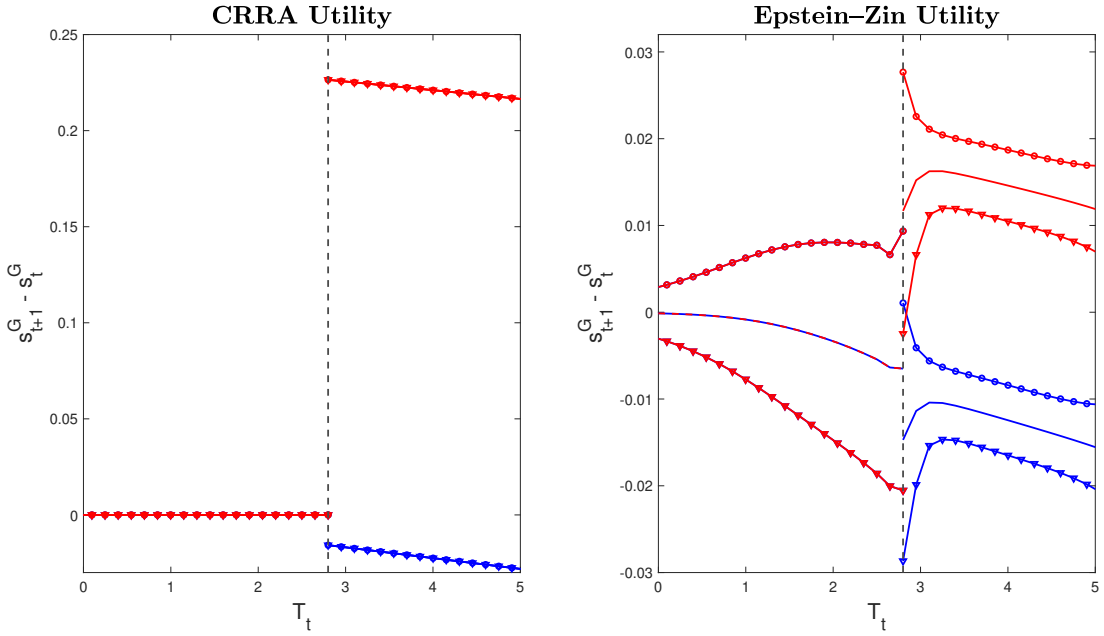

The figure plots changes in the consumption share of the green investor, $s^G_{t+1} - s^G_t$, as a function of temperature, T_t, for different shocks in period $t+1$. The left panel shows results for CRRA utility and the right for Epstein–Zin utility. Red lines depict the case where a disaster hits in $t+1$ and blue lines the case with no disaster in $t+1$. Lines with circles show the case of a positive shock in T_{t+1} ($T_{t+1} - E_t(T_{t+1}) = +0.0816$°C), lines with triangles that of a negative shock in T_{t+1} ($T_{t+1} - E_t(T_{t+1}) = -0.0816$°C), and the plain solid lines the average change in the consumption share. Results are shown for $s^G_t = 0.5$ and the vertical line marks the tipping threshold.

For Epstein–Zin preferences this does not hold true. Changes in temperature are a source of long-run consumption risk and hence affect the lifetime utility of the investors, similar to Bansal and Yaron (2004). Hence, investors have an incentive to trade temperature risks; see equation (15). In particular, the green investor, who believes in a larger impact of temperature changes on disaster probabilities, has an incentive to hedge positive shocks to temperature. Hence, her consumption share increases when a positive temperature shock materializes (circled lines) compared to the case of a negative temperature shock (lines with triangles). However, as in the CRRA case, as climate disasters can potentially occur as of today these risks are traded as well, implying that the average change in the consumption share of the green investor is significantly negative (given no disaster hits) as she is paying to insure against immediate disaster risk.

Panel (b) shows the corresponding results for our benchmark model with a distant tipping point of $T_{tipp} = 2.8$°C. For CRRA preferences, as long as $T_t < T_{tipp}$ investors agree on the distribution of climate disasters and hence have no incentive to trade. Only once the tipping point is crossed do they disagree about the probability of a climate disaster and trade with each other as in the case without the tipping point. Hence, for CRRA preferences climate news has no effect on the equilibrium consumption shares independent of whether the climate disaster risk is immediate or only occurs once the distant tipping point is crossed.

In contrast, for Epstein–Zin preferences temperature risks are traded even if $T_t < T_{tipp}$ as the risk that the tipping point will be crossed in the future is reflected in continuation utility v_t^h. Hence, green investors buy insurance against bad climate shocks so that when temperature increases they can compensate the decline in utility by an increased consumption share. In contrast to the immediate disaster risk case, climate disaster risks are not traded as long as $T_t < T_{tipp}$ as investors agree on disaster probabilities and hence have no incentive to trade these risks. This implies that green investors are also not paying a premium to hedge disaster risks such that the average change in the consumption share is close to 0 for low temperature levels.

So, our model implies that as long as the tipping point has not been crossed the only sources of variation in the market shares of green and of brown investors are climate news shocks. In particular, bad news about the climate (positive shocks to temperature) leads to an increase in the market share of green investors in line with the increase in green investing over the past decade as reported in Section 2.2. We discuss this finding as well as the equilibrium implication for the carbon risk premium in more detail in the following section.

4.3 Mean-Variance Trade-off of the Continuation Utilities

In this section, we explain the economic intuition behind the trading in the two-agent economy with Epstein–Zin preferences in more detail.[15] Colacito and Croce (2013) show that for Epstein–Zin investors the equilibrium consumption shares in the infinite-horizon economy can be characterized by a mean-variance trade-off of the continuation utilities of the investors. To show this analytically, they rewrite the value functions (9) of the investors. Let $\overline{v}_t^h = \frac{(v_t^h)^{\rho^h}}{\rho^h}$. The value functions are then given by

$$\overline{v}_t^h = (1-\delta^h)\frac{(s_t^h)^{\rho^h}}{\rho^h} + \delta E_t^h\left((\overline{v}_{t+1}^h)^{\frac{\alpha^h}{\rho^h}} e^{\alpha^h \Delta c_{t+1}}\right)^{\frac{\rho^h}{\alpha^h}}, h \in \{B, G\}. \tag{20}$$

In the model presented in this paper, all investors share the same preference parameters and only disagree about the disaster probability. Hence, we can simply write $\gamma^h = \gamma$, $\psi^h = \psi$ and $\delta^h = \delta$. Assuming log-normality for $\overline{v}_t^h$, Colacito and Croce (2013) show that the value functions can be approximated by

$$\overline{v}_t^h \approx (1-\delta)\frac{(s_t^h)^{\rho}}{\rho} + \delta k_t^h E_t^h(\overline{v}_{t+1}^h) - \delta k_t^h \frac{\rho-\alpha}{2\rho}\frac{Var_t^h(\overline{v}_{t+1}^h)}{E_t^h(\overline{v}_{t+1}^h)}, h \in \{B, G\}, \tag{21}$$

with $k_t^h = E_t^h(e^{\alpha \Delta c_{t+1}})^{\frac{\rho}{\alpha}}$. For investors with CRRA preferences, it holds that $\rho = \alpha$, so the last term of the equation vanishes in this case. Hence, the continuation utility of these investors solely depends on the expected future utility, and not on the volatility of future utility. In our baseline calibration we choose $\gamma > \frac{1}{\psi}$, so agents have a preference for the early resolution of risks. This implies $(\rho - \alpha) > 0$, and since $\rho E_t^h(\overline{v}_{t+1}^h)$ is also positive, a higher subjective variance of the continuation utility, $Var_t^h(\overline{v}_{t+1}^h)$, reduces welfare today. In other words, the investors are willing to trade off expected future utility, $E_t^h(\overline{v}_{t+1}^h)$, to reduce today's uncertainty about future utility $Var_t^h(\overline{v}_{t+1}^h)$. This is what we refer to as the mean-variance trade-off in this section. Moreover, this trade-off can also be interpreted in terms of effects on the wealth shares of the two investors, as there is a one-to-one mapping between the continuation utility values v_t^h and the lifetime wealth of the investors.

Figure 5 shows the conditional mean and variance of the continuation utilities for the baseline economy with $T_t = 1°\text{C}$. The upper panel displays the subjective expectations of the continuation utilities for the green investor (left plot) and brown investor (right plot) in the trade minus no-trade economy. In this context, the trade case refers to the baseline economy, where agents can freely trade with each other and insure against future states of the economy they particularly dislike. On the other hand, the no-trade case refers to an autarky economy, where the consumption shares of the two agents remain constant over time, as they are not

[15] The analysis in this chapter is inspired by Pohl et al. (2021), while the narrative and economic intuition have been tailored to align with the specific model outlined in this paper.

allowed to trade risks with each other. The 'trade minus no-trade' curve is positive across almost the entire s_t^G state space, indicating positive gains from trade for both agents.

Figure 5: Conditional Mean and Variance of Continuation Utilities

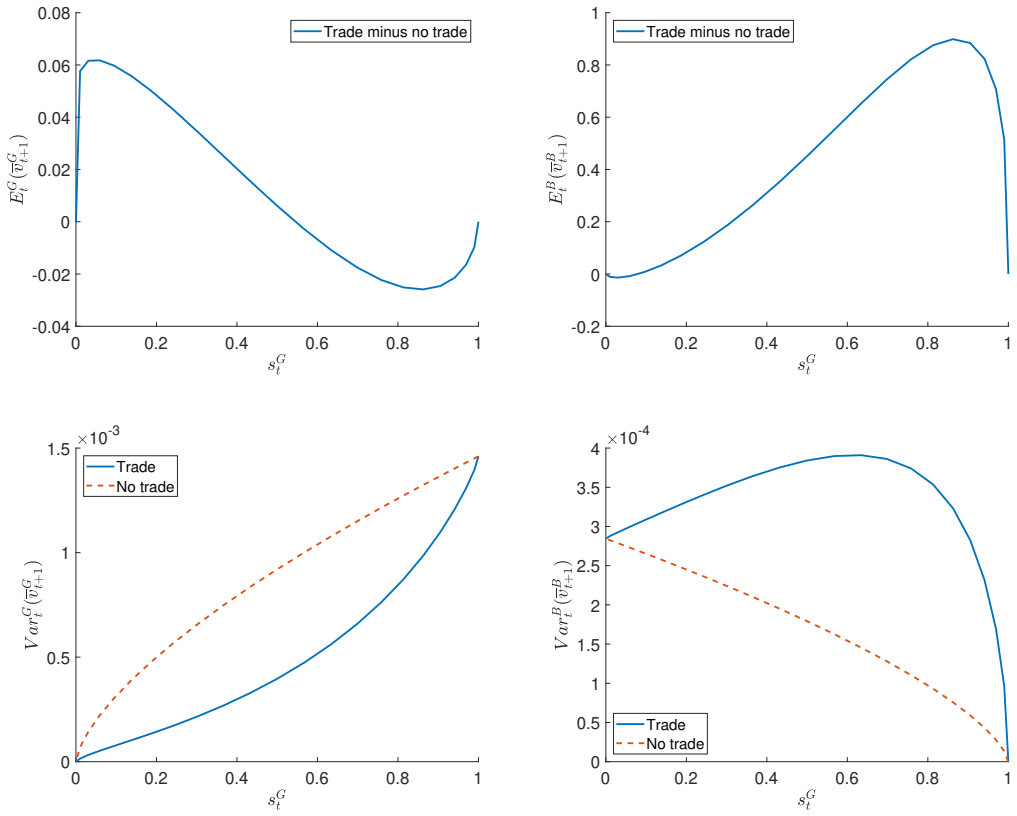

The figure shows the conditional mean and variance of continuation utilities as a function of the consumption share of the green investor, s_t^G, for the baseline model with a tipping threshold at 2.8°C. The top panel displays the difference in expected utility between an economy in which the agents are allowed to trade and a no-trade assumption. The lower panel shows the conditional variance for both, the trade and no-trade case. The left panel presents the results for the green investor, who beliefs in a higher temperature-induced disaster probability, and the right panel shows the results for the brown investor, who believes in a lower temperature-induced disaster probability. Results are shown for $T_t = 1$°C.

For the green investor, the gains from trade are largest when there is only a small fraction of green investors in the economy. This can be explained by the risk sharing motive introduced in Section 3.3 The green investors believe in a higher impact of global warming on disaster probabilities, and due to Epstein–Zin preferences with a preference for the early resolution of risks, the investors care about these long-run consumption risks and want to hedge against low growth states. The brown investors, on the other hand, believe in a smaller impact of

higher temperatures on consumption growth and provide insurance for these bad states in exchange for an insurance premium in the form of higher future wealth during normal times.

For a small share of green investors, the demand for insurance against high temperature states is low, while the supply of this insurance is high due to the larger share of brown investors. This drives down the price of this insurance, allowing green investors to insure against future consumption volatility without paying a high premium today. In contrast, when the share of green investors is large in the economy, there is a high demand for this insurance but limited supply, leading to a higher insurance price. The upper left plot of Figure 5 demonstrates, that green investors are even willing to give up some (subjective) future expected utility, to buy insurance and reduce volatility of future consumption. On the other hand, the gains of trade for brown investors (upper right plot) are largest when there is only a small share of brown investors in the economy, as the premium they collect for providing the insurance is higher in such an economy.

The lower panel of Figure 5 plots the conditional variance of the continuation utility for both investors in the trade (solid blue line) and no-trade (dashed orange line) case. The green investor can significantly reduce her volatility of future utility by hedging against states of high marginal utility, particularly high temperature states. In contrast, the brown investor is willing to accept more uncertainty about future utility in exchange for a higher expected continuation utility.

Similar analysis about the effects of risk sharing with recursive preferences have also been made in different settings. Pohl et al. (2021) show the risk sharing for an economy in which agents have different beliefs about the persistence of shocks to the long-run risk process. Colacito and Croce (2013) and Colacito et al. (2022) analyze the risk sharing in a two-country model, in which trade is a response to different idiosyncratic endowment shocks.

4.4 Carbon Premium

Our model yields predictions regarding the pricing of green and of brown assets. Figures 6 and 7 show the carbon premium for CRRA and Epstein–Zin preferences, respectively.[16] We define the carbon premium as the expected return of brown stocks minus the expected return of green stocks, and show the premium as a function of T_t for the beliefs of the brown investor and a fixed wealth share of $w_t^G = 0.5$.[17]

The red line in Figure 6 shows results for the immediate disaster risk case and the blue line

[16] For CRRA preferences, results are shown for $\gamma = 2$, as for higher degrees of risk aversion existence issues occur (see Pohl et al. (2023) for a detailed discussion of the existence problem). However, while this lowers the carbon premium quantitatively, it does not have any effect on the qualitative conclusions we draw based on these results.

[17] Figures 33 and 34 in Appendix A show the corresponding results for the beliefs of the green investor, which are qualitatively the same; only the magnitude of the carbon premium decreases.

Figure 6: Carbon Premium for CRRA Preferences

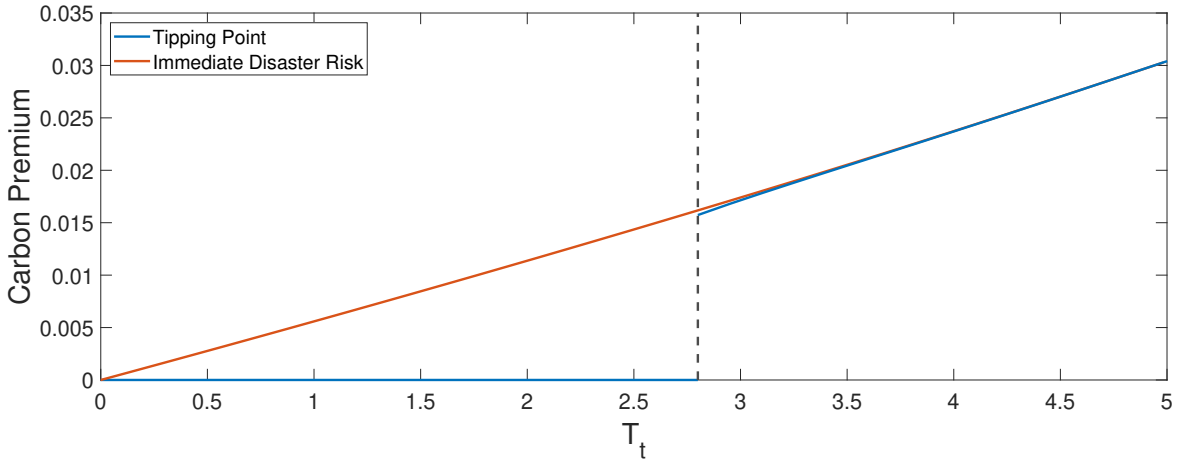

The figure plots the expected return of the brown stock minus the expected return of the green stock as a function of temperature, T_t, for $w_t^G = 0.5$ for CRRA preferences with $\gamma = 1/\psi = 2$. Results are shown for the case with immediate disaster risk and for the case with the distant tipping threshold for the beliefs of the brown investor. The vertical dashed line marks the tipping threshold.

Figure 7: Carbon Premium for Epstein–Zin Preferences

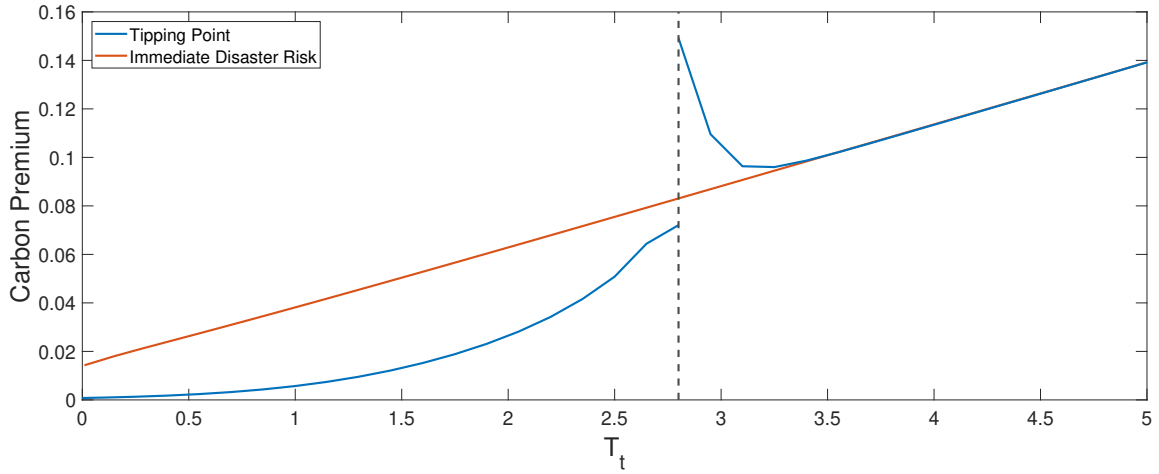

The figure plots the expected return of the brown stock minus the expected return of the green stock as a function of temperature, T_t, for $w_t^G = 0.5$ for Epstein–Zin preferences. Results are shown for the case with immediate disaster risk and for the case with the distant tipping threshold for the beliefs of the brown investor. The vertical dashed line marks the tipping threshold.

for our benchmark model with the distant tipping point. In the case of CRRA preferences, the carbon premium is zero as long as $T_t < T_{tipp}$. Investors with CRRA preferences do not price in long-term risks and, as the disaster risk can only occur in the future, the premium for assets with different exposures to climate risk is the same across assets and is equal to zero. Only once the tipping threshold is crossed does the carbon premium become large and significant and increase with the disaster probability driven by T_t. Hence, for temperature levels below the temperature threshold as observed in the past decade, CRRA investors would not require a premium for holding assets that are more exposed to climate risks. This is in contrast with the findings of Bolton and Kacperczyk (2021, 2022), who report a significant carbon premium.

In turn, for Epstein–Zin preferences the carbon risk premium is positive as long-run climate risks are priced in and brown stocks have a higher exposure to climate risks than green stocks ($k^B = 3.0$ versus $k^G = 0.75$). The carbon premium increases with temperature as it positively affects the probability of a disaster. Note that this is true in the tipping point model even if $T_t < T_{tipp}$ as temperature changes are a source of long-run risk, which is priced under Epstein–Zin utility. So even if temperatures are well below the tipping point, an increase in temperature increases the carbon premium.

If climate disasters pose a potential risk as of today (red line), the carbon premium will be large even for low temperature levels. For example, for the temperature level of 2020 of 1°C the carbon premium is 3.5 percent. In contrast, when we appropriately account for the distant tipping point when modeling climate disaster risks the implied carbon premium is significantly smaller for lower temperatures as the tipping point is sufficiently far away, in line with the small carbon premium reported on financial markets. Pástor et al. (2022) compute an expected carbon premium of approximately 0.5–1.5 % respectively in the period from 2012–2020, depending on the estimation method used, which is in line with our carbon premium in the tipping threshold model. However, our model predicts that the carbon premium will increase significantly if climate risks increase in the future. These results highlight the importance of appropriately accounting for the specific properties of climate risks in financial models. More precisely, when climate risks are analyzed in financial models, it is crucial to include tipping thresholds when modeling these risks and not to model them as imminent disaster risks, which is standard in the asset-pricing literature. Moreover, for CRRA preferences long-term climate risks are not priced, so it is crucial to use preferences that take long-term trade-offs into account.

The carbon premium depends not only on the temperature level but also on the market share of the green investor. Figure 8 plots the carbon premium as a function of the wealth share of the green investor for a low temperature level, $T_t = 1$°C, and a high temperature level close to the tipping point, $T_t = 2$°C, which—in line with the pessimistic RCP8.5 emission

scenario—could be reached in 2050.

Figure 8: Carbon Premium as a Function of the Wealth Share

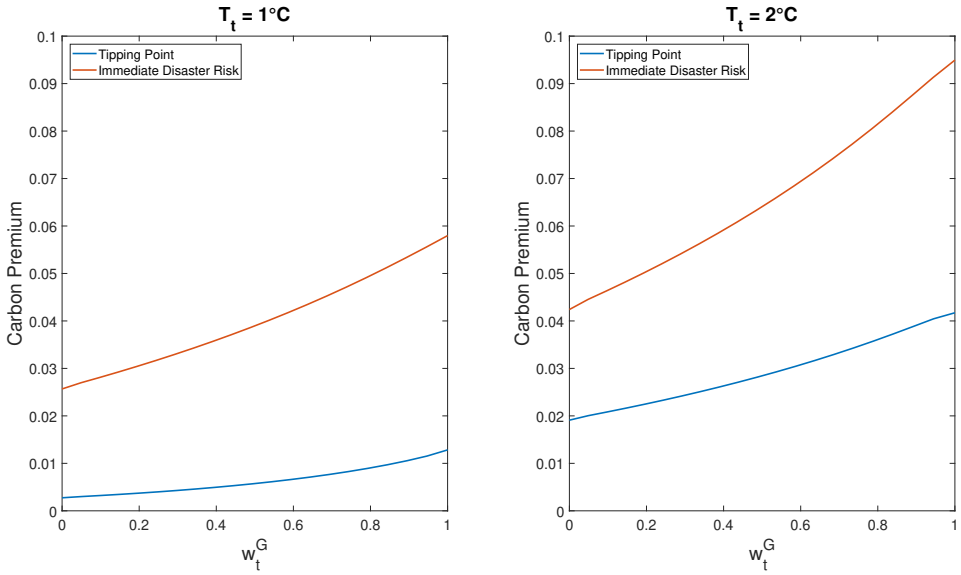

The figure plots the expected return of the brown stock minus the expected return of the green stock as a function of the wealth share of the green investor, w_t^G, for different levels of temperature, T_t. Results are shown for the case with immediate disaster risk and for the case with the distant tipping threshold for the beliefs of the brown investor.

Green investors are more afraid of climate risks and hence require a larger premium for holding the brown asset. So in equilibrium, the larger the market share of the green investor, the larger is the carbon premium. While this effect is quantitatively small for the low temperature level of today ($T_t = 1°\text{C}$), with a carbon premium only slightly above 1 percent for any wealth share of the green investor, it significantly increases once the temperature gets closer to the tipping point, with a carbon premium of up to 4 percent for $T_t = 2°\text{C}$.

Our model hence yields a positive carbon premium that increases with temperature risks as well as with the share of green investors. So the increase in the market share of green investors over the past decade has likely contributed to an increase in the carbon premium, and our model predicts that the carbon premium will increase significantly if the market share of green investors keeps rising.

4.5 Green Investing

How can this evidence be reconciled with the recent outperformance of green stocks as for example reported in Huij et al. (2021) and Pástor et al. (2022)? We show that unexpected bad news about the climate drives up the wealth shares of green investors and pushes up the relative valuations of green versus brown firms. Ardia et al. (2023) provide empirical evidence

for this mechanism. They construct a climate concern index based on newspaper articles and show that green stocks react more positively to bad climate news compared to brown stocks. Pástor et al. (2022) use this climate concern index and show that forecasting errors have a strong downward trend implying that news about the climate has been consistently worse than expected.

In our model, unexpected bad news about the climate—that is, positive shocks to T_t—has two effects on the pricing of green and brown assets, one direct and one indirect: Positive shocks to T_t lead to a decrease in the price of stocks that have a large exposure to climate risks. In turn, green stocks that provide a (partial) hedge against climate risks increase in value in response to bad climate news; see the left panel of Figure 9, which plots the price–dividend ratios of the green and the brown asset as well as the market portfolio as a function of T_t. Simultaneously, the increase in temperature increases the market share of green investors as argued in Section 4.2. Green investors require a larger compensation for holding brown assets compared to brown investors, and hence the increase in their market share leads to a further decrease in the prices of the brown asset (see the right panel of Figure 9, which plots price–dividend ratios as a function of w_t^G). As a result, increases in temperature endogenously drive up the market share of green investors and lead to an outperformance of green over brown stocks.

Figure 9: Price–Dividend Ratio

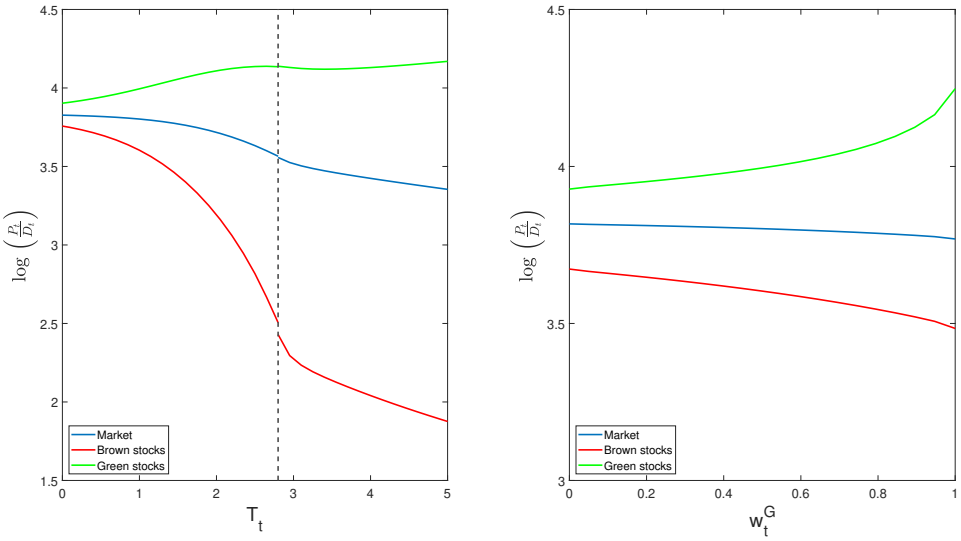

The figure plots the log price–dividend ratio for the green and the brown stocks and for the market portfolio. In the left panel, the price–dividend (pd) ratios are shown as a function of temperature, T_t, for $w_t^G = 0.5$. The right panel shows the pd ratios as a function of the wealth share of the green investor for $T_t = 1$°C. Results are shown for the baseline calibration with a tipping threshold at 2.8°C.

We demonstrate this mechanism in Figures 10 and 11. Figure 10 shows the impact of a bad climate shock on the market share of the green investor and on the returns of green and of brown stocks. Starting at $T_0 = 1°\text{C}$, the temperature level today, and $w_0^G = 0.5$, it shows the effect of a one standard deviation climate shock of $\sigma_\zeta \zeta_{t+1} = +0.1°\text{C}$ in period 2, assuming that all shocks in other periods are zero.[18] The bad climate shock increases the market share of the green investor, who buys insurance against climate risk from the brown investor as argued in Section 3.3. Hence, a series of bad shocks leads to an increased market share of green investors over time. Green and brown stocks are differently affected by bad climate news. Brown stocks with a large climate exposure depreciate in value when bad news about the climate arrives, as shown in the right panel of Figure 10. In contrast, green stocks provide a (partial) hedge against climate risks such that their prices increase in response to bad news about the climate. Hence, positive shocks to T_t imply an outperformance of green over brown stocks in our model.

Figure 10: Impulse Responses for Temperature Shock

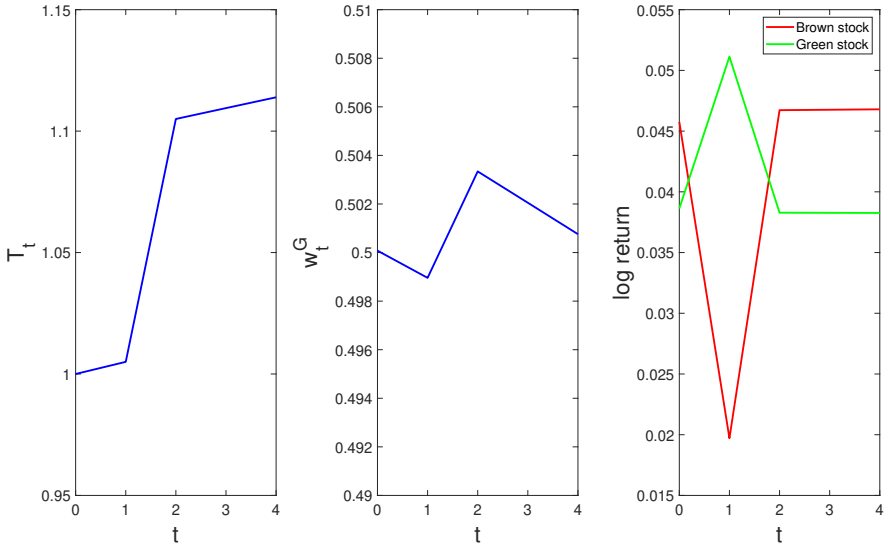

The figure plots changes in the wealth share of the green investor and the log returns of green and of brown stocks for a one-time shock in temperature of 0.1°C in period 2. All other shocks are set to zero and results are shown for $w_0^G = 0.5$.

Figure 11 shows corresponding results assuming that no news about the climate occurs, but that there is an exogenous shift in the market share of green investors in period 2. Green investors are more afraid of climate risks and hence are willing to pay a lower (higher) price for the brown (green) asset. As a consequence, the increase in market share implies temporarily

[18] Note that due to mean reversion, T_t is slightly sloping upward and the market share of green investors is sloping downward in the absence of shocks as green investors pay a premium to hedge climate news; see Figure 4.

higher returns for green stocks compared to brown stocks. So, both the bad climate news and the resulting increase in the market share of the green investor lead to an outperformance of green over brown stocks.

Figure 11: Impulse Responses for Wealth Share Shock

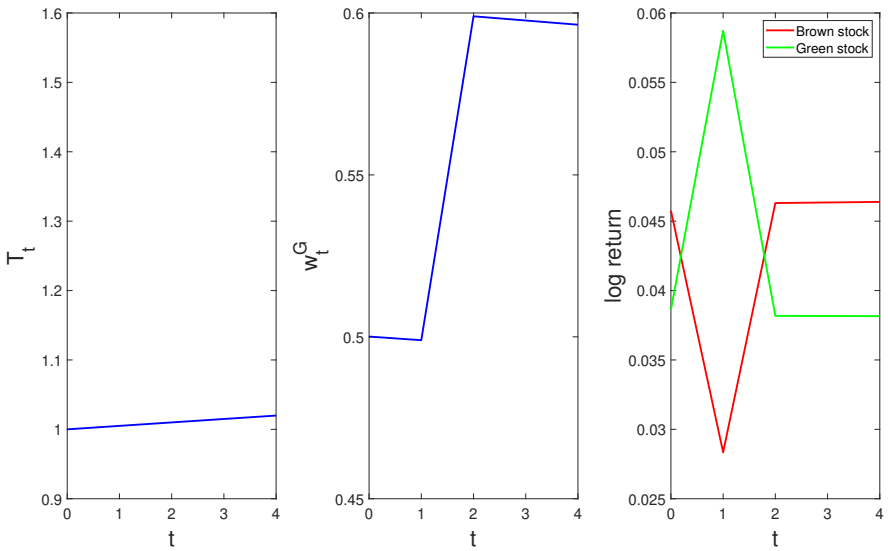

The figure plots changes in the wealth share of the green investor and the log returns of green and of brown stocks for a one-time shock in the wealth share of the green investor of 10% in period 2. All other shocks are set to zero and results are shown for $w_0^G = 0.5$.

Ardia et al. (2023) find that there was a series of bad climate news items in the period 2010–2021. Our model predicts that such a series of bad climate news items will lead to an outperformance of green stocks over brown stocks in line with the outperformance of green stocks in the past decade reported by Huij et al. (2021) and Pástor et al. (2022). We demonstrate the impact of a series of bad climate news items in Table 2. For this, we simulate 1,000 sample paths each containing 11 years of data. We consider two scenarios. In the first, climate news shocks ζ_{t+1} are simply drawn from a random normal distribution. This describes a scenario with no particularly bad news about the climate. In the second scenario, in each period we exogenously add a bad climate news shock of $\sigma_\zeta \zeta_{t+1} = 0.1$°C to the temperature process. We assume that the green agent holds the correct beliefs about disaster probability, so $l = l^G = 0.03$. However, given the 90% quantile of the temperature process in Figure 12, it becomes evident that the speculation motive has minimal impact in these simulations.

Table 2 shows selected annualized asset-pricing moments for the two scenarios. In the first scenario, without unexpectedly bad climate news, brown stocks slightly outperform green stocks reflecting the small but positive carbon premium for low temperature levels reported in Figure 7. As brown stocks are more exposed to climate risks, they have a smaller price–

dividend ratio compared to green stocks and are slightly more volatile. The wealth share of green investors is slightly decreasing over time as green investors are paying a premium to insure against climate risks; see Figure 4.

In contrast, a series of bad climate news items leads to a strong outperformance of green stocks. In our calibrated economy, we obtain an annual outperformance of 3.70% with a standard deviation across the sample paths of 1.65%, which is roughly in line with the outperformance of 4.08% reported in Huij et al. (2021) and that of 5.4% reported in Pástor et al. (2022).

Table 2: Annual Asset-Pricing Moments of Brown and Green Stock

	$E(p_t^i - d_t^i)$	$\sigma(p_t^i - d_t^i)$	$E(log(R_t^i))$	$\sigma(log(R_t^i))$	$R_t^B - R_t^G$	$E(w_T^G)$
Normal Shocks to T_{t+1}						
Green Stock	3.9567	0.0146	0.0412	0.0496	0.0031	0.4942
	(0.0198)	(0.0069)	(0.0158)	(0.0111)	(0.0077)	
Brown Stock	3.6728	0.0255	0.0442	0.0519		
	(0.0351)	(0.0150)	(0.0162)	(0.0118)		
Unexpectedly bad climate news						
Green Stock	4.0235	0.0499	0.0520	0.0501	-0.0370	0.5559
	(0.0235)	(0.0135)	(0.0160)	(0.0113)	(0.0165)	
Brown Stock	3.5173	0.1353	0.0151	0.0605		
	(0.0738)	(0.0600)	(0.0205)	(0.0145)		

The table reports annual asset-pricing moments for green and for brown stocks from simulating 1,000 sample paths each containing 11 years of data. We set $T_{start} = 0.6$°C and $w_{start}^G = 0.5$. The top panel shows results when shocks to temperature, ζ_{t+1}, are drawn from a standard normal distribution. In the bottom panel we assume that, additional to the normal shocks, there is bad climate news of +0.1°C per period. Standard deviations of the time series moments across the sample paths are shown in parentheses.

Figure 12 shows the impact of a series of bad news about the climate on the performance of green over brown stocks, corresponding to the second scenario from above. We do not aim to precisely match the size of outperformance (note that the return spreads reported in Huij et al. (2021) and Pástor et al. (2022) have large standard errors) but rather provide an intuitive mechanism on how bad news about the climate have affected the market share of green investors and the pricing of green and brown assets. As empirically shown in Pástor et al. (2022), we assume that there has been a series of bad news about the climate in the past decade. More precisely, we assume that there has been a climate news shock of $\sigma_\zeta \zeta_{t+1} = 0.1$°C each period from 2010 until 2021 additional to the random variation in T_{t+1}. That is, we draw

ζ_{t+1} from a normal distribution and exogenously add +0.1°C each period. Figure 12 shows the median path together with the 10% and 90% quantiles of T_t, w_t^G as well as cumulative log returns and the return spread of the brown and green asset using 1,000 simulated paths.

Figure 12: Performance of Green and Brown Stocks

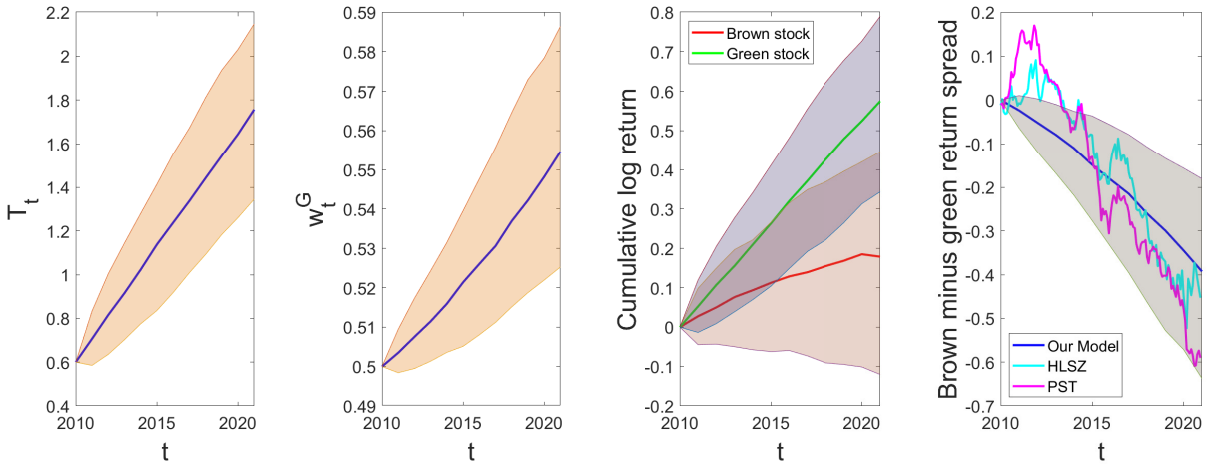

The figure shows the median path together with the 10% and 90% quantiles of T_t, w_t^G as well as cumulative log returns and the return spread of the brown and green asset using 1000 simulated paths for a 11-year period from 2010 to 2021. Shocks to temperature ζ_{t+1} are drawn from normal distribution and additionally an exogenous climate news shock of +0.1°C is added each period. The right panel also shows the performance of the Brown-Minus-Green factors from Huij et al. (2021) and Pástor et al. (2022).

The left panel plots the implied path of T_t which increases by approximately 1.2°C in the 11 year period. In line with the arguments above, the unexpectedly bad climate news lead to a steady increase in the market share of green investors, consistent with the evidence provided in Section 2.2. Both, the increases in T_t as well as the increase in the market share of the green investor lead to an outperformance of green over brown stocks. The right panel shows the performance of a portfolio that goes long the brown stock and short the green stock. Additional to the model implied performance, the figure also shows the performance of the brown-minus-green portfolios of Huij et al. (2021) based on emission data, and the portfolio of Pástor et al. (2022) based an environmental-scores. We find that a series of bad climate shocks can explain the outperformance of green over brown stocks reported in the two papers.

Bad climate news leads to a strong increase in the valuations of green assets while the average price–dividend ratio of brown assets is significantly smaller compared to the scenario without unexpectedly bad climate news. As green investors buy insurance against climate shocks, their market share increases in response to the bad climate news resulting in an increase in their market share of about 5 percent over the 11 year period. This is approximately in line

with the survey evidence provided by Howe et al. (2015), who find that the fraction of people who believe that climate change will significantly harm future generations has increased by roughly 6 percentage points between 2014 and 2021. Furthermore, as brown stocks are more exposed to climate risks their prices react more strongly to climate news leading to a larger volatility of brown stocks compared to green stocks.

Finally, Table 3 shows annual moments for aggregate consumption growth, dividend growth of the market portfolio, the market risk premium, and the carbon premium, as well as the risk-free rate. As the climate tipping point is not crossed in the simulations, climate shocks have no effect on consumption and dividend growth. Our calibration implies average aggregate consumption growth of about 2% per year with a volatility of 1.88%, in line with the US data. Dividends also have a growth rate of about 2% per year but are significantly more volatile, in line with the moments in the data (see, for example, Wachter (2013)). Our model implies a market risk premium of below 1% per year. Note that climate risks are the only priced risks in our model and hence we do not target a matching of the aggregate market premium of about 7% per year in the US. Finally, the risk-free rate in our model is about 3.45% per year as precautionary savings due to disasters are low for temperature levels significantly below the tipping point. Figure 13 plots the risk-free rate as a function of T_t. In the case of immediate disaster risk, the risk-free rate is monotonically decreasing in T_t, as precautionary savings increase with the probability of a disaster (Wachter, 2013). Precautionary savings only become economically relevant once the tipping point is crossed. Hence, for low temperature levels the risk-free rate is relatively large. Note that the model would produce both a large risk premium and a low risk-free rate if, for example, other consumption disaster risks as in Barro (2009) and Wachter (2013) were added to it. This would increase the disaster risk premium and lower the risk-free rate due to precautionary savings, such that aggregate moments could be matched. As we are primarily interested in the consequences of belief disagreement for the pricing of green and of brown assets, we abstract from this level of complexity here.

Figure 13: Risk-free Rate

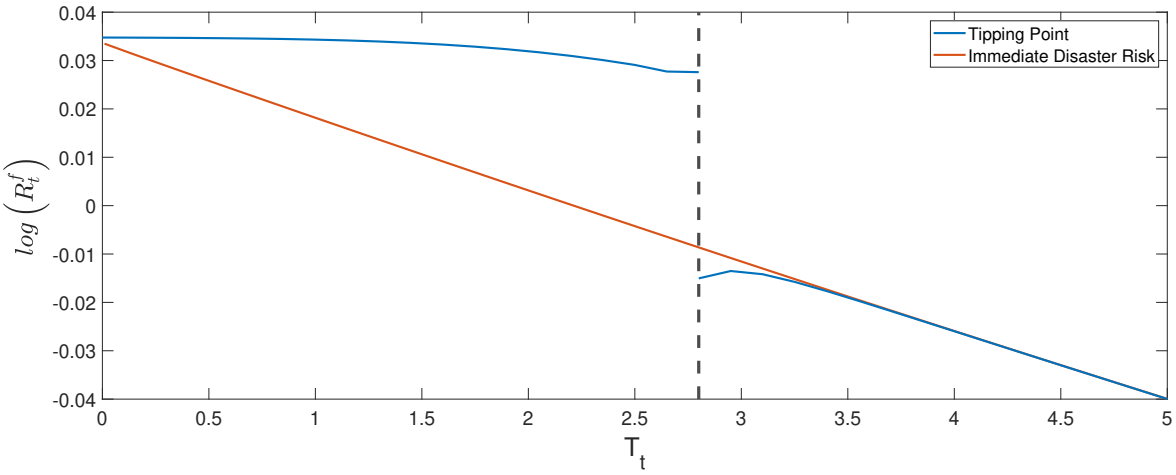

The figure plots the risk-free rate as a function of temperature, T_t, for $w_t^G = 0.5$. Results are shown for the case with immediate disaster risk and for the case with the distant tipping threshold. The vertical dashed line marks the tipping threshold.

Table 3: Annual Asset-Pricing Moments of Market Portfolio and Risk-free Rate

	Δc_{t+1}	Δd_{t+1}^M	$\log(R_t^f)$	$R_t^M - R_t^f$
Normal Shocks to T_{t+1}				
mean	0.0205	0.0213	0.0345	0.0081
	(0.0055)	(0.0142)	(1.1946e-04)	(0.0155)
σ	0.0188	0.0488	0.0001	0.0486
	(0.0040)	(0.0103)	(6.8924e-05)	(0.0109)
Unexpectedly large climate news shocks				
mean	0.0205	0.0213	0.0338	0.0025
	(0.0055)	(0.0142)	(4.7979e-04)	(0.0157)
σ	0.0188	0.0488	0.0008	0.0492
	(0.0040)	(0.0103)	(6.2944e-04)	(0.0111)

The table reports annual asset-pricing moments from simulating 1,000 sample paths each containing 11 years of data. We set $T_{start} = 0.6$°C and $w_{start}^G = 0.5$. The top panel shows results when shocks to temperature, ζ_{t+1}, are drawn from a standard normal distribution. In the bottom panel we assume that, additional to the normal shocks, there is an unexpected increase in temperature of +0.1°C per period. Standard deviations of the time series moments across the sample paths are shown in parentheses.

4.6 Welfare Cost of Carbon

In our asset-pricing model, we measure the impact of climate risks on equity valuations and the wealth of the investors. In line with Bansal et al. (2021), we refer to our measure in the following as the welfare cost of carbon (WCC). We interpret the WCC as a marginal concept—the monetary loss that is caused by an additional metric ton of carbon emissions. It is important to note that carbon emissions only affect the WCC to the extent that they are already reflected in equity valuations. In contrast, the social cost of carbon (SCC) measures the full extent of emissions' negative externality [19].

Thus, if (a part of) emissions impose(s) a negative externality and are (is) not correctly priced yet, the SCC would exceed the WCC. The WCC sets a lower bound to the "true" SCC in this scenario. This concept of measuring the impact of temperature increases on future wealth is also related to the "welfare cost of consumption uncertainty," introduced by Barro (2009), who shows that society would be willing to reduce GDP by around 20 percent yearly to eliminate the possibility of rare disasters. This is around 15 times as much as the welfare cost of usual economic fluctuations. So as long as $\psi > 1$, we would expect to see a sizeable WCC since agents want to reduce the risk of future consumption disasters.

In our model we do not explicitly include carbon emissions, but instead directly model the dynamics of global temperature, which is affected by increases in emissions. We use the estimate of Bansal et al. (2021) for the sensitivity of global temperature to changes in emissions to quantitatively analyze the WCC implied by our model. We express that cost in terms of a numeraire good, in our case current consumption. Hence, the WCC is defined as the ratio of two marginal values:

$$WCC_t = -\frac{\frac{\partial V_t}{\partial E_t}}{\frac{\partial V_t}{\partial C_t}}. \tag{22}$$

For Epstein–Zin preferences, the value function is a function of the aggregate wealth–consumption ratio $Z_t \equiv \frac{W_t}{C_t}$.

$$\frac{V_t}{C_t} = [(1-\delta)Z_t]^{\frac{\psi}{\psi-1}},$$

so that the WCC can be written as

$$WCC_t = \frac{\psi}{\psi-1}\frac{-\partial log Z_t}{\partial T_t}\frac{\partial T_t}{\partial E_t}C_t. \tag{23}$$

In Appendix B we provide the derivations of equation (23). Note that WCC_t measures

[19] The SCC is an attempt to put a monetary value on the negative consequences of climate change, now and in the future. There is a wide range of different estimates for the SCC in the literature. These differences result mainly from different assumptions of parameter values regarding, for example, preferences, discounting, damage, climate response to emissions, and uncertainties in general.

aggregate welfare effects—that is, how changes in climate risks affect aggregate wealth in the economy. We discuss the impact of climate risks on individual wealth in Section 4.7. As Bansal et al. (2021), we use a semi-parametric approach to calculate WCC_t. The sensitivity of the log wealth–consumption ratio, $\frac{\partial log Z_t}{\partial T_t}$, follows from our climate economy and depends on both the temperature level and the wealth share of the green and the brown investors at time t. In line with Bansal et al. (2021), we set the temperature sensitivity to cumulative carbon emissions to $\frac{\partial T_t}{\partial E_t} = 1.71°C$ per trillion tonnes of carbon. They obtain the value by matching the mean value of carbon sensitivity to emissions estimated in MacDougall et al. (2017).[20] For C_t we use the purchasing power parity adjusted world gross domestic product, which was about 146.71 trillion international dollars in 2021[21].

Figure 14 shows the WCC as a function of global temperature for the benchmark case with a distant tipping point as well as for the case with immediate climate disaster risks. First, consider the case with immediate disaster risks. The WCC is slightly decreasing in T_t as the marginal decline in utility due to an increase in T_t is decreasing in temperature. Note that Bansal et al. (2021) report a constant WCC, which, however, only arises as they use a linear approximation to solve the model. Once the model is solved accurately using global methods as proposed by Pohl et al. (2018), the wealth–consumption ratio is a convex function of T_t; see Figure 15. Hence, immediate climate disaster risks imply that the WCC is high as of today, but should decrease in the future if global temperature keeps increasing.

In contrast, our benchmark model—accounting for the fact that climate disasters can only occur once the tipping point is crossed—implies a low WCC for low temperature levels, as observed until now. The marginal decline in utility due to an increase in temperature is small as long as the tipping point is sufficiently far away. However, once temperature approaches the tipping point, the WCC increases significantly and can almost triple compared to the case with immediate climate disaster risks. Close to the tipping point, a reduction in temperature leads to a large utility gain for the investors as it significantly decreases the probability of crossing the tipping point. So the wealth–consumption ratio is strongly decreasing in T_t close to the tipping point—see Figure 15—such that the WCC is high.

Thus, our model provides a potential explanation of why investments to reduce climate risks have been low in the past: as the tipping point was sufficiently far away, the welfare gains from such investments were small. However, with increasing temperatures, as predicted by climate scientists for the coming years, the WCC is likely to increase significantly. Put differently, the marginal gain from investments to slow down climate change should increase in the future.

[20] They base their results on the carbon–climate response; see Matthews et al. (2009) for the scientific background to these estimations.

[21] This value is provided by the World Bank, using the current international dollar value (https://data.worldbank.org/indicator/NY.GDP.MKTP.PP.CD).

Figure 14: Welfare Cost of Carbon

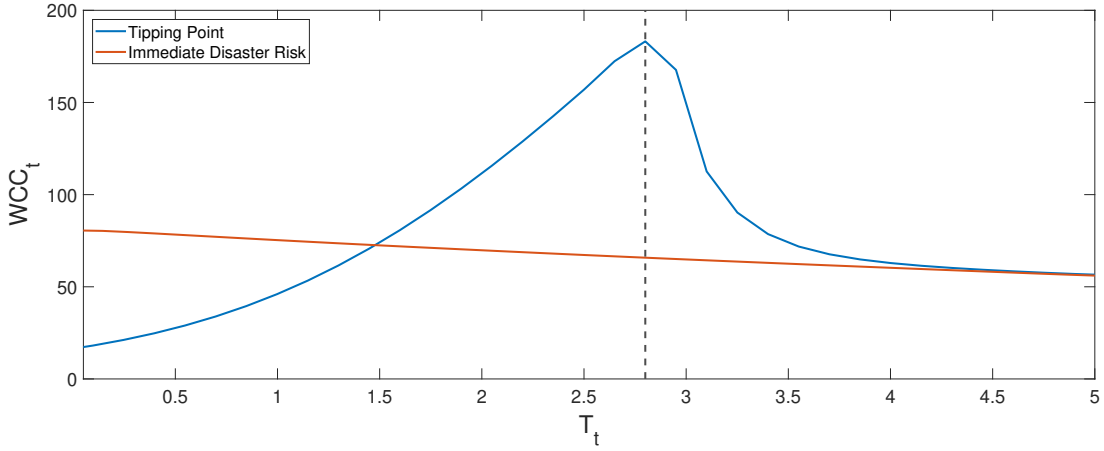

The figure plots the welfare cost of carbon as a function of T_t for $w_t^G = 0.5$. Results are shown for the case with immediate disaster risk and for the case with the distant tipping threshold. The vertical dashed line marks the tipping threshold.

Figure 15: Wealth–Consumption Ratio

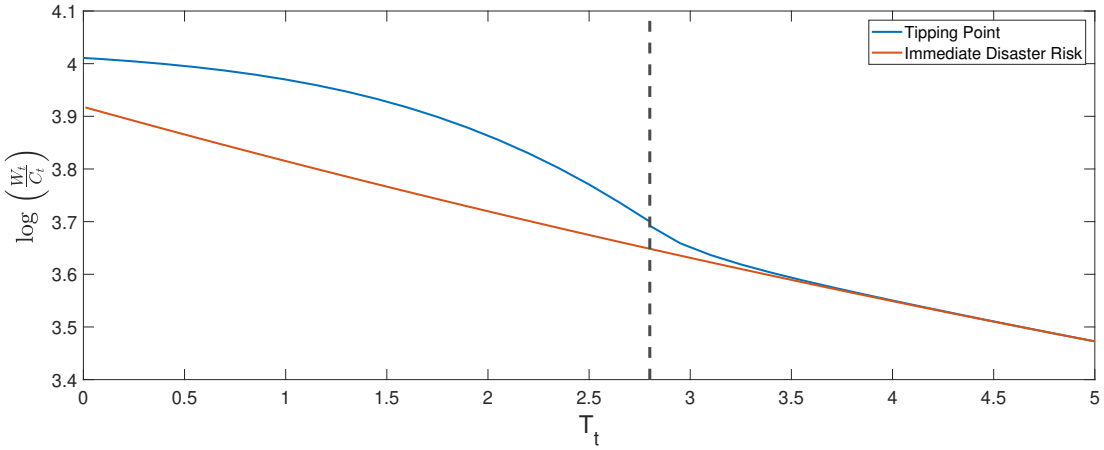

The figure plots the aggregate log wealth–consumption ratio as a function of T_t for $w_t^G = 0.5$. Results are shown for the case with immediate disaster risk and for the case with the distant tipping threshold. The vertical dashed line marks the tipping threshold.

Figure 16: Welfare Cost of Carbon as a Function of Wealth

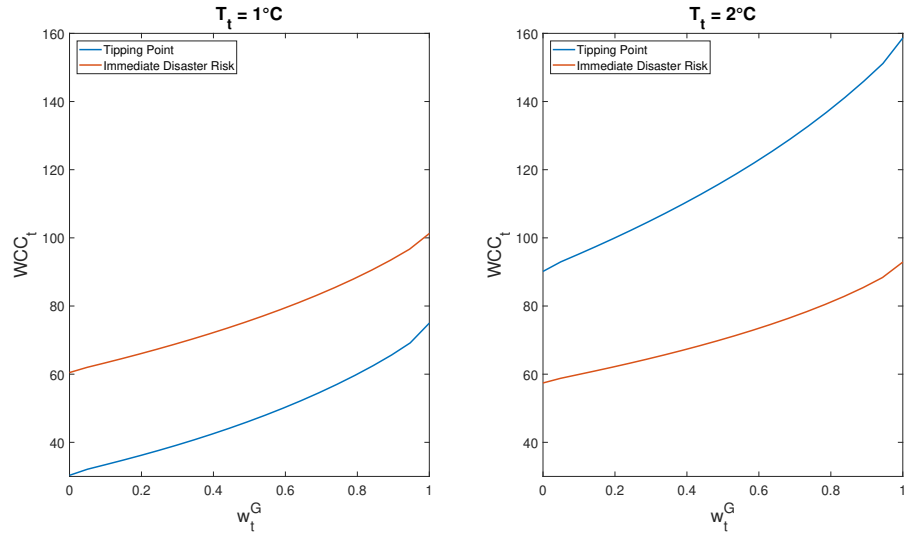

The figure plots the welfare cost of carbon as a function of the wealth share, w_t^G, of the green investor for different levels of temperature, T_t. Results are shown for the case with immediate disaster risk and for the case with the distant tipping threshold.

Figure 16 plots the WCC as a function of the market share of the green investor for the current temperature level of $T_t = 1°\text{C}$ as well as for a global temperature of $T_t = 2°\text{C}$. It shows that the WCC strongly increases with the market share of green investors. Green investors believe in a larger impact of temperature increases on the probability of a climate-induced disaster. Hence, their utility increases more strongly in response to a reduction in temperature compared to that of brown investors. This effect is particularly strong once global temperature approaches the tipping point. For $T_t = 2°\text{C}$, the WCC is significantly larger for the model with the distant tipping point compared to the immediate disaster risk model and, in particular, the difference increases with the wealth share of the green investor. Hence, the welfare gains from policies to slow down climate change are going to increase if the market share of green investors keeps on increasing in the future.

Using the insights from Figures 14 and 16, we can also analyze the impact of (bad) news about climate change on the welfare cost of carbon. When bad news about climate change is interpreted as an unexpected increase in temperature, as done in Section 4.5, such news have two effects on the WCC. The direct, first-order effect is an increase in the WCC if the tipping threshold has not been reached yet, as the WCC increases with temperature below the tipping point. Additionally, the unexpected shock to temperature increases the wealth share of the green investors, as they hedge against these states. Since the WCC also increases with the wealth share of the green investors, this second-order effect leads to a further increase in the WCC.

Having an exogenous increase in the market share of the green investor would also increase the WCC. This increase in the WCC can be motivated by an increased awareness of the population about the impact of climate change on future economic growth, leading to a higher willingness to pay to slow down climate change. For example, using survey evidence provided by Howe et al. (2015), who find that the fraction of people who believe that climate change will significantly harm future generations has increased from 58% in 2014 to 64% in 2021, this alone would imply an increase in the WCC from approximately \$49 to \$52, assuming T_t is held constant at 1°C.

4.7 Individual Welfare Cost of Carbon

In the previous section, the (aggregate) welfare cost of carbon was computed via the elasticity of the aggregate wealth–consumption ratio to temperature. Instead, we could also re-write the welfare cost of carbon as the (by consumption share) weighted individual welfare cost of carbon of the two agents. In Section C we show that the aggregate WCC is then given as a function of the individual wealth–consumption ratios by:

$$WCC_t = \frac{\psi}{\psi - 1} s_t^G \frac{-\partial log Z_t^G}{\partial E_t} C_t + \frac{\psi}{\psi - 1} s_t^B \frac{-\partial log Z_t^B}{\partial E_t} C_t, \tag{24}$$

with $Z_t^h = \frac{W_t^h}{C_t^h}$ being the individual wealth–consumption ratio of investor h.

Figure 17 shows the individual WCC for the green and brown investor, along with the aggregate WCC in an economy where both agents hold a wealth share of 50%. The aggregate WCC in this case is the same as shown in Figure 14 for the tipping threshold economy. The figure illustrates that as the wealth share of the green (brown) investor increases, the aggregate WCC moves closer to the individual WCC of the green (brown) investor. The individual WCCs for both agents are increasing in temperature before reaching the tipping threshold and declining afterwards. The individual WCC of the green agent is consistently higher than the individual WCC of the brown agent, since her future utility is more affected by higher temperatures. This can also be seen by looking at the individual wealth–consumption ratio of the two agents in Figure 18, where the wealth–consumption ratio of the green investor decreases more in T_t, leading to a corresponding higher WCC for her.

Figure 17: Individual Welfare Cost of Carbon

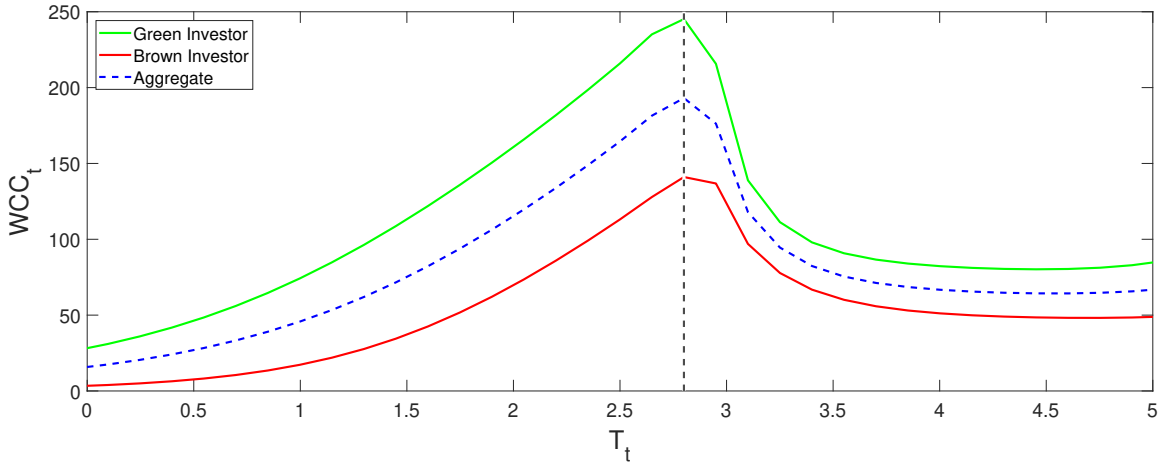

The figure plots the individual welfare cost of carbon for the green and brown investor, along with the aggregate welfare cost of carbon for an economy with $w_t^G = 0.5$, as a function of T_t. Results are shown for the model with the distant tipping threshold. The vertical dashed line marks the tipping threshold.

Figure 18: Individual Wealth–Consumption Ratios

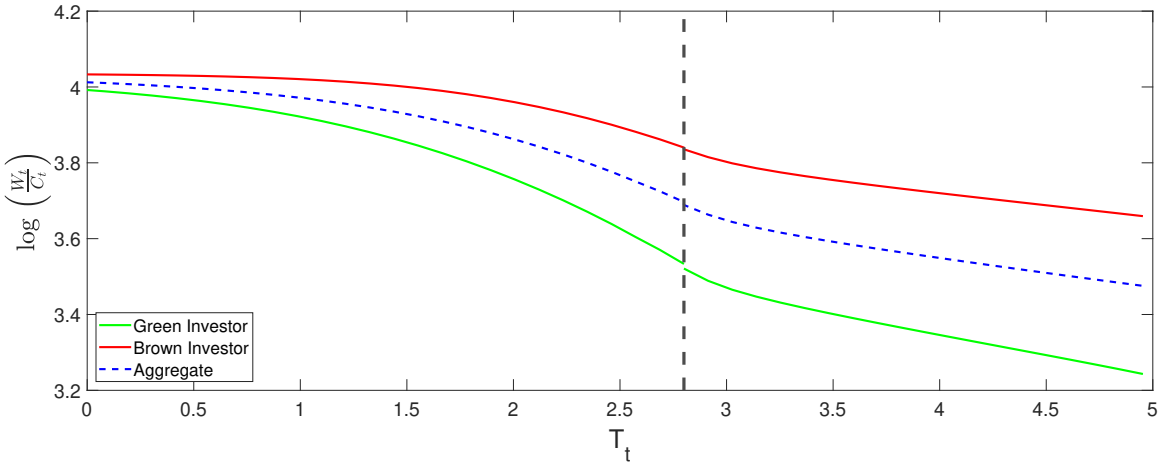

The figure plots the individual log wealth–consumption ratio of the green and brown investor, along with the aggregate log wealth–consumption ratio for an economy with $w_t^G = 0.5$, as a function of T_t. Results are shown for the model with the distant tipping threshold. The vertical dashed line marks the tipping threshold.

Figure 19 shows the individual WCC of the green and brown investor, along with the aggregate WCC, as a function of the wealth share of the green investor. Results are shown for the current temperature level of $T_t = 1°\text{C}$, as well as for a global temperature of $T_t = 2°\text{C}$. For $w_t^G = 1$, the individual WCC of the green agent equals the aggregate WCC, and for $w_t^G = 0$, the individual WCC of the brown agent equals the aggregate WCC. The results are cut at the boundaries, as the individual WCC for an investor with a market share of zero is not defined. The aggregate WCC increases with the wealth share of the green agent, while the individual WCC of the brown agent decreases with the wealth share of the green agent and even becomes negative in the left panel. This phenomenon occurs in economies dominated by many green investors and only a few brown investors, which results in a high demand for hedging climate risks, yet the supply of insurance is limited. This observation is evident in the upper-right plot of Figure 5, where the wealth of the brown investor experiences the most significant increase through trading with green investors under such circumstances. In these scenarios, the gains from trade can even outweigh the negative consequences of climate change for future consumption growth for the brown investor. He benefits from climate risks by selling insurance to the green investor. Figure 18 in Appendix A plots the corresponding individual wealth–consumption ratios as a function of wealth. The individual wealth–consumption ratio of the brown agent increases monotonically with the share of w_t^G, with the increase being particularly pronounced as $w_t^G \to 1$, coinciding with the most substantial decrease in the corresponding WCC for these cases.

Figure 19: Individual Welfare Cost of Carbon as a Function of Wealth

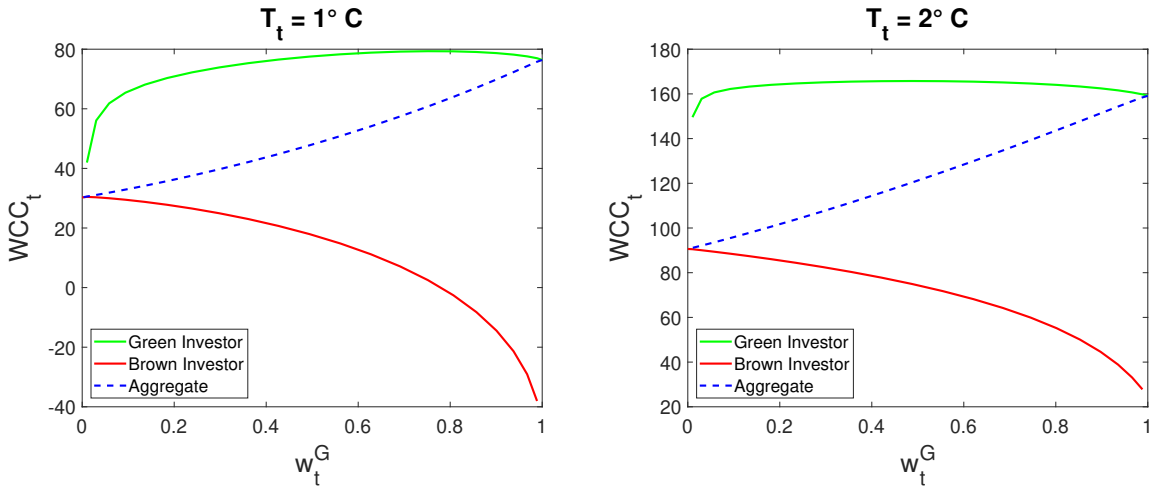

The figure plots the individual welfare cost of carbon for the green and brown investor, along with the aggregate welfare cost of carbon, as a function of the wealth share, w_t^G, of the green investor, for different levels of temperature T_t. Results are shown for the economy with a distant tipping threshold.

4.8 Robustness

In this section we conduct several robustness checks to show that the qualitative conclusions we draw based on our benchmark calibration do not depend on the specific choice of parameters. We consider the following cases: lowering the tipping threshold, changing the degree of disagreement, changing the climate exposure of green and of brown stocks, changing the risk aversion of the investors, changing the disaster size, and changing the long-run mean global temperature. Figures 20 - 22 plot the carbon premium and the WCC as a function of temperature for these different cases. First, consider the case with a lower tipping threshold. A report from the OECD (2022) shows that important tipping points may become "likely" already within the Paris Agreement range of 1.5°C to 2°C of global warming. The possibility that tipping points could already be crossed under moderate levels of global warming adds further urgency to the climate challenge. Hence, we also discuss results for a tipping point of $T_{tipp} = 2.0$°C instead of $T_{tipp} = 2.8$°C as in the benchmark model. All other parameters are kept at the level of the baseline calibration provided in Table 1. The carbon premium plotted in Figure 20 is qualitatively similar to the case with the distant tipping point of 2.8°C with the exception that for low temperature levels it is slightly larger. This larger premium arises as the tipping point is not as far away, so investors demand a higher risk premium for holding more carbon-exposed (brown) stocks. For the WCC plotted in Figure 21 we also find that it is slightly higher for lower temperature levels, as climate disaster risks are a more imminent threat. Otherwise, the results are qualitatively similar to those for the benchmark model.

We also consider cases in which we either change the amount of risk by decreasing the parameters that determine the disaster probabilities (l^B from 0.015 to 0.01 and l^G from 0.03 to 0.02) or by decreasing the climate exposure of the brown stock, k^B, from 3 to 1.5, or change the price of risk by decreasing risk aversion, γ, from 8 to 5. All three cases have similar effects on the carbon premium, leading to a lower premium relative to the benchmark case. However, qualitatively our findings do not change, which also holds for the WCC shown in Figure 21.[22]

We also consider the case in which we increase the mean temperature to $\mu_T = 2.5$°C which has negligible impact on equilibrium outcomes. Finally, we analyze the impact of different disaster sizes on our results. There is not only uncertainty about disaster probabilities after crossing the tipping threshold, but the impact itself of disasters is also unknown. Figure 22 shows that, as expected, the carbon premium increases (decreases) for a higher (lower) disaster size. However, the qualitative implications remain unchanged.

[22]Note that changing k^B does not affect the WCC, which is why we do not consider this case in Figure 21.

Figure 20: Robustness Checks for Carbon Premium

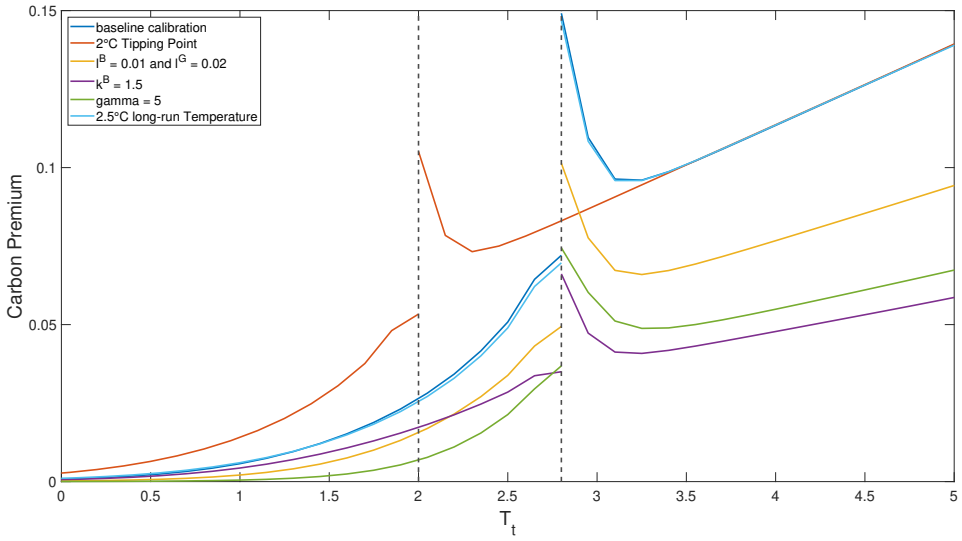

The figure plots the expected return of the brown stock minus the expected return of the green stock for the beliefs of the brown investor as a function of temperature, T_t, for $w_t^G = 0.5$. The dark blue line depicts the case of our benchmark model with parameters provided in Table 1. The red line assumes a lower tipping threshold of $T_{tipp} = 2.0°$ C. The yellow line assumes more moderate beliefs about climate change, with $l^B = 0.01$ and $l^G = 0.02$. The purple line depicts the case with less climate exposure of the brown stock, with $k^B = 1.5$, and the green line shows results for a lower risk aversion of $\gamma = 5$. The light blue line depicts the case with a long-run mean temperature of $\mu_T = 2.5$°C. The vertical dashed lines mark the tipping threshold at 2°C and 2.8°C, respectively.

Figure 21: Robustness Checks for Welfare Cost of Carbon

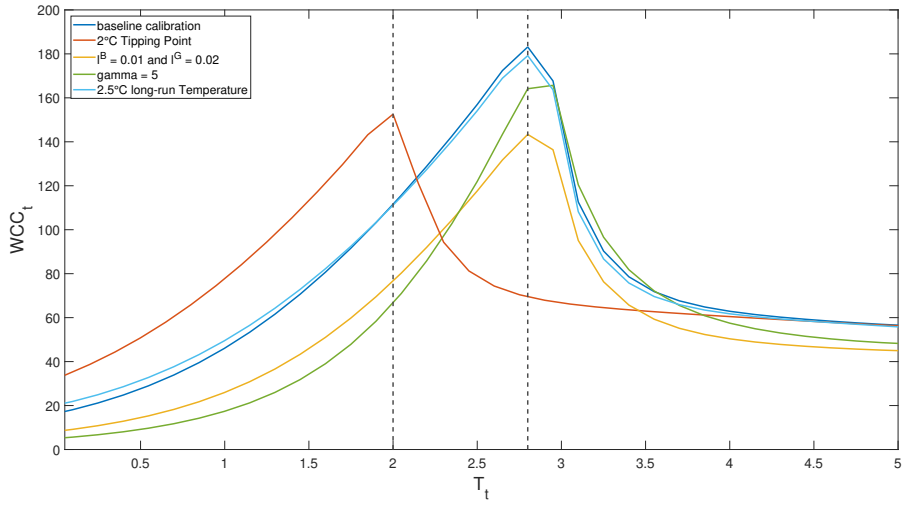

The figure plots the welfare cost of carbon as a function of temperature, T_t, for $w_t^G = 0.5$. The dark blue line depicts the case of our benchmark model with parameters provided in Table 1. The red line assumes a lower tipping threshold of $T_{tipp} = 2.0$°C. The yellow line shows the welfare cost of carbon for more moderate beliefs about climate change, with $l^B = 0.01$ and $l^G = 0.02$, and the green line shows results for a lower risk aversion of $\gamma = 5$. The light blue line depicts the case with a long-run mean temperature of $\mu_T = 2.5$°C. The vertical dashed lines mark the tipping threshold at 2°C and 2.8°C, respectively.

Figure 22: Robustness Checks for different Disaster Size

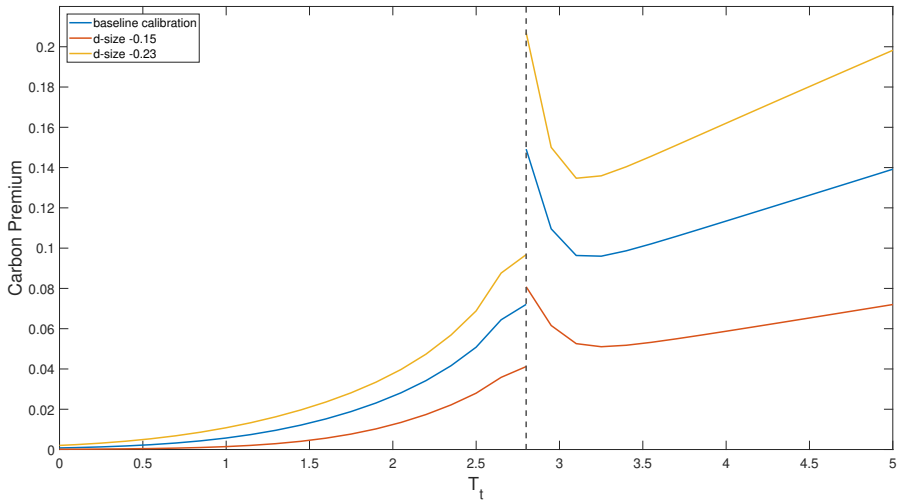

The figure plots the expected return of the brown stock minus the expected return of the green stock for the beliefs of the brown investor as a function of temperature, T_t, for $w_t^G = 0.5$. The blue line depicts the case of our benchmark model with parameters provided in Table 1, especially $d = -0.2$. The red line assumes a lower disaster impact of $d = -0.15$. The yellow line assumes a higher disaster impact of $d = -0.23$. The vertical dashed line marks the tipping threshold.

4.9 Long-Run Simulations

In this chapter we study the long-run equilibrium of our model, specifically examining the dynamics of the wealth share of the two investors over an extensive time horizon spanning several hundred years. Our primary objective is to demonstrate that, based on the baseline calibration and some robustness checks, no investor will be entirely forced out of the market within this extended 500-year period. It's important to note that our emphasis lies on investigating the behavior of the system over this substantial time frame, rather than solely focusing on the traditional $t \to \infty$ scenario typically explored in survival literature.

As shown in Section 3.3, the evolution of consumption shares for investors with Epstein–Zin preferences depends on the interplay of the speculation motive and risk sharing motive. In contrast, for investors with CRRA preferences, only the speculation motive matters. This has important implications for the survival of agents with different beliefs in the long-run. Investors with CRRA preferences only bet on different realizations for the state in the next period, which in our case are different beliefs about the probability of climate-induced disasters. In the long run, only the investors with the (more) correct beliefs will survive, as they bet on the correct states more frequently. This is also known as the classical market selection hypothesis, which was already developed by Alchian (1950) and Friedman (1953). Hence, only the investor with the (more) correct beliefs has an impact on asset prices in the long-run.

The interesting new feature that arises for EZ preferences is the risk sharing channel. Agents are willing to pay a premium to hedge future (long–run) risks. In our case, the brown investor, believing in a lower impact of climate change on future consumption growth, provides insurance for the green agent, who is more concerned about climate change. During normal times–in the absence of climate disasters or unexpected shocks to temperature–this leads to an increased consumption share of the brown investor. Thus, even if the brown investor has the wrong beliefs, he can survive in the long-run and possibly even dominate the economy by collecting the insurance premium from the green investor.

In the following, we demonstrate that for different calibrations, both agents will maintain a significant wealth share in the long-run, and thus, also have an impact on asset prices. Table 4 reports the median, 10%, and 90% quantile paths using 1,000 simulations, each consisting of 200 or 500 years of simulated data, respectively. In the initial period, the wealth is distributed equally among the two investors with $w_0^G = w_0^B = 0.5$. The temperature in the initial period is set to its long-run mean $T_0 = \mu_T = 2°\text{C}$ and evolves according to equation 6 over time. We assume that the green investor holds the true beliefs regarding the probability of a climate-induced disaster, hence $l = l^G$. Consequently, the speculation motive works on average in favor of the green investor. The results for the same exercise, but starting at the current temperature anomaly $T_0 = 1°\text{C}$ instead of at its long-run mean of $T_0 = \mu_T = 2°\text{C}$, are presented in Table 12 in Appendix A.

Table 4: Wealth Shares – Different Simulations

	200 years			500 years		
	10%	median	90%	10%	median	90%
Baseline TP	0.0515	0.1293	0.2325	0.0042	0.0262	0.0896
$T_{Tipp} = 2°C$	0.0415	0.0723	0.1380	0.0023	0.0103	0.0386
$\gamma = 5$	0.1702	0.3014	0.4024	0.0477	0.1265	0.2754
$l^G = 2\%$; $l^B = 1\%$	0.1159	0.2183	0.3204	0.0205	0.0659	0.1730
$d = -0.15$	0.1476	0.2459	0.3436	0.0286	0.0845	0.2070
Imm. Disaster Risk	0.0405	0.0671	0.1108	0.0023	0.0080	0.0231

The table shows the median, 10% and 90% quantiles of the wealth share of the green investor w^G from 1,000 samples – each containing 200 or 500 years of simulated data. The starting distribution is $w_0^G = w_0^B = 0.5$. Temperature at the beginning is $T_0 = \mu_T = 2°C$. Results are shown for different calibrations of the economy. 'Baseline TP' refers to the model calibration presented in Table 1. Additionally, results are also shown for a lower tipping threshold ($T_{Tipp} = 2.0°C$ instead of $T_{Tipp} = 2.8°C$), lower risk aversion ($\gamma = 5$ instead of $\gamma = 8$), lower subjective disaster probabilities ($l = l^G = 0.02$ and $l^B = 0.01$ instead of $l = l^G = 0.03$ and $l^B = 0.015$), a lower impact of disasters ($d = -0.15$ instead of $d = -0.2$) and an immediate disaster risk economy ($T_{Tipp} = 0.01°C$ instead of $T_{Tipp} = 2.8°C$).

Table 4 shows that in all considered cases the wealth share of the brown investor increases over time. This is due to the risk sharing channel as explained in Section 3.3. Note that the speculation motive is only relevant once the tipping threshold is crossed, so for most of the time of the simulations only the risk sharing motive matters. The size of the risk sharing channel increases with the degree of risk aversion of the investors, see equation 15. By lowering the risk aversion from $\gamma = 8$ to $\gamma = 5$, the median wealth share of the green investor increases from 13% to 30% after 200 years, and from 3% to 13% after 500 years, since she pays less to insure against climate risks.

Table 4 also reports several other robustness checks for the evolution of the wealth shares over time. For a lower tipping threshold of $T_{Tipp} = 2.0°C$ instead of $T_{Tipp} = 2.8°C$, the wealth shifts even faster to the brown investor on average, as climate disaster risks are a more imminent threat. A closer tipping threshold increases the chance of passing it in a given interval of time, and hence, increases the demand for hedging against theses states. This drives down the median wealth share of the green investor to 7% after 200 years (compared to 13% with $T_{Tipp} = 2.8°C$) and only 1% after 500 years (compared to 3% with $T_{Tipp} = 2.8°C$).

The intuition behind the two next robustness checks is similar: both, a decrease in the subjective disaster probabilities as well as a decrease of the disaster impact lowers the demand for hedging against these states. Hence, in both of these scenarios, the wealth share of the

green investor decreases less over time compared to the baseline scenario.

Finally, we consider the evolution of the wealth shares in the immediate disaster risk economy. In this case, the disaster probability is positive in each period of the simulation, so according to equation 15, the dynamics of the consumption shares do not only depend on the risk sharing channel but also on the speculation motive in each period of the simulation. On average, the speculation motive works in favor of the green investor in the long-run, since we assume that she holds the correct beliefs about the disaster probabilities ($l = l^G$). However, the wealth share of the brown investor increases even faster in this case compared to the tipping point case, so the risk sharing motive clearly dominates the speculation motive here. The demand for risk sharing already increased when lowering the tipping threshold from 2.8°C to 2°C, and further increases when lowering the disaster threshold further to 0.01°C.

While we do not focus on the equilibrium at the limit here ($t \to \infty$), we conducted some tests for the baseline economy and found that in the (very) long-run, the wealth share of the green investor vanishes. Given the simulation above, after 1,000 years of simulation her mean wealth share declines to $w^G_{1000} = 0.0032$. After 2,000 years of simulation, the median wealth share further declines to $w^G_{2000} = 2.3716\text{e-}5$, and after 10,000 years of simulation it declines to $w^G_{10000} = 1.9618\text{e-}7$.

5 Numerical Solution

In this section, we describe the solution methods employed to solve our baseline-model: a long-run risk asset-pricing model incorporating disasters with heterogeneous agents and recursive preferences. Since there are–to the best of our knowledge–no closed-form solutions for this model framework available, we rely on a numerical solution approach as proposed in Pohl et al. (2018). This approach is based on projection methods to approximate for the equilibrium functions. We also give a brief introduction to collocation methods and Gauss-Hermite quadrature in general, but focus on its application for our model framework. For a more comprehensive discussion of projection methods used to solve asset-pricing models, interested readers can refer to Pohl et al. (2018).

To simplify notation, the subsequent procedures are described for the two-agent economy presented in Chapter 3 and a single state variable $y_t \in \mathbb{R}^1$, representing the temperature state T_t in our model. The described approach can be extended analogously to the general case involving more than two agents and multiple states. As proposed by Pohl et al. (2021), we solve the social planer's problem using a collocation projection. This involves reformulating the equilibrium into an alternative representation involving functions of the state variables on our state space. To simplify notation further, the current exogenous state of the economy will be denoted by T and the subsequent state in the next period by T'. Analogously, the current endogenous state of the Negishi weight is denoted by λ and the the corresponding state in the subsequent period by λ', within the bounded state space $\Lambda \in (0, 1)$. In the following, we will write the equilibrium conditions as a function of λ^B. Remember, that we have normalized the Negishi weights, so once we solve for λ^B, we can directly calculate λ^G, using the equation $\lambda^G = 1 - \lambda^B$.

We use a piecewise-linear approximation for the value functions of the two agents $v^h(\lambda, T)$, with $h \in \{B, G\}$. The approximated value functions are then denoted by $\hat{v}^h(\lambda, T)$. We tested different interpolation methods to handle the discontinuity around the tipping threshold, and piecewise-linear approximation turned out to deliver the best approximations for values close to the tipping threshold. For the model with immediate disaster risk, the value functions can also be interpolated using other methods, such as cubic splines, with high accuracy. The results presented below use piecewise-linear interpolation for both models, since they are faster to compute and deliver sufficiently accurate results as we show. This way, we can also directly compare the accuracy of the case with a tipping threshold and without. The primary aim of this section is not to achieve the highest level of accuracy possible in our solution. Instead, our focus is on showcasing the sufficient accuracy of our solution method and demonstrating the numerical robustness of all our economic outcomes even when we increase the number of collocation nodes further.

To compute the expectations over the i.i.d. shocks in our model, we rely on Gauss-

Hermite quadrature, a powerful numerical integration method. By strategically placing sample points (quadrature nodes) at the specific roots of Hermite polynomials and leveraging the weighting mechanism of the Gaussian probability distribution, Gauss-Hermite quadrature excels in accurately estimating expectations. This makes this method particularly well-suited for handling expectations over independent and identically distributed (i.i.d.) shocks with remarkable efficiency.[23]

For the collocation projection, we need to select a set of collocation nodes at which we evaluate $\hat{v}^h(\lambda, T)$. For the Negishi weights, we choose a vector of length n_l ($\{\lambda_a\}_{a=1}^{n_l}$) and for the temperature state, we use a vector of length n_T ($\{T_b\}_{b=1}^{n_T}$). Altogether, we have a matrix with $n_l \times n_T$ collocation nodes for which the equilibrium conditions need to hold.

The Negishi weight of the subsequent period λ' and the value function of the next period v' are given by a vector of size $n_l \times n_T \times n_{GHT} \times n_D$, where '$n_l$' denotes the number of collocation nodes for λ, 'n_T' denotes the number of collocation nodes for T, 'n_{GHT}' denotes the number of quadrature nodes for the i.i.d. temperature shock and 'n_D' represents the number of states for the Poisson counting process over which we compute the expectations. Note that the dynamics of the Negishi weights are independent of the realization of the i.i.d. shock η_{t+1} in the consumption process. As a result, the corresponding quadrature can be computed in a separate step instead of being solved together with the equilibrium conditions each time, to save computing time.

5.1 Collocation Projection Approach

We showed in Section 3.2 that the dynamics of the Negishi weights depend on the value functions (9) of the two investors, which in turn depend on the consumption decisions (10). Hence, we need to jointly solve for the value functions v^h of the two investors and the dynamics of the equilibrium Negishi weights λ. We do this in a two step procedure.

Step 1: Computing Optimal Consumption Allocations

In the first step, we compute the optimal consumption allocations in equilibrium. The transformation from Negishi weights to individual consumption shares is necessary, since the individual value functions v^h depend on the consumption shares. We see that the consumption decisions today – as given by equations (10) and (11) – depend only on the current endogenous state λ_t and can be solved independently of the utility functions and the dynamics of the Negishi weights next period. Equation (10) has to hold at each collocation node $\{\lambda_a\}_{a=1}^{nl}$.

[23] For a more extensive review of numerical integration methods in economics, we refer the interested reader to Judd (1998).

Together with the market-clearing condition we get

$$\lambda_a^B(1-\delta)(s_a^B)^{\rho-1} = (1-\lambda_a^B)(1-\delta)(1-s_a^B)^{\rho-1}. \tag{25}$$

Since the agents share the same preference parameters, we can reformulate this condition and get a closed-form solution for the consumption share of the brown agent [24]:

$$s_a^B = \frac{(\lambda_a^G)^{\frac{1}{\rho-1}}}{(\lambda_a^B)^{\frac{1}{\rho-1}} + (\lambda_a^G)^{\frac{1}{\rho-1}}} \tag{26}$$

We can solve for s_a^B to get the optimal consumption choice for the brown investor at each collocation node. The optimal consumption choice for the green agent, s_a^G is obtained by using the market-clearing condition, thus $s_a^G = 1 - s_a^B$.

Step 2: Solving for the Value Functions and the Dynamics of the Negishi Weights

In a second step, we solve jointly for the value functions of the two agents together with the dynamics of the Negishi weights, hence for equations (9) - (14). The reason we have to solve these equations jointly is that the value functions depend on the dynamics of the Negishi weights – which depend themselves on the utility functions.

The expectation over the exogenous T-state in the subsequent period is computed by a Gaussian quadrature, using n_{GHT} quadrature nodes. The corresponding values for T' at which we need to evaluate v^h are given by the quadrature rule. For the temperature state T, the corresponding quadrature nodes depend on the temperature state today $\{T_b\}_{b=1}^{n_T}$, and are given by $\{T'_{b,c}\}_{b=1,c=1}^{n_T,n_{GHT}}$. The accompanying weights for the Gaussian quadrature are given by $\{w_c\}_{c=1}^{n_{GHT}}$.

Although closed-form solutions exist for the expectation over the Poisson disaster process, we opt for a numerical solution to account for the divergence in beliefs between the two investors regarding the probability of a disaster in the next period. To compute agent h's expectation over the disaster term, the possible number of disasters (x) next period is weighted by the subjective probability π_t^h of each of these states, as given by the probability mass functions from equation (17):

$$E_t^h[D_{t+1}] = E_t^h[N_{t+1}] \cdot d = \sum_{x=0}^{\infty} \frac{(\pi_t^h)^x}{x!} e^{-\pi_t^h} \cdot x \cdot d \tag{27}$$

Theoretically, there is an infinite number of possible disasters to consider, albeit with diminishing probabilities. We show at the end of this chapter how we could choose a cutoff value

[24] We could analogously solve for the consumption share of the green agent first. In the following, we solve all equilibrium conditions for the brown agent.

for the maximum number of disasters x considered, in order to compute an accurate solution while remaining numerical tractability.

We can solve equation (13) for a given pair of collocation nodes $\{\lambda_a^B, T_b\}_{a=1,b=1}^{n_l,n_T}$, the corresponding quadrature nodes $\{T'_{b,c}\}_{b=1,c=1}^{n_T,n_{GHT}}$ and the probability mass function for having x disasters next period, given current temperature T_b. With this input, we compute a vector for $\lambda^{B'}$ of size $n_l \times n_T \times n_{GHT} \times n_D$. [25] For each $\lambda^{B'}_{a,b,c,x}$, equation (13) then reads

$$\lambda^{B'}_{a,b,c,x} = \frac{\lambda_a^B \Pi^B}{(1-\lambda_a^B)\Pi^G + \lambda_a^B \Pi^B},$$

with

$$\Pi^h = \left(\frac{v^h(\lambda^{B'}_{a,b,c,x}, T'_{b,c})}{R^h\left[v^h(\lambda^{B'}, T')e^{\Delta c(N')} | \lambda_a^B, T_b\right]} \right)^{\alpha-\rho} \cdot \frac{dP^h(N'|T_b)}{dP(N'|T_b)}, \tag{28}$$

where

$$R^h\left[v^h(\lambda^{B'}, T')e^{\Delta c(N')} | \lambda_a^B, T_b\right] = G_h^{-1}\left(E\left[G_h\left(v^h(\lambda^{B'}, T')e^{\Delta c(N')} \right) \frac{dP^h(N')}{dP(N')} \middle| \lambda_a^B, T_b \right] \right).$$

Due to the expectation operator, the values of $\lambda^{B'}_{a,b,c,x}$ depend on the entire distribution of $\lambda^{B'}$. We apply the Gaussian quadrature to compute the expectation over the i.i.d temperature-shock and use the probability mass function to compute the expectation over the disaster state next period:

$$E\left[G_h\left(v^h(\lambda^{B'}, T')e^{\Delta c(N')} \right) \frac{dP^h(N')}{dP(N')} \middle| \lambda_a^B, T_b \right] \approx$$
$$\sum_{x=0}^{n_D} \sum_{c=1}^{n_{GHT}} G_h\left(v^h(\lambda^{B'}_{a,b,c,x}, T_{b,c}) \cdot e^{\Delta c(N')} \right) \cdot \omega_c \cdot \frac{(\pi^h(T_b))^x}{x!} e^{-\pi^h(T_b)} \cdot x \cdot d.$$

The collocation nodes $\{\lambda_a^B, T_b\}_{a=1,b=1}^{n_l,n_T}$ together with the quadrature nodes $\{T'_{b,c}\}_{b=1,c=1}^{n_T,n_{GHT}}$ and the maximum number of considered disasters in the Poisson counting process (n_D) determine the values $\lambda^{B'}_{a,b,c,x}$ at which we need to evaluate the value functions v^h. This yields a square system of equations with $n_L \times n_T \times n_{GHT} \times n_D$ unknowns, and as many equations (28) for each point $\{a, b, c, x\}$.

As noted earlier, the value functions are not known and need to be computed in the same step when solving for $\lambda^{B'}_{a,b,c,x}$. By plugging in the approximation $\hat{v}^h(\lambda^B, T)$ into equation (9), the value functions can be described as:

$$\hat{v}^h(\lambda_a^B, T_b) = \left[(1-\delta)(s_a^h)^\rho + \delta R_t^h\left(\hat{v}^h(\lambda^{B'}, T') \cdot e^{\Delta c(N')} \right)^\rho \middle| \lambda_a^B, T_b \right]^{\frac{1}{\rho}}. \tag{29}$$

[25] The vector for $\lambda^{B'}$ depends on the temperature shock as well as on temperature today and the realization of the disaster state: $\{\lambda^{B'}_{a,b,c,x}\}_{a=1,b=1,c=1,x=0}^{n_l,n_T,n_{GHT},n_D}$.

The collocation projection conditions require that equation (29) must hold at each collocation node $\{\lambda_a^B, T_b\}_{a=1,b=1}^{n_l,n_T}$. This yields a square system of equations with $n_L \times n_T$ equations for each agent, resulting in $n_l \times n_T \times 2$ equations and as many unknowns for the linear interpolation at each collocation node. We solve this system of equations jointly with the system for $\{\lambda_{a,b,c,x}^{B'}\}_{a=1,b=1,c=1,x=0}^{n_l,n_T,n_{GHT},n_D}$ described before.

We use the built-in interp-functions of Matlab for the function interpolation, using the interpolation option 'linear'. However, the built-in Matlab function 'interp2', which returns interpolated values of a function of two variables at specific query points using linear interpolation, cannot handle linear extrapolation, so we have to adjust the function accordingly[26]. We could not find any significant performance differences whether we used the solver 'fsolve', 'fmincon' or 'knitro'. All of these were able to solve for the equilibrium conditions described above. We provide the solvers with additional information for the boundary cases. For $\lambda^B = 1$ for example, the brown investor holds all the wealth in the economy. We can compute $v^B(1, T_b)$ in this case in the representative agent economy of the brown agent. The value function of the green agent, $v^G(1, T_b)$, will be zero in this case for all temperature states. The same can be done for the case of $\lambda^B = 0$, which is equal to the solution for the representative agent economy of the green agent.

In the following subsections, we provide details about the accuracy of the numerical solution method. In particular, we show that further increasing the number of collocation nodes does not affect the results. The Euler errors are computed for collocation grids with different numbers and distributions of collocation nodes. Additionally, we control for the number of Gauss-Hermite nodes and the cutoff value for the number of disasters in the next period, for which we compute the expectations. In a first step, we consider the immediate disaster risk model, which is a long-run risk disaster model with immediate disaster risk but without a tipping threshold. Afterward, we show how to adapt the grid to deal with nonlinearities, such as the temperature threshold, and still maintain a sufficient level of accuracy. While the methods presented in this chapter work for long-run risk models including disasters and heterogeneous agents in general, the specific choice of the grids and the reported errors refer to the baseline calibration presented in Chapter 4.1.

The collocation grids which are compared in the following contain two states: the endogenous Negishi-weight λ_t^B, and the current temperature anomaly T_t. To solve the model numerically, we need one additional dimension to compute the expectation for each i.i.d. shock. In the baseline-model presented in Section 3 are two i.i.d. shocks: one shock enters into the equations for consumption growth (1) and dividend growth (7) and the other shock affects the dynamics of temperature (6). Note that η in the equations for consumption and dividend growth represents the same shock, but is scaled by the leverage parameter Φ in the

[26] For the Matlab function 'interp1' instead, which returns interpolated values of a 1-D function at specific query points using linear interpolation, Matlab has a built-in option for extrapolation.

latter, as consumption and dividend growth are correlated. As a consequence, we only need one quadrature to compute the expectations over this shock. In addition to the two dimensions for the normally distributed shocks, we need an extra dimension to compute the expectations over the expected value of the climate-induced disasters. Hence, the largest matrices to work with in this model will be 5-dimensional of size $n_L \times n_T \times n_{GHT} \times n_{GHC} \times n_D$.

Table 5: Cumulative Subjective Disaster Probabilities

	$T_t = 0$	$T_t = 1$	$T_t = 2$	$T_t = 3$	$T_t = 4$	$T_t = 5$
$P(x = 0\|T_t)$	0	0.9704	0.9418	0.9139	0.8869	0.8607
$P(x \geq 1\|T_t)$	0	0.0296	0.0582	0.0861	0.1131	0.1393
$P(x \geq 2\|T_t)$	0	4.4110e-4	0.0017	0.0038	0.0066	0.0102
$P(x \geq 3\|T_t)$	0	4.4000e-6	3.4418e-5	1.1359e-4	2.6328e-4	5.0286e-4
$P(x \geq 4\|T_t)$	0	3.2950e-8	5.1472e-7	2.5441e-6	7.8506e-6	1.8714e-5
$P(x \geq 5\|T_t)$	0	1.9750e-10	6.1642e-9	4.5656e-8	1.8765e-7	5.5858e-7
$P(x \geq 6\|T_t)$	0	9.8683e-13	6.1553e-11	6.8336e-10	3.7423e-9	1.3914e-8

The table shows the cumulative subjective probability for the green agent that the number of disasters next period is greater or equal to x, given the current temperature T_t: $P^G(N_{t+1} \geq x|T_t)$. Values are shown for the immediate disaster risk case. In the tipping point case, it holds that $P^h(N_{t+1} = 0|T_t < T_{Tipp}) = 1$. After passing the tipping threshold, the probabilities are the same as in the immediate disaster risk case.

As mentioned earlier, in theory, the possible number of disasters over which we have to compute expectations is infinite, with the probability of multiple simultaneous disasters declining as we consider more disasters per period. Table 5 denotes the cumulative disaster probabilities for having at least x disasters next period, as a function of the current temperature anomaly. The numbers are computed for the beliefs of the green agent. Assuming a current temperature anomaly of approximately 1°C for example, it is even in the immediate disaster risk case very unlikely to have more than one disaster next period. For the tipping threshold economy, the disaster probability is zero anyways below the temperature threshold. Although the current temperatures are far from reaching 5 degrees global warming, these are the most extreme cases that require accurate solving using our global approximation method. Having a 5°C world, the probability of having more than 2 (3) disasters next period is in the order of 5e-4 (1.9e-5). We will show in the following that cutoff values in this range are sufficient to solve numerically accurate for the Poisson disaster process. Note that all values in Table 5 are computed using the subjective beliefs of the green investor. Since $l^B < l^G$, the chance of having multiple disasters within a period is even smaller for the subjective beliefs of the brown investor.

5.2 Accuracy: Immediate Disaster Risk Model

In this chapter, we present the numerical errors for different collocation grids in the immediate disaster risk case, and show how the number of collocation nodes impacts the accuracy of the results. After choosing the collocation nodes, we vary the number of quadrature nodes and the cutoff value for the maximum length of the disaster state to ensure that these do not change the results. The numerical errors (Euler errors) are computed using a 100×100 uniform grid[27] for the two states of the model: the exogenous temperature state T_t and the endogenous Negishi weight λ_t^B. We report the errors for the value functions (9) of the two agents and the error in the dynamics of the equilibrium conditions (13) for different grid sizes. In a second step, we investigate whether these errors have a relevant economic impact on our results. To do so, we analyze how the asset pricing moments of interest and the WCC change with different approximation degrees.

All collocation grids for the immediate disaster risk model are uniformly distributed in both dimensions. While the equilibrium conditions depend on the Negishi weights, the value function, wealth–consumption ratio and price–dividend ratio depend on the corresponding consumption shares. As shown in Section 3.2, consumption shares and Negishi weights are linked together via the following equation:

$$\frac{\lambda_t^G}{\lambda_t^B} = \left(\frac{s_t^G}{s_t^B}\right)^{\frac{1}{\psi}}.$$

For $\psi > 1$, a uniform distribution of λ implies that the corresponding consumption shares are concentrated more heavily on the boundaries of the state space. This effect gets stronger, the higher the value for ψ is chosen. In the special case of $\psi = 1$, it holds that $s_t^G = \lambda_t^G$. Figure 23 shows the mapping between λ^G and s^G for $\psi = 1.5$, as in our baseline calibration computed for $n_l = 45$ collocation nodes. We also tested collocation grids that are uniformly distributed with respect to the consumption shares, i.e. choosing a uniform distribution of s_t^B, and then computing the corresponding Negishi weights to solve for the equilibrium. While a uniform λ^B-distribution was numerically more stable in computing the equilibrium conditions, a uniform s^B-distribution delivered better results when solving for the wealth–consumption and price–dividend ratio. For the rest of this section, whenever we mention 'uniformly distributed,' it pertains to the uniform distribution in the λ-dimension.

[27] We also checked errors for some collocation grids on a 200×200 grid. However, since the differences were marginal and computing the numerical errors on a 200×200 grid takes four times more computing time compared to a 100×100 grid, we report the errors for the 100×100 grids.

Figure 23: Mapping between Negishi Weights and Consumption Shares

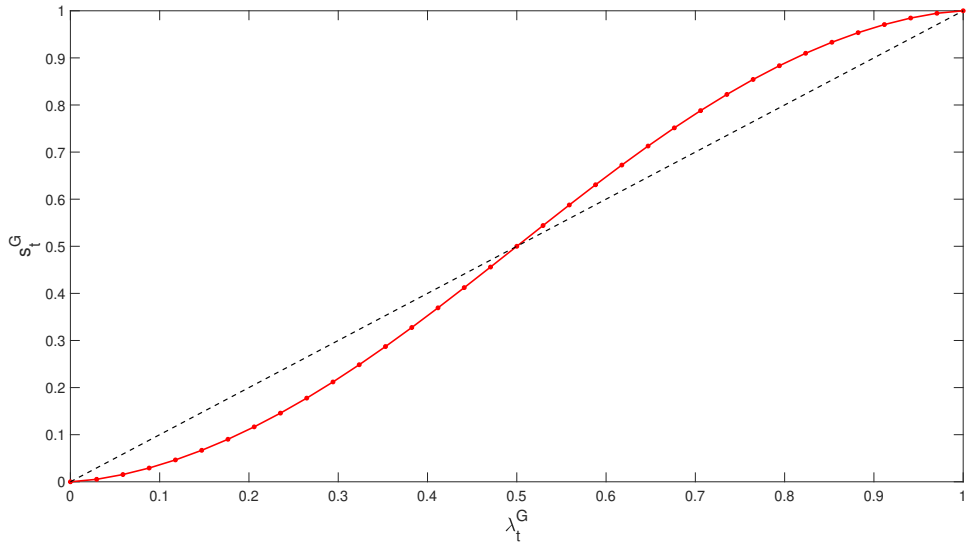

The figure plots the consumption share, s_t^G, of the green investor as a function of her Negishi weight, λ_t^G. The dashed lines mark the 45-degree line. Values are computed for $\psi = 1.5$, as in the baseline calibration. The dots mark the collocation nodes for $n_l = 45$.

Table 6 shows the root-mean-square errors (RMSEs) and the maximum absolute errors (MAEs) in the value functions (9) as well as in the equilibrium conditions of the Negishi weights (13). Errors are reported on a state grid covering ±3 standard deviations around the unconditional long-run mean of T, which is approximately from -1 to 5°C. We set the disaster probability to zero for all $T_t < 0$, to avoid negative disaster probabilities according to equation (5).[28] A different way to deal with negative disaster probabilities is to exclude the possibility of negative temperature values, i.e. set $T_{min} = 0.01$°C as a lower bound for the T-dimension of the state space. Using the latter approach, we could avoid nonlinear behavior around 0°C. Outside of that area, it would not affect the approximation results, as can be seen in Figure 26. Since the errors are largest around zero degrees (see Figure 24 and 25), solving a model with a lower bound of $T_{min} = 0.01$°C would decrease the approximation errors. We show the respective approximation errors in Appendix A (Table 13) for some collocation grids with $T_{min} = 0.01$, but focus the discussion in the following on the model that is solved on a state space from -1 to 5°C, using different collocation grids.

We exclude all error terms for $\lambda_t^{B'}$ values, for which the corresponding T'-value is outside of the collocation grid. The reason to exclude these errors is that the main focus of the analysis lies on the errors and accuracy of the results within the collocation grid. Given that the errors at the boundaries are considerably large and depend on extrapolation, they could potentially

[28] Technically, we set the tipping threshold to 0.01°C in the immediate disaster risk case.

skew the accuracy statistics. For the Negishi weights, the full state space is included between 0 and 1. We observe that for $n_l = 15$ and $n_T = 30$, the errors in the value functions of the two agents are already small with a maximum absolute error of 0.001 and 0.0012, respectively. By increasing the approximation degree further, there are small improvements in the accuracy of the value functions. The maximum error in the Negishi weights, however, can be reduced by roughly a factor of three from 0.0116 to 0.0043, by increasing the approximation degree to $n_l = 35$ and $n_T = 35$. We argue that this approximation degree is already sufficient for our model statistics.

Table 6: Numerical Errors – Immediate Disaster Risk Case

		v_t^G		v_t^B		$\lambda_t^{B'}$		$E[\lambda_t^{B'}]$	
n_l	n_T	RMSE	MAE	RMSE	MAE	RMSE	MAE	RMSE	MAE
15	20	4.215e-4	0.0021	4.237e-4	0.0020	6.936e-4	0.0117	2.665e-4	0.0030
15	30	2.101e-4	0.0010	2.256e-4	0.0012	6.780e-4	0.0116	2.416e-4	0.0030
15	35	1.587e-4	8.661e-4	1.764e-4	0.0012	6.759e-4	0.0116	2.379e-4	0.0030
15	55	8.754e-5	7.736e-4	1.118e-4	0.0012	6.719e-4	0.0116	2.336e-4	0.0029
25	35	1.502e-4	8.021e-4	1.572e-4	9.544e-4	6.617e-4	0.0069	1.684e-4	0.0016
35	35	1.506e-4	7.819e-4	1.560e-4	9.324e-4	5.598e-4	0.0043	1.389e-4	0.0011
45	45	5.627e-5	4.194e-4	6.304e-5	4.475e-4	6.975e-4	0.0076	1.207e-4	9.562e-4

The table shows root-mean-square errors (RMSEs) and maximum absolute errors (MAEs) in the value functions and equilibrium conditions for the Negishi weights for different numbers of collocation nodes for the immediate disaster risk model. Errors are reported for a state grid of ± 3 standard deviations around the unconditional mean of T_t. For λ_t^B the full grid between 0 and 1 is used. We denote the number of collocation nodes for the λ_t^B-dimension by n_l and the number of collocation nodes for the T_t-dimension by n_T. Errors are computed on a grid of size 100×100.

Figure 24 shows the numerical errors in the two value functions for a uniform grid with 35 collocation nodes in the λ^B- and T_t- dimension. The most substantial approximation errors occur in the area close to the 'hypothetical' tipping threshold of 0.01°C. However, even in this area, the value functions are computed with high accuracy with a maximum absolute error of 7.819e-4 and 9.324e-4 for the two agents.

For the dynamics of the Negishi weights, the maximum absolute error is orders of magnitude larger. Since $\lambda_t^{B'}$ is 4-dimensional of size $n_l \times n_T \times n_{GHT} \times n_D$, Figure 25 shows the errors for a zero-shock in temperature ($\sigma_\zeta \zeta_{t+1} = 0$) and different number of disasters next period. The plots for different positive or negative shocks to temperature can be found in Appendix A (Figure 37). The approximation is most inaccurate at the borders of the state grid. We see in all three subplots that the errors are largest when λ^B is close to the boundaries of the state

Figure 24: Numerical Errors in the Value Functions – Immediate Disaster Risk Case

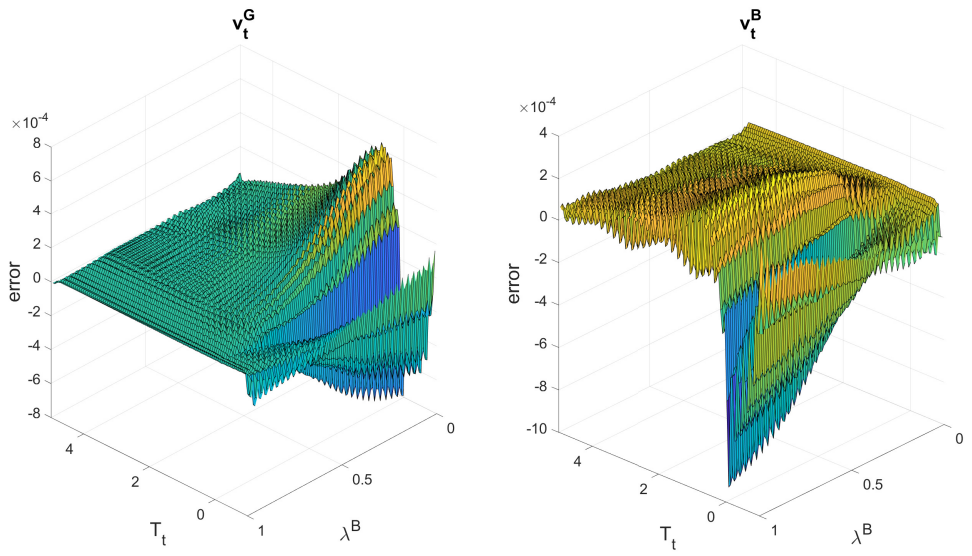

The figure plots numerical errors in the value functions for the two agents in the immediate disaster risk case. Errors are reported for a state grid covering ±3 standard deviations around the unconditional mean of T_t. For λ_t^B the full grid between 0 and 1 is used. The projection method uses a 35×35 uniform grid for the λ^B- and T_t- dimension. Numerical errors are computed on a 100×100 uniform grid.

space, hence, when λ^B gets close to 0 or 1. For the states covering a disaster next period, it can be seen that the errors are larger for positive temperatures, since the disaster probability is zero for negative temperatures. Since our economic analysis focuses on economies that are inhabited by a significant share of both investors, the economic impact of the errors at the boundaries of the λ-space should be limited.

All values in Table 6 are computed using $n_{GHC} = 3$, $n_{GHT} = 7$ and $n_D = 4$[29]. In Table 7, we demonstrate that the number of nodes chosen for the Gauss-Hermite quadrature and the cutoff value for the expectation over the disaster term are sufficient. Generally, a larger number of quadrature nodes increases the accuracy of the approximation, but at the same time increases the computation time needed to solve the model. For this reason, our objective is to determine the minimum number of quadrature nodes required, while ensuring that any further increase in the number of nodes has only a marginal impact on the accuracy of the results. Table 7 reports the effect of increasing the number of Gauss-Hermite nodes compared to the baseline grid. The distribution of the i.i.d. consumption shock can be approximated with high accuracy by using only 3 Gauss-Hermite nodes. Using 5 Gauss-Hermite nodes instead would not affect the results. The i.i.d. temperature shock is approximated using 7

[29]This refers to a cutoff value of $x = 3$, as $x = 0$ also counts as a state.

Figure 25: Numerical Errors in the Negishi Weights – Immediate Disaster Risk Case

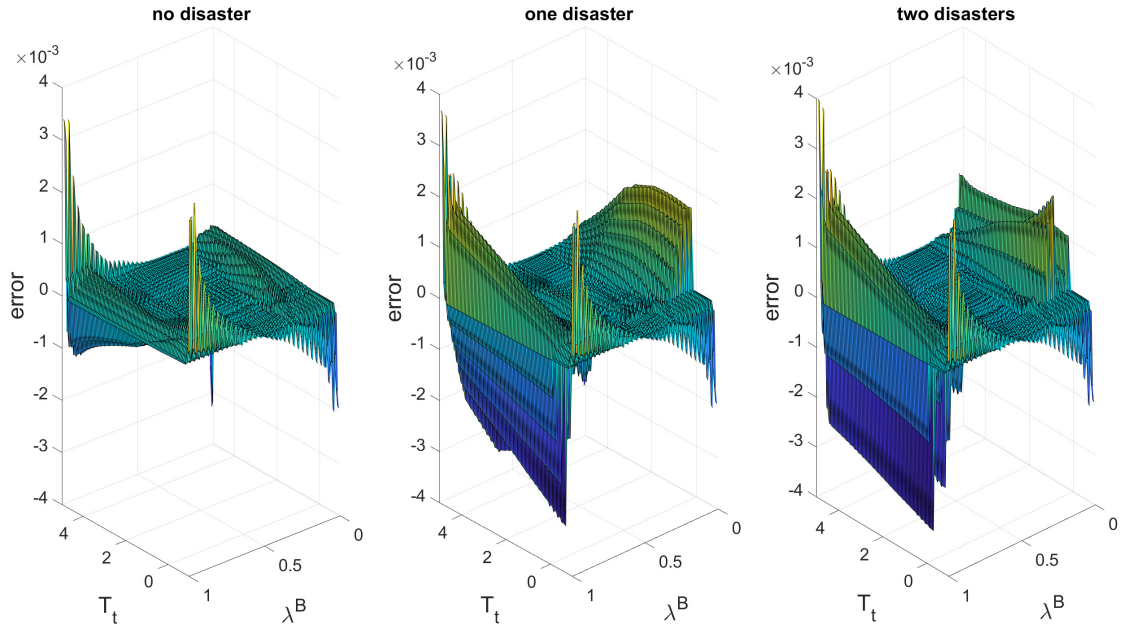

The figure plots numerical errors in the dynamics of the Negishi weights for a different number of disasters next period in the immediate disaster risk case. The i.i.d. temperature shock is set to zero ($\sigma_\zeta \zeta_{t+1} = 0$). Errors are reported for a state grid covering ± 3 standard deviations around the unconditional mean of T_t. For λ_t^B the full grid between 0 and 1 is used. The projection method uses a 35×35 uniform grid for the λ^B- and T_t- dimension. Numerical errors are computed on a 100×100 uniform grid.

Gauss-Hermite nodes. Changing to 9 nodes would only have a marginal effect on the errors. The expectation over the disaster impact is already approximated with high accuracy using a cutoff value of 3, which itself has only very little difference to a higher cutoff value of 4.

Table 7: Robustness Numerical Errors – Immediate Disaster Risk Case

	v_t^G		v_t^B		$\lambda_t^{B'}$	
	RMSE	MAE	RMSE	MAE	RMSE	MAE
baseline	1.5058e-4	7.8186e-4	1.5598e-4	9.3240e-4	5.5975e-4	0.0043
$n_{GHC} = 5$	1.5058e-4	7.8186e-4	1.5598e-4	9.3240e-4	5.5975e-4	0.0043
$n_{GHT} = 9$	1.5231e-4	8.0383e-4	1.6127e-4	9.5582e-4	5.7180e-4	0.0048
$N_{max} = 4$	1.5041e-4	7.8096e-4	1.5596e-4	9.3239e-4	5.6396e-4	0.0047

The table shows root-mean-square errors (RMSEs) and maximum absolute errors (MAEs) in the value functions as well as the equilibrium conditions for the Negishi weights for a different number of Gauss-Hermite nodes and a different cutoff value for the disaster state. Errors are reported for a state grid covering ±3 standard deviations around the unconditional mean of T_t. For λ_t^B the full grid between 0 and 1 is used. The number of collocation nodes for the λ_t^B-dimension and for the T_t-dimension is given $n_l = n_T = 35$. Errors are computed on a grid of size 100×100.

.

Finally, we conduct two exercises to analyze the economic significance of the numerical errors. As noted before, the errors are largest at the boundaries of the collocation grid and around $T_t = 0.01$°C. However, these are not the states on which we focus in our economic analysis, since we assume that the belief disagreement about climate change will not be resolved in the near future. Instead, we assume that we will have a significant share of green as well as brown investors over the next decades, which is also the result of the simulations shown in Section 4.9. Also, given a current temperature anomaly of around 1.2°C and its high persistency, we argue that (without geo-engineering) global warming will not be reversed to preindustrial levels in the near future. We show the impact of the numerical errors on asset prices by running a simulation over 100 years, starting at a temperature of $T_0 = 1$°C. At the beginning, both agents have an equal consumption share, hence $s_0^G = s_0^B = 0.5$. We run this simulation 100 times for several collocation grids and report selected mean annualized asset-pricing moments from these simulations in Table 8.[30] At the end of the simulation, the mean consumption share of the brown agent is $s_{100}^B = 0.75$ and mean temperature at the end is $T_{100} = 1.45$°C.

[30]Table 14 in Appendix A shows the corresponding price–dividend ratio from the simulations for the green stock, brown stock, and the market portfolio.

Table 8: Annualized Asset-Pricing Moments – Immediate Disaster Risk Case

n_l	n_T	$\log(R_t^M)$	$\sigma(\log(R_t^M))$	$\log(R_t^G)$	$\sigma(\log(R_t^G))$	$\log(R_t^B)$	$\sigma(\log(R_t^B))$
15	20	0.0410	0.0642	0.0351	0.0588	0.0621	0.1258
15	55	0.0404	0.0654	0.0347	0.0594	0.0607	0.1308
35	35	0.0406	0.0655	0.0349	0.0597	0.0609	0.1298
45	45	0.0408	0.0650	0.0352	0.0594	0.0616	0.1273

The table reports selected annualized asset-pricing moments for different approximation degrees for the green stock, brown stock, and the market portfolio in the immediate disaster risk model. Moments are computed by simulating 100 sample paths each containing 100 years of data. We set $T_{start} = 1.0$°C and $w_{start}^G = 0.5$. The number of collocation nodes for the λ_t^B-dimension is denoted by n_l and the number of collocation nodes for the T_t-dimension by n_T. Shocks to temperature, ζ_{t+1}, are drawn from a standard normal distribution, and no exogenous shocks are added.

The differences in the returns for different grids are relatively small and do not significantly impact the economic interpretation of the model outcomes. The model economy produces a significant carbon premium over the simulation period, as brown stocks outperform green stocks during normal times. The return of the market portfolio lies somewhere in between, reflecting the climate risk exposure that is also between that of green and brown stocks. However, the simulation does not cover the whole state space as can be seen in Figure 32 in Appendix A. To demonstrate the accuracy of our solution for much higher and lower temperature states, we show the carbon premium as well as the welfare cost of carbon for a temperature space from -1 to 5°C in an economy with $w^G = w^B = 0.5$ in Figure 26. While there are some differences observed when using a 15×20 collocation grid, the results show a convergence when comparing grids of 15×35 and 35×35.

The green line in Figure 26 shows the respective economy with a lower limit to the temperature state space, hence setting $T_{min} = 0.01$°C. The effect is very limited for the carbon premium. For the welfare cost of carbon instead, the difference is significant around $T_t = 0$°C but the results converge around $T_t = 1$°C. This difference can be explained since the marginal gain of reducing temperature is higher in a world in which negative temperatures are possible, compared to a world in which negative temperature values are not possible, and hence, the disaster probability will always be positive. While we show in the main part of our paper results for an immediate disaster risk model with a lower bound to temperature of 0.01°C to get a monotone declining welfare cost of carbon, all other results are robust to that assumption.

In Appendix A, we show the corresponding figures closer to the λ-dimension boundaries within the state space. Specifically, Figure 39 shows the carbon premium and WCC for an economy with $w_t^G = 0.05$ and for an economy with $w_t^G = 0.95$. The carbon premium remains

relatively consistent across different approximation degrees, displaying only minimal variation. In the WCC plot, there is a slight distinction between the 15×20 grid and the larger grids, all of which ultimately converge near 1°C.

Figure 26: Carbon Premium and Welfare Cost of Carbon for different Collocation Grids – Immediate Disaster Risk Case

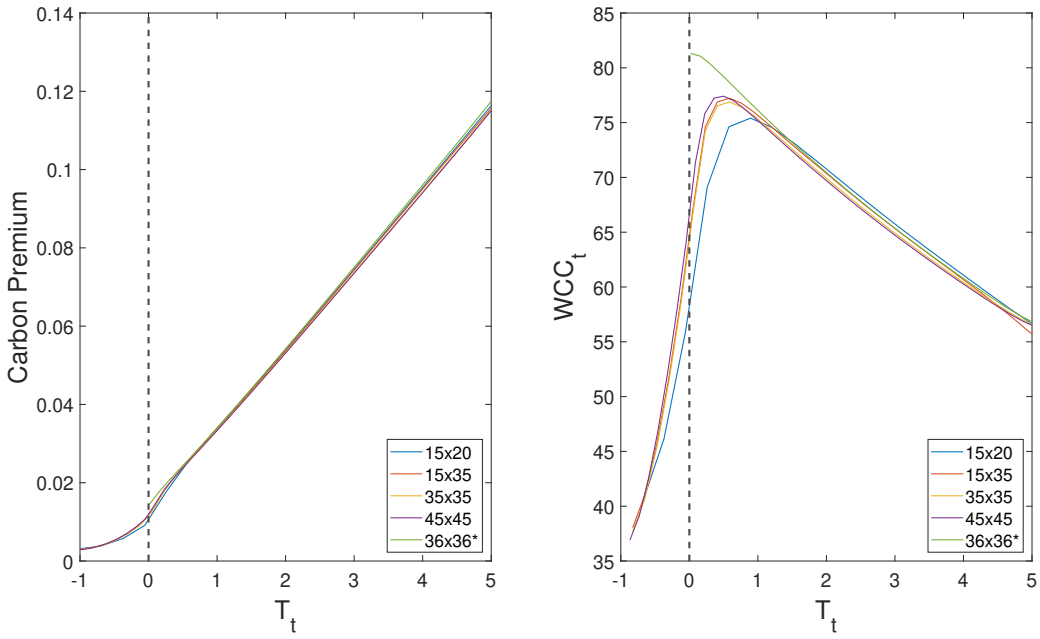

The figure plots the carbon premium and the welfare cost of carbon for different collocation grids. The four grids without an asterisk cover a T-space from approximately -1 to 5°C, while the grid with an asterisk (green line) refers to the collocation grid with a lower boundary of $T_{min} = 0.01$°C. Results are shown for an economy with $w_t^G = 0.5$. The vertical dashed line marks 0°C.

5.3 Accuracy: Tipping Threshold Model

In this section, we show how to adapt the uniform grid to handle the discontinuity around the tipping threshold. The numerical errors for the tipping point case are reported for a state grid covering ±3 standard deviations around the unconditional mean of T, which is approximately from -1 to 5°C temperature anomaly. We do not need to distinguish between cutting off the temperature state space at 0°C or not for this case, since disaster probabilities are zero for any $T_t < T_{Tipp}$, which is at 2.8°C in our baseline calibration. For this reason, the discontinuity of interest is no longer at a temperature of zero degrees but at the positive tipping threshold.

To get a better approximation around the tipping threshold, we include some additional collocation nodes in this area. In particular, we explicitly place a collocation node exactly at the tipping threshold ($T_t = 2.8$°C). Another collocation node is included infinitesimally before the tipping threshold: $T_t = (2.8 - \epsilon)$°C, with ϵ = 1e-6. This allows us to divide the grid in a state space with positive disaster probability and a state space with zero disaster probability. We tested for several other ways to adapt the grid around the tipping threshold, for example by using a finer collocation grid around this area. The method with including a node directly at the tipping threshold and infinitesimally before provided the best results in terms of convergence and accuracy, so we only discuss results for this method in the following in detail. The adjusted grids are all marked with an asterisk in the tables.

Table 9 shows the root-mean-square errors (RMSEs) and the maximum absolute errors (MAEs) in the value functions (9) as well as in the equilibrium conditions of the Negishi weights (13). As in the immediate disaster risk case, we exclude all error terms for $\lambda_t^{B'}$ values, for which the corresponding T'-value would be outside of the collocation grid. For the Negishi weights, the full state space is included between 0 and 1. We observe that for $n_l = 11$ and $n_T = 35$, the errors in the value functions of the two agents are already small with a maximum absolute error of 0.0078 and 0.0082, respectively. By increasing the approximation degree further up to $n_l = 23$ and $n_T = 55$, the maximum errors in the value functions go down to 0.0055 and 0.0052 for the two agents, and the root-mean-square errors can be lowered to 4.0e-4 and 6.1e-4, respectively. The numerical errors in the value functions for a collocation grid with $n_l = 23$ and $n_T = 55$ are plotted in Figure 27. The maximum errors in the value functions are concentrated in the area around the tipping threshold at 2.8°C and are rather evenly distributed across the remaining state space. As noted before, there is no spike in the errors around 0°C, in contrast to the immediate disaster risk case.

Table 9: Numerical Errors – Tipping Point Case

		v_t^G		v_t^B		$\lambda_t^{B'}$		$E[\lambda_t^{B'}]$	
nl	nT	RMSE	MAE	RMSE	MAE	RMSE	MAE	RMSE	MAE
11	21*	0.0013	0.0113	0.0019	0.0121	0.0013	0.0192	5.246e-4	0.0037
11	35*	8.877e-4	0.0078	0.0011	0.0082	0.0012	0.0192	4.427e-4	0.0037
11	55*	4.294e-4	0.0055	6.317e-4	0.0052	0.0011	0.0167	3.156e-4	0.0036
15	55*	4.038e-4	0.0055	6.100e-4	0.0052	9.029e-4	0.0161	2.405e-4	0.0025
19	55*	3.978e-4	0.0055	6.065e-4	0.0052	9.253e-4	0.0161	2.234e-4	0.0019
23	55*	3.962e-4	0.0055	6.064e-4	0.0052	8.813e-4	0.0161	2.010e-4	0.0015

The table shows root-mean-square errors (RMSEs) and maximum absolute errors (MAEs) in the value functions as well as the equilibrium conditions for the Negishi weights for different numbers of collocation nodes for the tipping threshold model. Errors are reported for a state grid covering ±3 standard deviations around the unconditional mean of T_t. For λ_t^B the full grid between 0 and 1 is used. We denote the number of collocation nodes for the λ_t^B-dimension by n_l and the number of collocation nodes for the T_t-dimension by n_T. Errors are computed on a grid of size 100×100. An asterisk (*) denotes cases where we used an adjusted grid by placing a collocation node exactly on the tipping point and an additional node infinitesimally before the tipping threshold. The remaining state space is uniformly distributed.

Figure 27: Numerical Errors in the Value Functions – Tipping Point Case

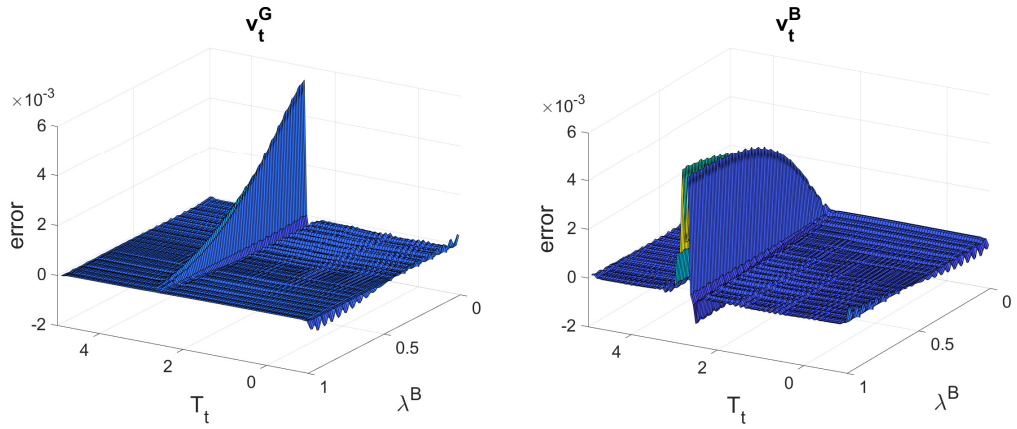

The figure plots numerical errors in the value functions for the two agents in the tipping point case. Errors are reported for a state grid covering ±3 standard deviations around the unconditional mean of T_t. For λ_t^B the full grid between 0 and 1 is used. The projection method uses a collocation grid with $n_l = 23$ and $n_T = 55$ nodes, with a collocation node exactly on the tipping point and an additional node infinitesimally before the tipping threshold. The remaining state space is uniformly distributed. Numerical errors are computed on a 100×100 uniform grid.

The maximum errors in the Negishi weights are significantly larger in the tipping threshold case compared to the immediate disaster risk case. This holds especially true for temperature values around the tipping area. These values are driven by outliers, however, and do not affect the economic interpretation of our results. While the maximum absolute error in $\lambda_t^{B'}$ is quite significant with a value of 0.0161, the maximum absolute error in the expectation over the Negishi weight next period, $E[\lambda_t^{B'}]$, is around ten times lower with a value of 0.0015. This is a first indication that the maximum errors occur in very unlikely states of nature, which have accordingly only a little weight when computing the expectations of each agent. Note that the asset-pricing moments in our model also depend on the subjective expectations of the two agents on the future states of the economy. Figure 28 visualizes the errors in the dynamics of the Negishi weights. Since the matrices of $\lambda^{B'}$ are 4-dimensional, we plot the figures for a zero-shock in temperature ($\sigma_\zeta \zeta_{t+1} = 0$), and for no disaster, one disaster and two disasters occurring in the next period. The largest errors are around the area of the tipping threshold and at the boundaries of the state space. The plots for different positive or negative shocks to temperature can be found in Appendix A (Figure 38).

The results in Table 9 are computed using $n_{GHC} = 3$, $n_{GHT} = 7$ and $n_D = 4$[31]. We refer to these errors as 'baseline' in Table 10 and show that the number of nodes chosen for the Gauss-Hermite quadrature and the numerical cutoff value for the expectation over the disaster term are sufficient. The distribution of the i.i.d. consumption shock can be accurately approximated using only 3 Gauss-Hermite nodes; using 5 Gauss-Hermite nodes instead would not affect the results. For the i.i.d. temperature shock, 7 Gauss-Hermite nodes are used, and increasing the number of nodes to 9 would only slightly affect the numerical errors.[32] The disaster impact is already approximated with high accuracy using a cutoff value of 3. For comparison, results with a cutoff value of 4 are reported in the table. Note that the cutoff value only affects the accuracy for T_t-values above the tipping threshold on the collocation grid, as the disaster probability is always zero for values below the threshold.

Finally, as a last exercise, we try to use a finer grid around the tipping threshold, since the numerical errors are largest in this area. We do this by including some additional collocation nodes in the region of $T_{Tipp} \pm 0.3$°C. While the errors can be further decreased by including additional nodes in this region, the economic results are nearly unaffected by this as shown in the following.

[31] This refers to a cutoff value of $x = 3$, as $x = 0$ also counts as a state.

[32] The observed difference in errors primarily arises from large jumps in temperature ($\sigma_\zeta \zeta_{t+1}$) around the tipping point.

Figure 28: Numerical Errors in the Negishi Weights – Tipping Point Case

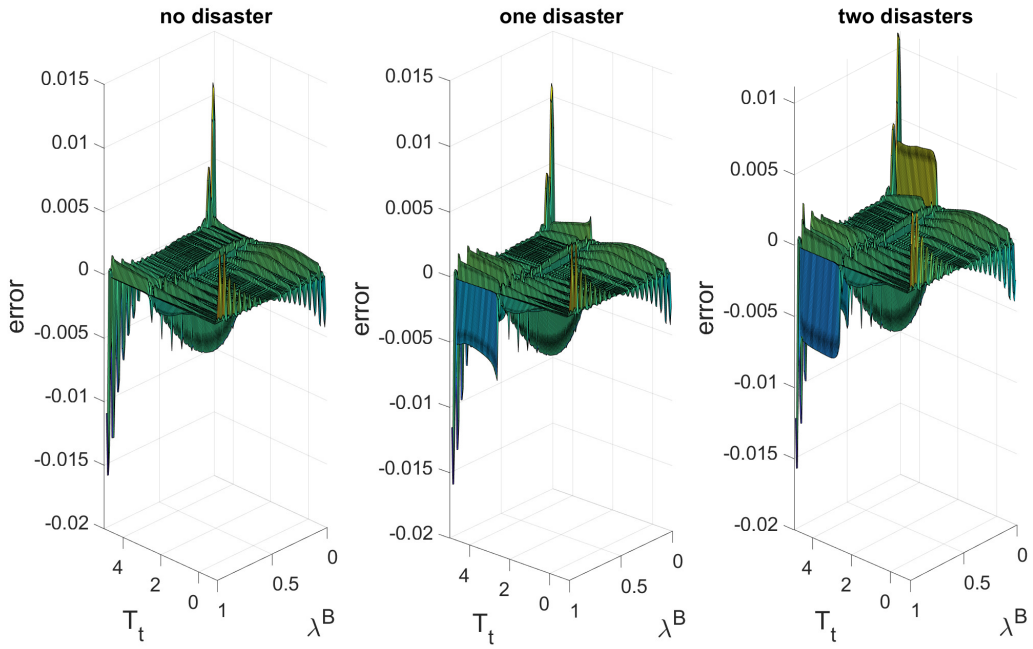

The figure plots numerical errors in the dynamics of the Negishi weights for a different number of disasters next period in the model including a tipping threshold at 2.8°C. The i.i.d. temperature shock is set to zero ($\sigma_\zeta \zeta_{t+1} = 0$). Errors are reported for a state grid covering ± 3 standard deviations around the unconditional mean of T_t. For λ_t^B the full grid between 0 and 1 is used. The projection method uses a collocation grid with $n_l = 23$ and $n_T = 55$ nodes, with a collocation node exactly on the tipping point and an additional node infinitesimally before the tipping threshold. The remaining state space is uniformly distributed. Numerical errors are computed on a 100×100 uniform grid.

Table 10: Robustness Numerical Errors – Tipping Point Case

	v_t^G		v_t^B		$\lambda_t^{B'}$	
	RMSE	MAE	RMSE	MAE	RMSE	MAE
baseline	3.9618e-4	0.0055	6.0637e-4	0.0052	8.8134e-4	0.0161
$n_{GHC} = 5$	3.9618e-4	0.0055	6.0636e-4	0.0052	8.8134e-4	0.0161
$n_{GHT} = 9$	2.9204e-4	0.0036	4.9529e-4	0.0043	0.0013	0.0209
$N_{max} = 4$	3.9512e-4	0.0055	6.0668e-4	0.0052	8.8005e-4	0.0161
finer TP	2.6772e-4	0.0046	4.3810e-4	0.0055	8.2381e-4	0.0117

The table shows root-mean-square errors (RMSEs) and maximum absolute errors (MAEs) in the value functions as well as the equilibrium conditions for the Negishi weights for a different number of Gauss-Hermite nodes, a different cutoff value for the disaster state and a finer grid around the tipping threshold. Errors are reported for a state grid covering ± 3 standard deviations around the unconditional mean of T_t. For λ_t^B the full grid between 0 and 1 is used. The number of collocation nodes for the λ_t^B-dimension and for the T_t-dimension is given $n_l = 23$ and $n_T = 55$, with a collocation node exactly on the tipping point and an additional node infinitesimally before the tipping threshold. The remaining state space is uniformly distributed. Errors are computed on a grid of size 100×100.

We argue that the approximation degree presented above is sufficient for our model statistics of interest. Table 11 shows asset pricing moments for different collocation grids by running a simulation over 100 years, starting at a temperature of $T_0 = 1°\text{C}$.[33] At the beginning, both agents have an equal consumption share, hence $s_0^G = s_0^B = 0.5$. We run this simulation 100 times for each of the collocation grids and report selected annualized asset-pricing moments from these simulations. At the end of the simulation, the mean temperature is $T_{100} = 1.45°\text{C}$ and the mean consumption share of the brown agent is $s_{100}^B = 0.63$. The differences between the tested collocation grids are marginal and do not significantly impact the qualitative predictions of the model.

Again, the simulation presented in Table 11 does not cover the whole state space, but rather focuses on the regions most likely to be encountered in the coming decades. To provide a more comprehensive analysis, we turn to Figure 29, which compares the carbon premium and WCC across the entirety of the state space of T_t for an economy with $w_t^G = 0.5$. Examining the carbon premium, we observe a slight variance between the 11×21 and 11×35 grids, though the difference diminishes when comparing the 11×35 and 23×55 collocation grids. The discrepancies in the WCC, however, are more apparent between the 11×21 and 11×35 grids, yet they also converge upon comparing the 11×35 and 23×55 collocation grids. It is

[33] Table 15 in Appendix A shows the corresponding price–dividend ratio from the simulations for the green stock, brown stock, and the market portfolio.

noteworthy that the WCC is particularly sensitive to even small approximation errors in the wealth–consumption ratio, given its dependency on its derivative (see equation 23).

Figure 40 in Appendix A presents the results for two scenarios closer to the boundaries of the λ-dimension: one with $w_t^G = 0.05$ and another with $w_t^G = 0.95$. Similar to the immediate disaster risk model, the differences between the various collocation grids do not significantly increase at the boundaries. Although the 11×21 collocation grid shows some variation, the solutions from the two larger grids converge, as seen before in the case of the economy with $w_t^G = 0.5$.

Finally, we tested whether the results change with an extended approximation interval for temperature. We increased the collocation grid to cover ± 4 standard deviations around the unconditional mean of temperature (approximately from -2°C to 6°C), instead of ± 3 standard deviations (approximately from -1°C to 5°C). We compare the carbon premium and WCC for both cases in Figure 30 and find no economically significant differences between the two choices for the approximation interval.

Table 11: Annualized Asset-Pricing Moments – Tipping Point Case

n_l	n_T	$\log(R_t^M)$	$\sigma(\log(R_t^M))$	$\log(R_t^G)$	$\sigma(\log(R_t^G))$	$\log(R_t^B)$	$\sigma(\log(R_t^B))$
11	21*	0.0443	0.0533	0.0403	0.0539	0.0506	0.0665
11	35*	0.0441	0.0535	0.0401	0.0540	0.0503	0.0679
11	55*	0.0441	0.0533	0.0400	0.0539	0.0503	0.0674
23	55*	0.0441	0.0534	0.0402	0.0539	0.0502	0.0679
23	55**	0.0441	0.0535	0.0401	0.0539	0.0503	0.0686

The table reports selected annualized asset-pricing moments for different approximation degrees for the green stock, brown stock, and the market portfolio. Moments are computed by simulating 100 sample paths each containing 100 years of data. We set $T_{start} = 1.0$°C and $w_{start}^G = 0.5$. The number of collocation nodes for the λ_t^B-dimension is denoted by n_l and the number of collocation nodes for the T_t-dimension by n_T. Shocks to temperature, ζ_{t+1}, are drawn from a standard normal distribution, and no exogenous shocks are added. An asterisk (*) denotes cases where we used an adjusted grid by placing a collocation node exactly on the tipping point and an additional node infinitesimally before the tipping threshold. Two asterisks (**) denote the case where we put some additional collocation nodes around the tipping point.

Figure 29: Carbon Premium and Welfare Cost of Carbon for different Collocation Grids – Tipping Point Case

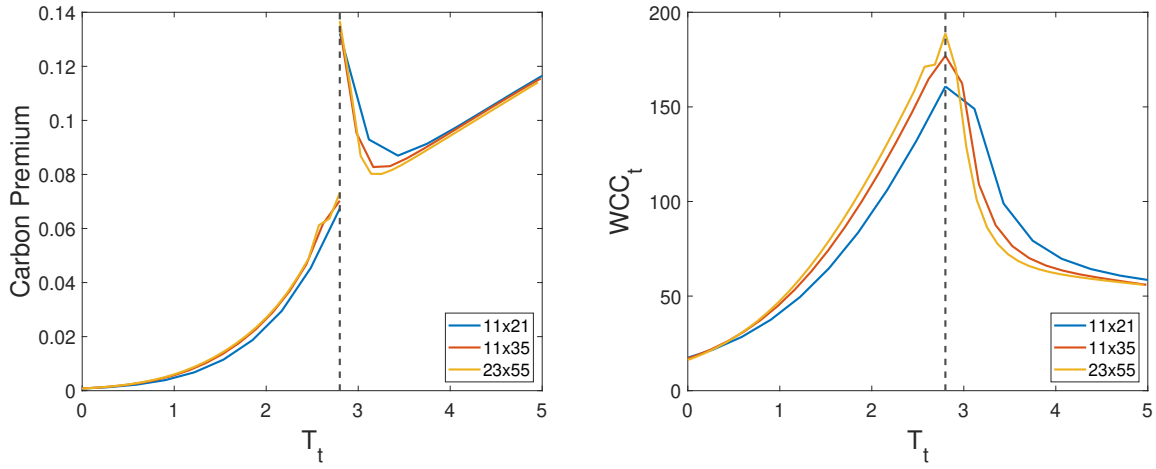

The figure plots the carbon premium and the welfare cost of carbon for different collocation grids as a function of T_t. The grids cover a T-space from approximately -1 to 5°C. Results are shown for an economy with $w_t^G = 0.5$. Collocation grids are adjusted by placing a collocation node exactly on the tipping point and an additional node infinitesimally before the tipping threshold. The remaining state space is uniformly distributed. The vertical dashed line marks the tipping threshold.

Figure 30: Carbon Premium and Welfare Cost of Carbon for a larger Approximation Space - Tipping Point Case

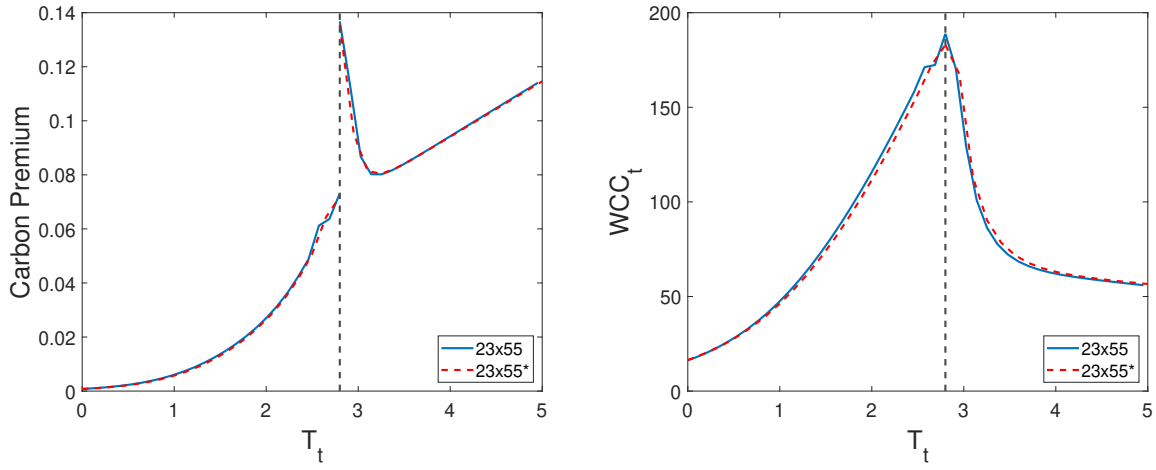

The figure plots the carbon premium and the welfare cost of carbon for different collocation grids as a function of T_t. The blue line corresponds to a grid that covers a T-space from ±3 standard deviations (approx. -1°C to 5°C), while the red line corresponds to a T-space from ±4 standard deviations (approx. -2°C to 6°C) around the unconditional mean of T_t. Results are shown for an economy with $w_t^G = 0.5$. Collocation grids are adjusted by placing a collocation node exactly on the tipping point and an additional node infinitesimally before the tipping threshold. The remaining state space is uniformly distributed. The vertical dashed line marks the tipping threshold.

6 Conclusion

We present an asset-pricing model for the analysis of climate financial risks. The persistent global average temperature anomaly is a natural source of long-run risk in financial markets. In our model, as long as the global temperature is below the temperature threshold of a tipping point, climate-induced disaster cannot occur. Once the global temperature crosses that threshold, disasters become increasingly likely. The economy is populated by two types of investor with divergent beliefs about climate change. Green investors believe that the disaster probability rises considerably faster than brown investors do. Both groups of investors have identical Epstein–Zin preferences with a preference for the early resolution of risk.

The model simultaneously explains several empirical findings that have recently been documented in the literature. First, not only is climate risk itself priced, but the risk of receiving bad news about the future climate is also priced. Brown investors implicitly sell insurance against this climate news risk to green investors. Second, bad news about the climate increases the market share of green investors, because they benefit from buying insurance against such news shocks. Third, brown stocks carry a carbon premium relative to green stocks due to their greater exposure to climate risks. Fourth, if the temperature threshold to trigger disaster events is sufficiently far away from the current temperature anomaly, then the corresponding carbon premium is only small. The news-channel effect dominates the carbon-premium effect and the model thus shows an outperformance of green over brown stocks in response to bad climate news.

The model provides predictions for the future evolution of asset prices. As per our model, there exists a positive carbon premium, which means that the expected return of brown stocks is higher than that of green stocks. For this reason, according to our model past performance is not a good predictor of future performance. While realized returns of green stocks have gone up in response to negative climate news, expected returns have gone down simultaneously. In the absence of further exogenous shocks and climate-induced disasters, our model predicts higher future returns for brown stocks. However, if temperatures continue to rise and approach the tipping point threshold, the potential benefits of investments to slow down climate change increase significantly. In this scenario, our model predicts a significant increase in the market share of green investors and the carbon premium.

The model also points out the differences in the gains from carbon-reducing investments between investors with different beliefs about climate change. By introducing multiple investors and allowing them to trade with each other, climate risks can also lead to substantial gains in the wealth of some investors as shown in the simulations. Hence, while climate risks pose a threat to overall societal welfare in the economy, they also offer financial opportunities for specific investors.

Our novel framework for the pricing of climate risks opens numerous directions for future

research. We assume, for example, that investors have constant beliefs about climate change. It would be interesting to understand how the pricing of climate risks changes when investors update their beliefs based on new climate data. As certain thresholds are surpassed in the future, investors will gain a better understanding of the 'true' impact of climate change, resulting in a partial resolution of uncertainty. We also do not model the large uncertainty and ambiguity investors face when pricing in climate risks. Our model underscores the increasing significance of climate-related financial risks within financial markets, which have substantial implications for firms that are most exposed to climate risks. Consequently, innovative metrics to assess firm-level climate risk exposure should incorporate predictive data on climate change, rather than solely relying on historical emission data. Our model highlights a potential shift in the carbon risk from transitional to physical climate risk in the future – with significant implications for identifying the companies that bear the highest carbon risk. A worthwhile augmentation for subsequent research would be to broaden our framework to accommodate varying regional exposures to large-scale climate catastrophes such as floods and heatwaves, and to study the implications of such exposure on societal welfare and climate risk hedging across different regions.

Bibliography

Acharya, V. V., T. Johnson, S. Sundaresan, and T. Tomunen (2022): "Is physical climate risk priced? Evidence from regional variation in exposure to heat stress," Tech. rep., National Bureau of Economic Research.

Ai, H. and R. Bansal (2018): "Risk Preferences and the Macroeconomic Announcement Premium," *Econometrica*, 86, 1383–1430.

Alchian, A. A. (1950): "Uncertainty, evolution, and economic theory," *Journal of political economy*, 58, 211–221.

Ardia, D., K. Bluteau, K. Boudt, and K. Inghelbrecht (2023): "Climate change concerns and the performance of green versus brown stocks," *Management Science*, forthcoming.

Armstrong McKay, D. I., A. Staal, J. F. Abrams, R. Winkelmann, B. Sakschewski, S. Loriani, I. Fetzer, S. E. Cornell, J. Rockström, and T. M. Lenton (2022): "Exceeding 1.5 C global warming could trigger multiple climate tipping points," *Science*, 377, eabn7950.

Aswani, J., A. Raghunandan, and S. Rajgopal (2023): "Are carbon emissions associated with stock returns?" *Review of Finance, forthcoming.*

Baldauf, M., L. Garlappi, and C. Yannelis (2020): "Does Climate Change Affect Real Estate Prices? Only If You Believe In It," *The Review of Financial Studies*, 33, 1256–1295.

Bansal, R., D. Kiku, and M. Ochoa (2016): "Price of long-run temperature shifts in capital markets," Tech. rep., National Bureau of Economic Research.

——— (2021): "Climate Change Risk," Tech. rep., National Bureau of Economic Research.

Bansal, R., D. Kiku, and A. Yaron (2012): "An Empirical Evaluation of the Long-Run Risks Model for Asset Prices," *Critical Finance Review*, 1, 183–221.

Bansal, R. and A. Yaron (2004): "Risks for the long run: A potential resolution of asset pricing puzzles," *The journal of Finance*, 59, 1481–1509.

Barro, R. J. (2006): "Rare Disasters and Asset Markets in the Twentieth Century," *Quarterly Journal of Economics*, 121, 823–866.

——— (2009): "Rare disasters, asset prices, and welfare costs," *American Economic Review*, 99, 243–64.

Bauer, M. D., D. Huber, G. D. Rudebusch, and O. Wilms (2022): "Where is the carbon premium? Global performance of green and brown stocks," *Journal of Climate Finance*, 1, 100006.

Bernstein, A., S. B. Billings, M. T. Gustafson, and R. Lewis (2022): "Partisan residential sorting on climate change risk," *Journal of Financial Economics*.

Bolton, P. and M. Kacperczyk (2021): "Do investors care about carbon risk?" *Journal of financial economics*, 142, 517–549.

——— (2022): "Global Pricing of Carbon-Transition Risk," *Journal of Finance, Forthcoming*.

Borovička, J. (2020): "Survival and long-run dynamics with heterogeneous beliefs under recursive preferences," *Journal of Political Economy*, 128, 206–251.

Branger, N., P. Konermann, and C. Schlag (2020): "Optimists and Pessimists in (In)Complete Markets," *Journal of Financial and Quantitative Analysis*, 55, 2466–2499.

Cai, Y. (2021): "The Role of Uncertainty in Controlling Climate Change," in *Oxford Research Encyclopedia of Economics and Finance*, Oxford University Press.

Cai, Y., K. L. Judd, and T. S. Lontzek (2017): "The Social Cost of Carbon with Economic and Climate Risks," Working Paper 18113, Hoover Institution, Stanford, CA.

Cai, Y., T. M. Lenton, and T. S. Lontzek (2016): "Risk of multiple interacting tipping points should encourage rapid CO2 emission reduction," *Nature Climate Change*, 520–525.

Cai, Y. and T. S. Lontzek (2019): "The social cost of carbon with economic and climate risks," *Journal of Political Economy*, 127, 2684–2734.

Chen, H., S. Joslin, and N.-K. Tran (2012): "Rare disasters and risk sharing with heterogeneous beliefs," *The Review of Financial Studies*, 25, 2189–2224.

Choi, D., Z. Gao, and W. Jiang (2020): "Attention to Global Warming," *The Review of Financial Studies*, 33, 1112–1145.

Cochrane, J. H. (2017): "Macro-finance," *Review of Finance*, 21, 945–985.

Colacito, R. and M. M. Croce (2013): "International asset pricing with recursive preferences," *The Journal of Finance*, 68, 2651–2686.

Colacito, R., M. M. Croce, Y. Liu, and I. Shaliastovich (2022): "Volatility risk pass-through," *The Review of Financial Studies*, 35, 2345–2385.

Daniel, K. D., R. B. Litterman, and G. Wagner (2016): "Applying asset pricing theory to calibrate the price of climate risk," Tech. rep., National Bureau of Economic Research.

Enders, A., T. Lontzek, K. Schmedders, and M. Thalhammer (2023): "Carbon Risk and Equity Prices," *Available at SSRN 4476587*.

Engle, R. F., S. Giglio, B. Kelly, H. Lee, and J. Stroebel (2020): "Hedging Climate Change News," *The Review of Financial Studies*, 33, 1184–1216.

Epstein, L. and S. E. Zin (1989): "Substitution, risk aversion, and the temporal behavior of consumption and asset returns: A theoretical framework," *Econometrica*, 57, 937–969.

Fischer, T. and F. Lundtofte (2021): "Green portfolios," *Available at SSRN 3923578*.

Folini, D., F. Kübler, A. Malova, and S. Scheidegger (2021): "The Climate in Climate Economics," *Available at SSRN 3885021*.

Friedman, M. (1953): *Essays in positive economics*, University of Chicago press.

Gabaix, X. (2012): " Variable Rare Disasters: An Exactly Solved Framework for Ten Puzzles in Macro-Finance *," *The Quarterly Journal of Economics*, 127, 645–700.

Gibson Brandon, R., S. Glossner, P. Krueger, P. Matos, and T. Steffen (2022): "Do responsible investors invest responsibly?" *Review of Finance*, 26, 1389–1432.

Giglio, S., B. Kelly, and J. Stroebel (2021a): "Climate Finance," *Annual Review of Financial Economics*, 13, 15–36.

Giglio, S., M. Maggiori, K. Rao, J. Stroebel, and A. Weber (2021b): "Climate change and long-run discount rates: Evidence from real estate," *The Review of Financial Studies*, 34, 3527–3571.

Global Sustainable Investment Alliance (2020): "Global Sustainable Investment Review," `http://www.gsi-alliance.org/wp-content/uploads/2021/08/GSIR-20201.pdf`.

Heeb, F., J. F. Kölbel, F. Paetzold, and S. Zeisberger (2022): "Do Investors Care about Impact?" *The Review of Financial Studies*.

Howe, P. D., M. Mildenberger, J. R. Marlon, and A. Leiserowitz (2015): "Geographic variation in opinions on climate change at state and local scales in the USA," *Nature Climate Change*, 5, 596–603.

Hsu, P.-H., K. Li, and C.-Y. Tsou (2023): "The Pollution Premium," *Journal of Finance*, forthcoming.

Huij, J., D. Laurs, P. A. Stork, and R. C. Zwinkels (2021): "Carbon Beta: A Market-Based Measure of Climate Risk," *Available at SSRN*.

Hulme, M. (2009): *Why We Disagree about Climate Change: Understanding Controversy, Inaction and Opportunity*, Cambridge University Press.

IPCC (2014): "Impacts, adaptation and vulnerability," *Part A: global and sectoral aspects. Contribution of working group II to the fifth assessment report of the intergovernmental Panel on Climate Change*, 1132.

——— (2022): *Climate Change 2022: Mitigation of Climate Change. Contribution of Working Group III to the Sixth Assessment Report of the Intergovernmental Panel on Climate Change*, Cambridge, UK and New York, NY, USA: Cambridge University Press.

Judd, K. L. (1998): *Numerical methods in economics*, MIT press.

Karydas, C. and A. Xepapadeas (2019): "Pricing climate change risks: CAPM with rare disasters and stochastic probabilities," *CER-ETH Working Paper Series Working Paper*, 19, 311.

Kriegler, E., J. W. Hall, H. Held, R. Dawson, and H. J. Schellnhuber (2009): "Imprecise probability assessment of tipping points in the climate system," *Proceedings of the national Academy of Sciences*, 106, 5041–5046.

Lemoine, D. and C. Traeger (2014): "Watch your step: optimal policy in a tipping climate," *American Economic Journal: Economic Policy*, 6, 137–166.

Lenton, T. M., H. Held, E. Kriegler, J. W. Hall, W. Lucht, S. Rahmstorf, and H. J. Schellnhuber (2008): "Tipping Elements in the Earth's Climate System," *Proceedings of the National Academy of Sciences*, 105, 1786–1793.

Lontzek, T. S., Y. Cai, K. L. Judd, and T. M. Lenton (2015): "Stochastic integrated assessment of climate tipping points indicates the need for strict climate policy," *Nature Climate Change*, 441–444.

MacDougall, A. H., N. C. Swart, and R. Knutti (2017): "The uncertainty in the transient climate response to cumulative CO2 emissions arising from the uncertainty in physical climate parameters," *Journal of Climate*, 30, 813–827.

Matthews, H. D., N. P. Gillett, P. A. Stott, and K. Zickfeld (2009): "The proportionality of global warming to cumulative carbon emissions," *Nature*, 459, 829.

Nauels, A., M. Meinshausen, M. Mengel, K. Lorbacher, and T. M. L. Wigley (2017): "Synthesizing long-term sea level rise projections – the MAGICC sea level model v2.0," *Geoscientific Model Development*, 10, 2495–2524.

OECD (2022): *Climate Tipping Points*, OECD.

Pástor, L., R. F. Stambaugh, and L. A. Taylor (2021): "Sustainable investing in equilibrium," *Journal of Financial Economics*, 142, 550–571.

——— (2022): "Dissecting green returns," *Journal of Financial Economics*, 146, 403–424.

Pohl, W., K. Schmedders, and O. Wilms (2018): "Higher Order Effects in Asset Pricing Models with Long-Run Risks," *The Journal of Finance*, 73, 1061–1111.

——— (2021): "Asset pricing with heterogeneous agents and long-run risk," *Journal of Financial Economics*, 140, 941–964.

——— (2023): "Existence Conditions for Asset Pricing Models with Recursive Utility," Working paper.

Principles of Responsible Investment (2021): "Annual Report of the UN Principles of Responsible Investment," `https://www.unpri.org/annual-report-2021`.

Rietz, T. A. (1988): "The equity risk premium a solution," *Journal of Monetary Economics*, 22, 117–131.

Saad, L. (2017): "Global warming concern at three-decade high in US," *Gallup poll social series*.

Sautner, Z., L. Van Lent, G. Vilkov, and R. Zhang (2023a): "Firm-level climate change exposure," *The Journal of Finance*, 78, 1449–1498.

——— (2023b): "Pricing climate change exposure," *Management Science*.

Smith, C. J., P. M. Forster, M. Allen, N. Leach, R. J. Millar, G. A. Passerello, and L. A. Regayre (2018): "FAIR v1. 3: a simple emissions-based impulse response and carbon cycle model," *Geoscientific Model Development*, 11, 2273–2297.

UNFCCC (2015): "Paris agreement," in *Report of the Conference of the Parties to the United Nations Framework Convention on Climate Change (21st Session, 2015: Paris). Retrieved December*, HeinOnline, vol. 4, 2017.

van der Beck, P. (2022): "Flow-Driven ESG Returns," Working paper.

van der Ploeg, F. and A. de Zeeuw (2018): "Climate tipping and economic growth: Precautionary capital and the price of carbon," *Journal of the European Economic Association*, 16, 1577–1617.

Wachter, J. A. (2013): "Can Time-Varying Risk of Rare Disasters Explain Aggregate Stock Market Volatility?" *Journal of Finance*, 68, 987–1035.

Weil, P. (1989): "The equity premium puzzle and the risk-free rate puzzle," *Journal of monetary economics*, 24, 401–421.

Zickfeld, K., A. Levermann, M. G. Morgan, T. Kuhlbrodt, S. Rahmstorf, and D. W. Keith (2007): "Expert judgements on the response of the Atlantic meridional overturning circulation to climate change," *Climatic Change*, 82, 235–265.

Appendix

A Additional Figures and Tables

Figure 31: Mapping between Wealth Shares and Consumption Shares

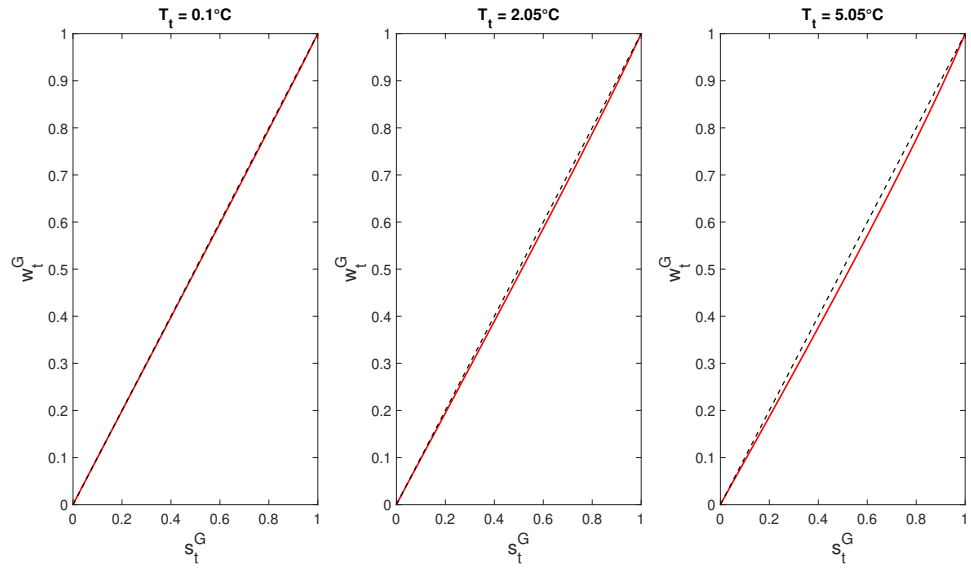

The figure plots the wealth share, w_t^G, of the green investor as a function of her consumption share, s_t^G, for different temperature states. The dashed lines mark the 45 degree line. Model parameters are calibrated using values reported in Table 1.

Figure 32: Temperature Pathways from 100 Simulations

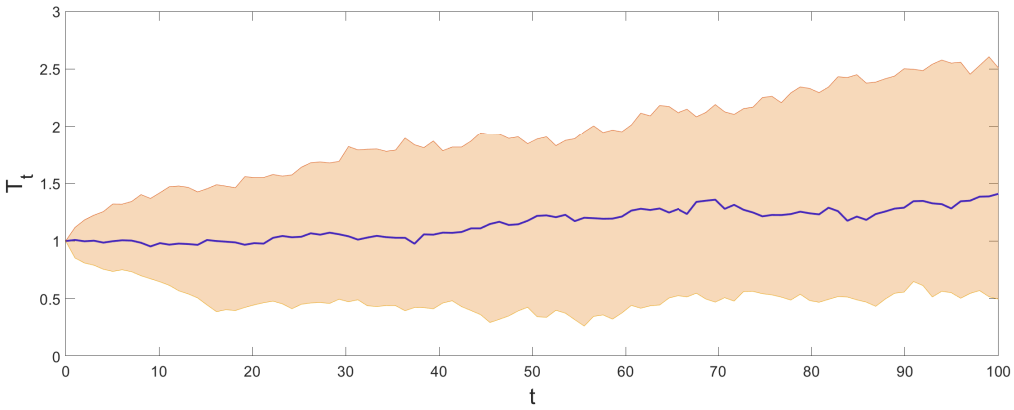

The figure shows the mean temperature path, along with the 10% and 90% quantiles for 100 simulations covering 100 years of simulated data each. The starting point is $T_0 = 1$°C and the mean temperature after 100 years is 1.45°C.

Figure 33: Carbon Premium for CRRA Preferences for the Beliefs of the Green Investor

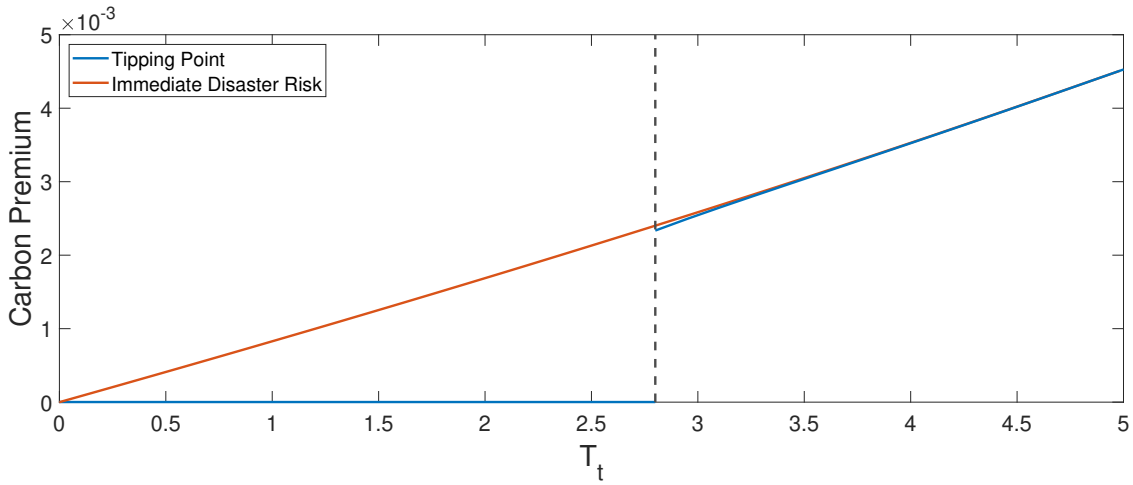

The figure plots the expected return of the brown stock minus the expected return of the green stock as a function of temperature, T_t, for $w_t^G = 0.5$ for CRRA preferences with $\gamma = 1/\psi = 2$. Results are shown for the case with immediate disaster risk and for the case with the distant tipping threshold for the beliefs of the green investor. The vertical dashed line marks the tipping threshold.

Figure 34: Carbon Premium for Epstein–Zin Preferences for the Beliefs of the Green Investor

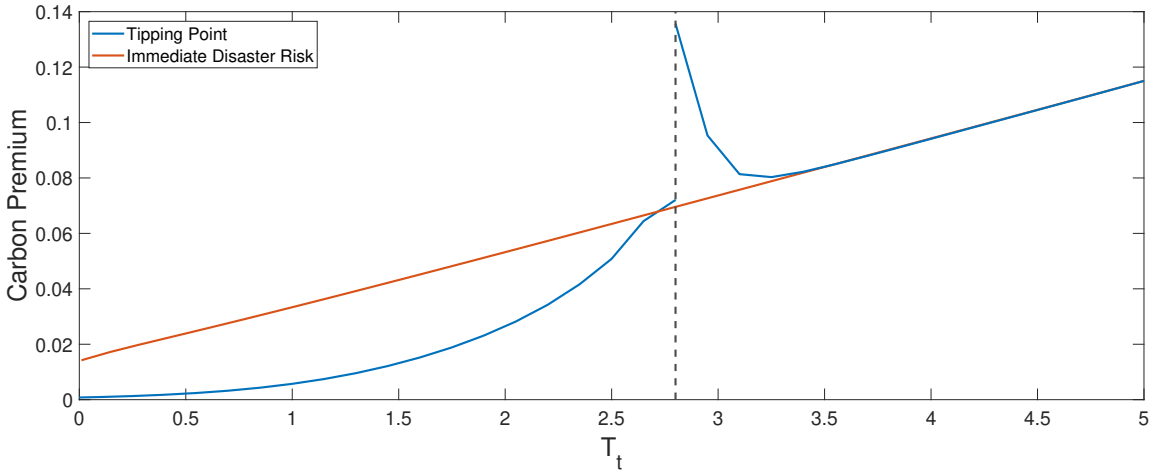

The figure plots the expected return of the brown stock minus the expected return of the green stock as a function of temperature, T_t, for $w_t^G = 0.5$ for Epstein–Zin preferences with $\gamma = 8$ and $\psi = 1.5$. Results are shown for the case with immediate disaster risk and for the case with the distant tipping threshold for the beliefs of the green investor. The vertical dashed line marks the tipping threshold.

Figure 35: Price–Dividend Ratio for Immediate and Distant Disaster Risk

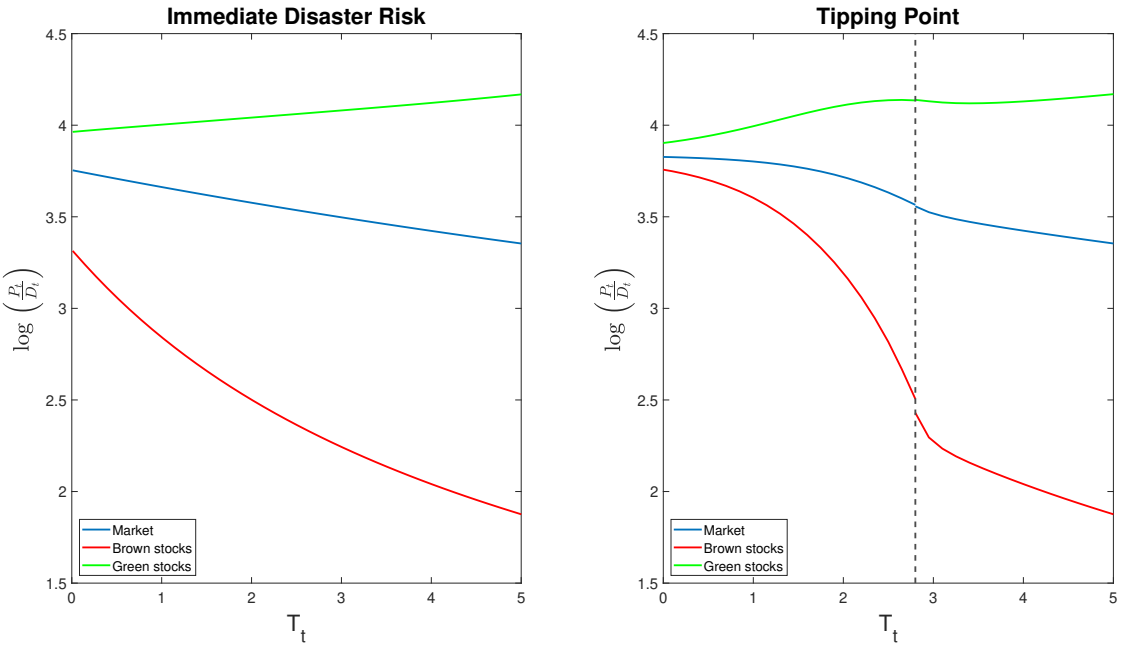

The figure plots the log price–dividend ratios for the green and the brown stock and for the market portfolio as a function of temperature, T_t, for $w_t^G = 0.5$. Results are shown for the case with immediate disaster risk and for the case with the distant tipping threshold. The vertical dashed line in the right panel marks the tipping threshold.

Figure 36: Individual Wealth–Consumption Ratio as a Function of Wealth

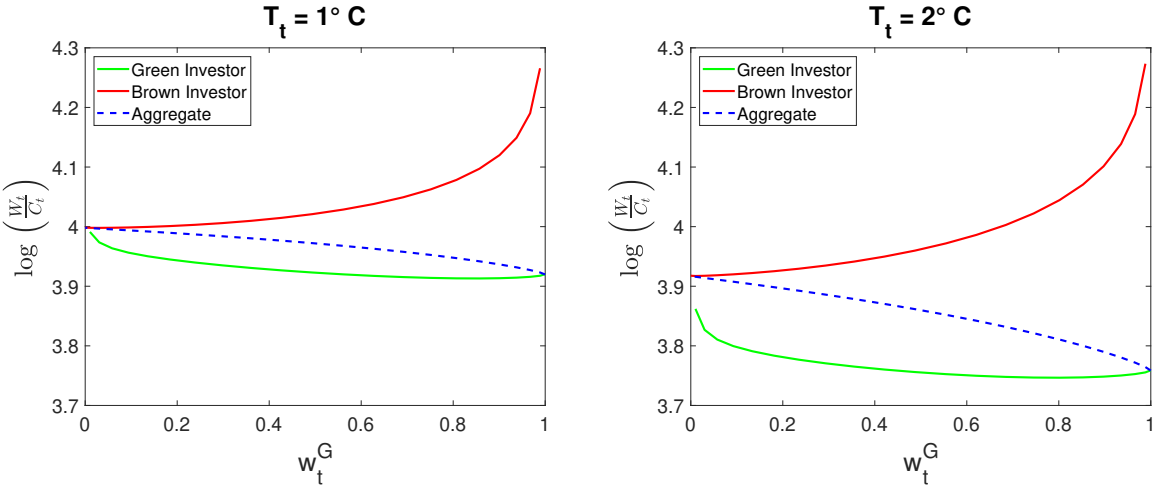

The figure plots the individual wealth–consumption ratio for the green and brown investor, along with the aggregate wealth–consumption ratio, as a function of the wealth share, w_t^G, of the green investor, for different levels of temperature T_t. Results are shown for the economy with a distant tipping threshold.

Figure 37: Numerical Errors in the Negishi Weights – Immediate Disaster Risk Case

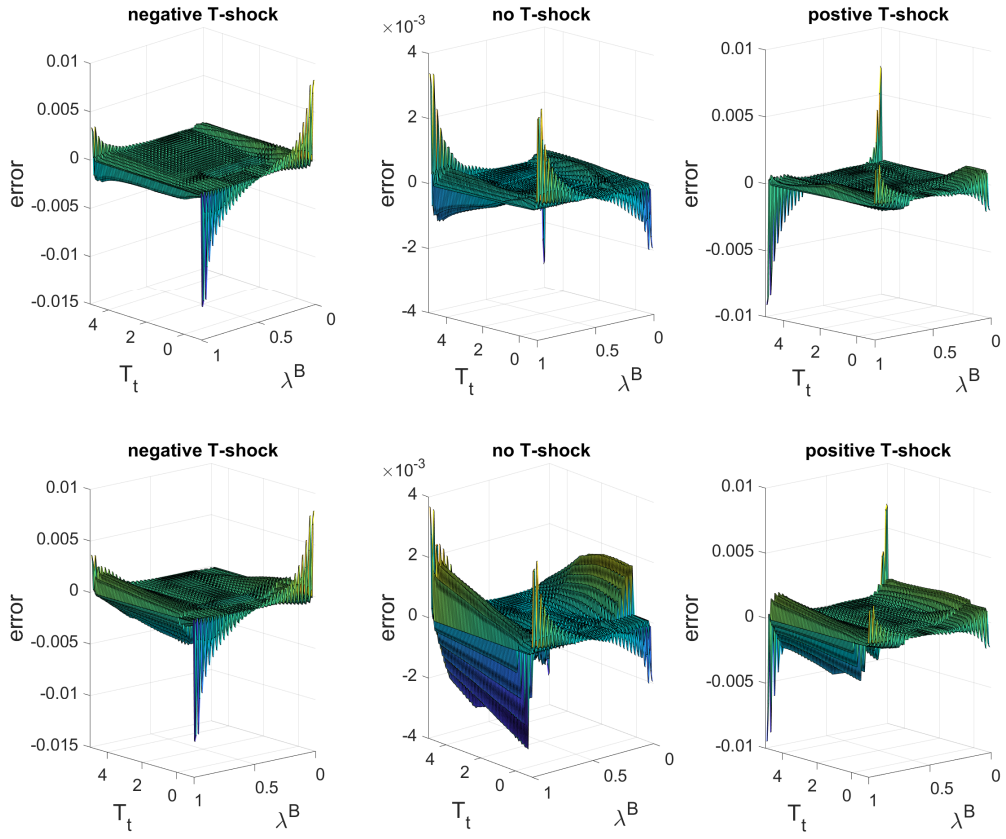

The figure plots the numerical errors in the dynamics of the Negishi weights for a no disaster state next period (upper row) and one disaster next period (bottom row) in the immediate disaster risk model. The i.i.d. temperature shock is set to $\sigma_\zeta \zeta_{t+1} = -0.0816$ in the left panel, $\sigma_\zeta \zeta_{t+1} = 0$ in the middle panel and $\sigma_\zeta \zeta_{t+1} = +0.0816$ in the right panel. Errors are reported for a state grid covering ± 3 standard deviations around the unconditional mean of T_t. For λ_t^B the full grid between 0 and 1 is used. The projection method uses a 35×35 uniform collocation grid for the λ^B- and T_t- dimension. Numerical errors are computed on a 100×100 uniform grid.

Figure 38: Numerical Errors in the Negishi Weights – Tipping Point Case

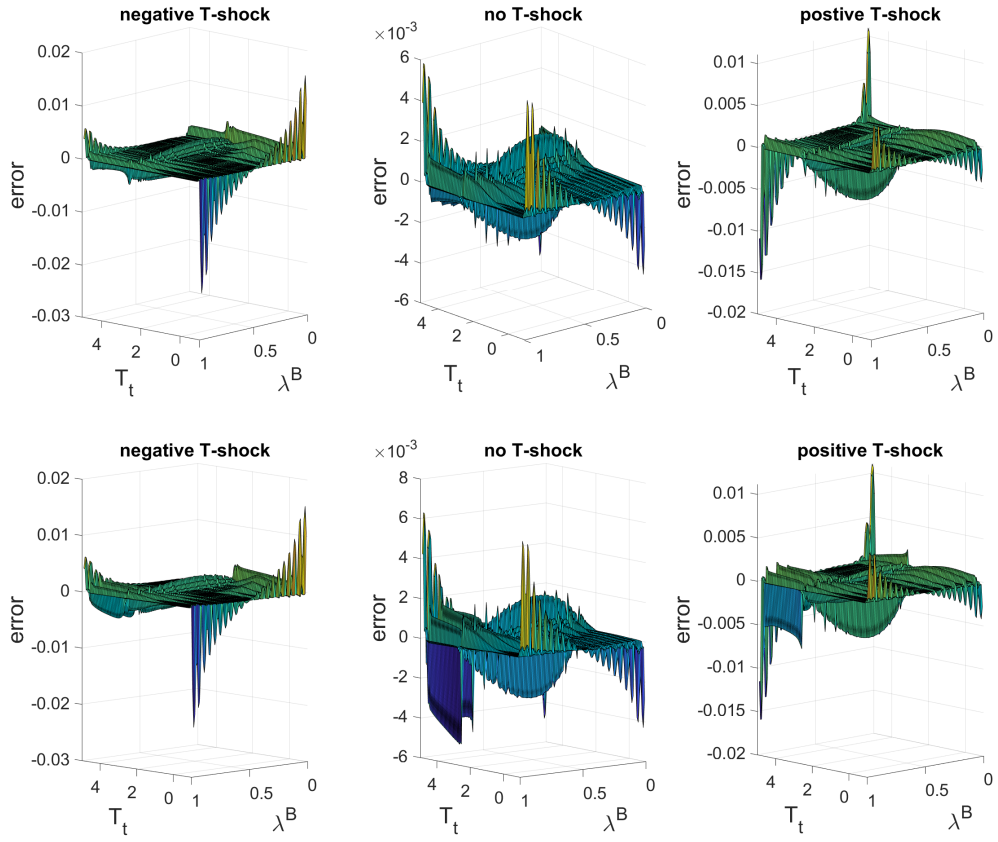

The figure plots the numerical errors in the dynamics of the Negishi weights for a no disaster state next period (upper row) and one disaster next period (bottom row) in the model including a tipping threshold at 2.8°C. The i.i.d. temperature shock is set to $\sigma_\zeta \zeta_{t+1} = -0.0816$ in the left panel, $\sigma_\zeta \zeta_{t+1} = 0$ in the middle panel and $\sigma_\zeta \zeta_{t+1} = +0.0816$ in the right panel. Errors are reported for a state grid covering ± 3 standard deviations around the unconditional mean of T_t. For λ_t^B the full grid between 0 and 1 is used. The projection method uses a collocation grid with $n_l = 23$ and $n_T = 55$ nodes, with a collocation node exactly on the tipping point and an additional node infinitesimally before the tipping threshold. The remaining state space is uniformly distributed. Numerical errors are computed on a 100×100 uniform grid.

Figure 39: Carbon Premium and Welfare Cost of Carbon for different Collocation Grids – Immediate Disaster Risk Case at the Boundaries

(a) Economy dominated by Brown Investors ($w_t^G = 0.05$)

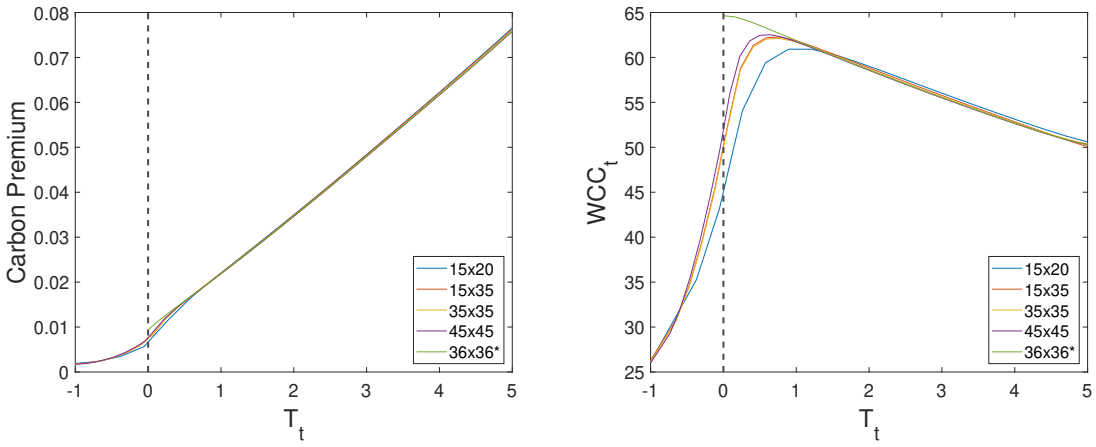

(b) Economy dominated by Green Investors ($w_t^G = 0.95$)

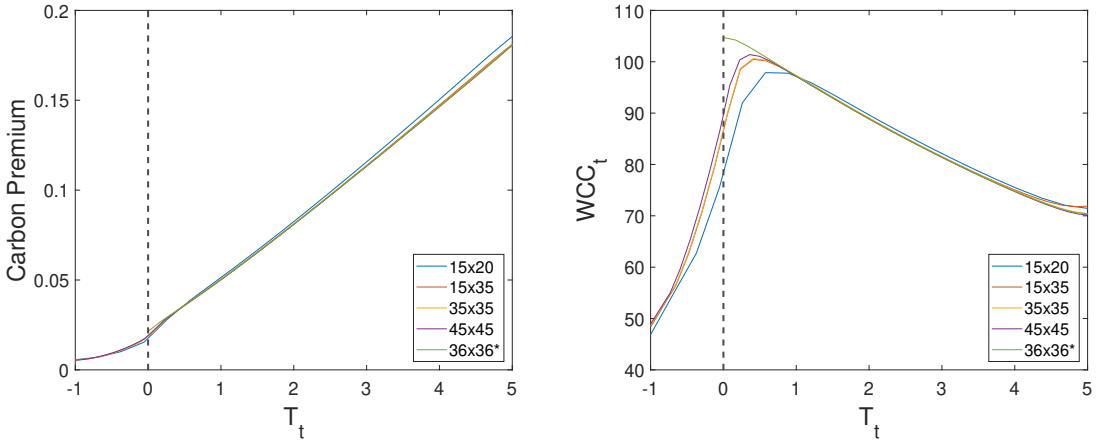

The figure plots the carbon premium and the welfare cost of carbon for different collocation grids as a function of temperature T_t. The upper two plots show the results for an economy with $w_t^G = 0.05$, and the lower two plots show results for an economy with $w_t^G = 0.95$. The four grids without an asterisk cover a T-space from approximately -1 to 5°C, while the grid with an asterisk (green line) refers to the collocation grid with a lower boundary of $T_{min} = 0.01$°C. The vertical dashed line marks 0°C.

Figure 40: Carbon Premium and Welfare Cost of Carbon for different Collocation Grids – Tipping Point Case at the Boundaries

(a) Economy dominated by Brown Investors ($w_t^G = 0.05$)

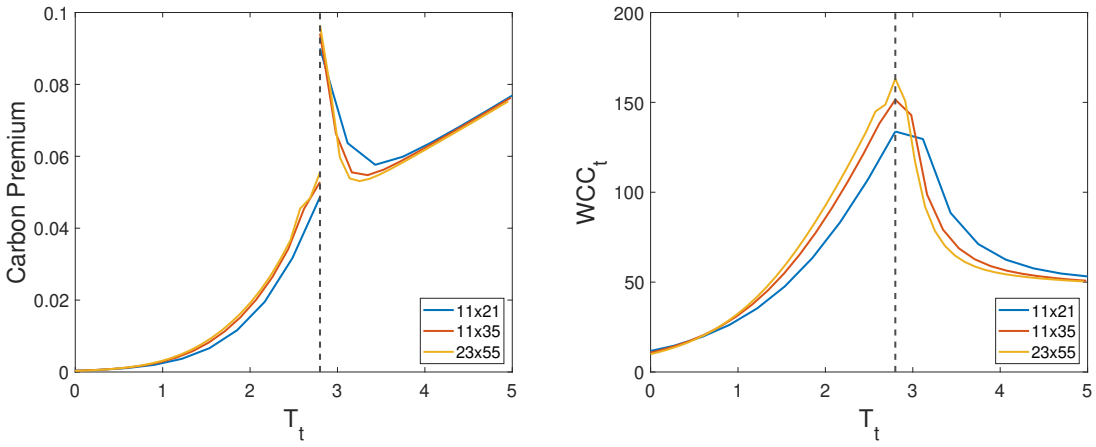

(b) Economy dominated by Green Investors ($w_t^G = 0.95$)

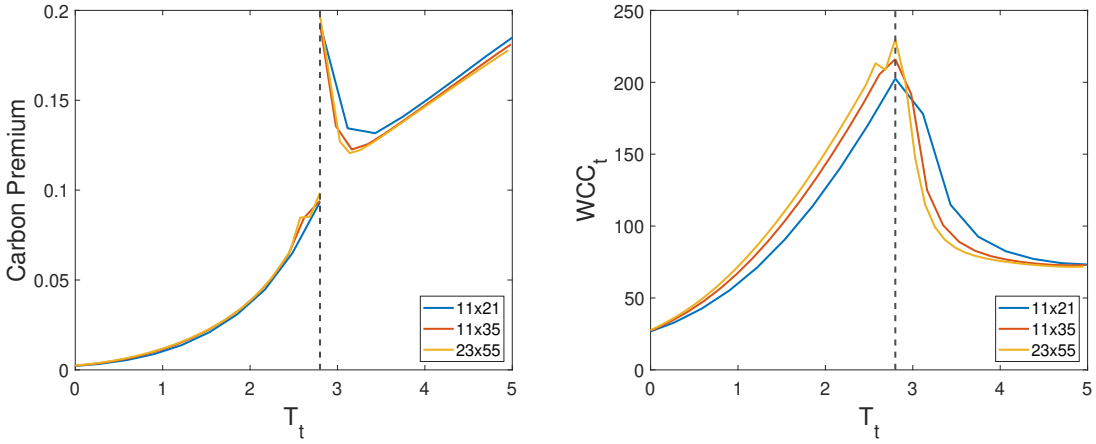

The figure plots the carbon premium and the welfare cost of carbon for different collocation grids as a function of temperature T_t. The upper two plots show the results for an economy with $w_t^G = 0.05$, and the lower two plots show results for an economy with $w_t^G = 0.95$. Collocation grids are adjusted by placing a collocation node exactly on the tipping point and an additional node infinitesimally before the tipping threshold. The remaining state space is uniformly distributed. The vertical dashed line marks the tipping threshold.

Table 12: Wealth Shares – Different Simulations with $T_0 = 1$°C

	200 years			500 years		
	10%	median	90%	10%	median	90%
Baseline TP	0.1271	0.2523	0.3584	0.0096	0.0504	0.1584
$T_{Tipp} = 2$°C	0.0745	0.1563	0.2643	0.0049	0.0217	0.0714
$\gamma = 5$	0.2991	0.4134	0.4727	0.0729	0.1997	0.3697
$l^G = 2\%$; $l^B = 1\%$	0.2181	0.3440	0.4233	0.0342	0.1138	0.2668
$d = -0.15$	0.2517	0.3662	0.4370	0.0464	0.1446	0.2971
Imm. Disaster Risk	0.0637	0.1066	0.1671	0.0040	0.0135	0.0358

The table shows the median, 10% and 90% quantiles of the wealth share of the green investor w^G from 1,000 samples – each containing 200 or 500 years of simulated years. The starting distribution is $w_0^G = w_0^B = 0.5$. Temperature at the beginning is $T_0 = 1$°C and mean temperature after 200 and 500 years is $T_{200} = 1.59$°C and $T_{500} = 1.92$°C, respectively. Results are shown for different calibrations of the economy. Baseline refers to the model calibration presented in Table 1. Results are also shown for a lower tipping threshold ($T_{Tipp} = 2.0$°C instead of 2.8°C), lower risk aversion ($\gamma = 5$ instead of $\gamma = 8$), lower subjective disaster probabilities($l = l^G = 0.02$ and $l^B = 0.01$ instead of $l = l^G = 0.03$ and $l^B = 0.015$), a lower impact of disasters ($d = -0.15$ instead of $d = -0.2$) and an immediate disaster risk economy ($T_{Tipp} = 0.01$°C instead of $T_{Tipp} = 2.8$°C).

Table 13: Numerical Errors – Immediate Disaster Risk Case with $T_{min} = 0.01$°C

		v_t^G		v_t^B		λ_t^B	
nl	nT	RMSE	MAE	RMSE	MAE	RMSE	MAE
18	18	4.081e-4	0.0022	3.688e-4	0.0011	8.246e-4	0.0098
18	36	7.382e-5	6.588e-4	8.464e-5	7.379e-4	8.037e-4	0.0096
36	36	7.233e-5	4.852e-4	6.848e-5	3.288e-4	6.376e-4	0.0058

The table shows root-mean-square errors (RMSEs) as well as maximum absolute errors (MAEs) in the value functions as well as the equilibrium conditions for the Negishi weights for different numbers of collocation nodes for the immediate disaster risk model. Errors are reported for a state grid from 0.01°C – 5°C, which is approximately from -2 to +3 standard deviations around the unconditional mean of T_t. For λ_t^B the full grid between 0 and 1 is used. We denote the number of collocation nodes for the λ_t^B-dimension by n_l and the number of collocation nodes for the T_t-dimension by n_T. Errors are computed on a grid of size 100×100.

Table 14: Price–Dividend Ratio from Simulations - Immediate Disaster Risk Case

	$E(p_t^M - d_t^M)$	$\sigma(p_t^M - d_t^M)$	$E(p_t^G - d_t^G)$	$\sigma(p_t^G - d_t^G)$	$E(p_t^B - d_t^B)$	$\sigma(p_t^B - d_t^B)$
15×20	3.6363	0.0294	3.9827	0.0166	2.7903	0.1388
15×55	3.6371	0.0295	3.9791	0.0153	2.7866	0.1373
35×35	3.6384	0.0294	3.9747	0.0151	2.7921	0.1375
45×45	3.6390	0.0291	3.9732	0.0146	2.7924	0.1363

The table reports the mean and standard deviation of the price–dividend ratio for the green stock, brown stock, and the market portfolio in the immediate disaster risk model. Results are computed by simulating 100 sample paths each containing 100 years of data. We set $T_{start} = 1.0$°C and $w_{start}^G = 0.5$. The number of collocation nodes for the λ_t^B-dimension is denoted by n_l and the number of collocation nodes for the T_t-dimension by n_T. Shocks to temperature, ζ_{t+1}, are drawn from a standard normal distribution, and no exogenous shocks are added.

Table 15: Price–Dividend Ratio from Simulations - Tipping Point Case

	$E(p_t^M - d_t^M)$	$\sigma(p_t^M - d_t^M)$	$E(p_t^G - d_t^G)$	$\sigma(p_t^G - d_t^G)$	$E(p_t^B - d_t^B)$	$\sigma(p_t^B - d_t^B)$
$11 \times 21^*$	3.7526	0.0255	3.9924	0.0409	3.4669	0.1322
$11 \times 35^*$	3.7569	0.0273	3.9982	0.0407	3.4716	0.1393
$11 \times 55^*$	3.7606	0.0278	3.9958	0.0394	3.4796	0.1410
$23 \times 55^*$	3.7613	0.0276	3.9912	0.0388	3.4814	0.1405
$23 \times 55^{**}$	3.7594	0.0282	3.9915	0.0382	3.4723	0.1432

The table reports the mean and standard deviation of the price–dividend ratio for the green stock, brown stock, and the market portfolio in the model with a distant tipping point. Results are computed by simulating 100 sample paths each containing 100 years of data. We set $T_{start} = 1.0$°C and $w_{start}^G = 0.5$. The number of collocation nodes for the λ_t^B-dimension is denoted by n_l and the number of collocation nodes for the T_t-dimension by n_T. Shocks to temperature, ζ_{t+1}, are drawn from a standard normal distribution, and no exogenous shocks are added. An asterisk (*) denotes cases where we used an adjusted grid by placing a collocation node exactly on the tipping point and an additional node infinitesimally before the tipping threshold. Two asterisks (**) denote the case where we put some additional collocation nodes around the tipping point.

B Derivations of the Welfare Cost of Carbon

The welfare cost of carbon (WCC) is defined as the ratio of two marginal values:

$$WCC_t = -\frac{\frac{\partial V_t}{\partial E_t}}{\frac{\partial V_t}{\partial C_t}}. \tag{30}$$

For Epstein–Zin preferences, the value function is a function of the aggregate wealth–consumption ratio, $Z_t \equiv \frac{W_t}{C_t}$:

$$\frac{V_t}{C_t} = [(1-\delta)Z_t]^{\frac{\psi}{\psi-1}},$$

where $Z_t \equiv \frac{W_t}{C_t}$. Using this relationship, the two derivatives in equation (30) yield

$$\begin{aligned} \frac{\partial V_t}{\partial E_t} &= \frac{\partial V_t}{\partial Z_t}\frac{\partial Z_t}{\partial E_t} = \frac{\psi}{\psi-1}(1-\delta)^{\frac{\psi}{\psi-1}} Z_t^{\frac{\frac{1}{\psi}}{1-\frac{1}{\psi}}} \frac{\partial Z_t}{\partial E_t}, \\ \frac{\partial V_t}{\partial C_t} &= [(1-\delta)Z_t]^{\frac{\psi}{\psi-1}}. \end{aligned}$$

Hence, the WCC depends on the elasticity of Z_t to emissions:

$$WCC_t = \frac{\psi}{\psi-1}\frac{-\partial Z_t}{\partial E_t}\frac{C_t}{Z_t}. \tag{31}$$

As $\frac{\partial log Z_t}{\partial E_t} = \frac{1}{Z_t}\frac{\partial Z_t}{\partial E_t}$, this is equivalent to

$$WCC_t = \frac{\psi}{\psi-1}\frac{-\partial log Z_t}{\partial E_t}C_t. \tag{32}$$

Dividing and multiplying by ∂T_t yields equation (23).

C Derivations of the Individual Welfare Cost of Carbon

We showed in section B that the welfare cost of carbon in the aggregate economy is given by:

$$WCC_t = -\frac{\frac{\partial V_t}{\partial E_t}}{\frac{\partial V_t}{\partial C_t}} = \frac{\psi}{\psi - 1}\frac{-\partial Z_t}{\partial E_t}\frac{C_t}{Z_t}$$

The wealth–consumption ratio of the individual investor h satisfies

$$\frac{W_t^h}{C_t^h} = \frac{1}{1-\delta} \cdot \left(\frac{v^h}{s^h}\right)^{1-\frac{1}{\psi}}.$$

Using $W^G + W^B = W$, we can re-write the aggregate wealth–consumption ratio as:

$$\frac{W}{C} = \frac{W^G}{C^G}\frac{C^G}{C} + \frac{W^B}{C^B}\frac{C^B}{C}$$

Inserting yields:

$$WCC_t = \frac{\psi}{\psi - 1}\frac{C_t}{Z_t}\left(\frac{\partial Z_t^G}{\partial E_t}\frac{C_t^G}{C_t} + \frac{\partial Z_t^B}{\partial E_t}\frac{C_t^B}{C_t}\right)$$

$$WCC_t = \underbrace{\frac{\psi}{\psi - 1} \cdot \frac{C_t}{Z_t}\frac{\partial Z_t^G}{\partial E_t}\frac{C_t^G}{C_t}}_{\text{effect on green agent}} + \underbrace{\frac{\psi}{\psi - 1} \cdot \frac{C_t}{Z_t}\frac{\partial Z_t^B}{\partial E_t}\frac{C_t^B}{C_t}}_{\text{effect on brown agent}}$$

As $\frac{\partial log Z_t^h}{\partial E_t} = \frac{1}{Z_t^h}\frac{\partial Z_t^h}{\partial E_t}$, and $\frac{C_t^h}{C_t} = s_t^h$, this is equivalent to:

$$WCC_t = \frac{\psi}{\psi - 1}s_t^G\frac{-\partial log Z_t^G}{\partial E_t}C_t + \frac{\psi}{\psi - 1}s_t^B\frac{-\partial log Z_t^B}{\partial E_t}C_t.$$

Thus, the aggregate welfare cost of carbon can be re-written as the weighted sum of the two individual welfare costs of carbon.

D Alternative Modelling of Disasters

In the main part of the paper, the impact of disasters on economic growth is modeled using a Poisson counting process. In theory, N_{t+1} could take any value in the next period, so there is a small, but positive probability for having more than one disaster in the next period (see the discussion in Section 5, in particular Table 5).

Another way to model the disaster process would be to implement disaster shocks in a way that N_{t+1} could only take two values each period: 0 or 1. In the following, we show how the probability ratios would look like under this case.

As in the case with Poisson disasters, the two agents disagree about the disaster term D_{t+1} in equation 1, given the information at time t. Let $P^h_{t,t+1}$ be the subjective conditional distribution of agent h about D_{t+1}, given T_t, and $P_{t,t+1}$ be the true conditional distribution. We assume that each agent's expectation can be written in terms of the true distribution as

$$E^h_t[D_{t+1}] = E_t\left[D_{t+1}\frac{dP^h_{t,t+1}}{dP_{t,t+1}}\right],$$

for some measurable function $\frac{dP^h_{t,t+1}}{dP_{t,t+1}}$.

Agent h believes with probability $p^h_t(T_t)$ that there will be a disaster next period and with probability $(1-p^h_t(T_t))$ that no disaster will occur. This yields the following probabilities for the green and brown investor:[34]

$$P^G_t = \begin{bmatrix} p^G_t \\ (1-p^G_t) \end{bmatrix}; P^B_t = \begin{bmatrix} p^B_t \\ (1-p^B_t) \end{bmatrix}.$$

The probability ratio in this case is given by:

$$\frac{dP^G_{t,t+1}}{dP^B_{t,t+1}} = \begin{bmatrix} \frac{p^G_t}{p^B_t} \\ \frac{(1-p^G_t)}{(1-p^B_t)} \end{bmatrix}.$$

If the disaster probabilities p^h_t are constant (independent of the state, i.e. temperature T_t), the probability ratio also has a constant value for the disaster and no disaster case. However, since the disaster probability is time-varying, depending on the current temperature anomaly T_t, the probability ratio becomes a matrix of the size $nT \times 2$, in which the "2" captures the two states "disaster" and "no disaster" and n_T represents the number of collocation nodes for the temperature state. Notably, in this case, we do not need to choose a cutoff value as in the Poisson disaster case, as the probabilies of the two disaster states already sum up to 1.

[34] For improved readability, we will suppress the state-dependency of the probabilities in the following.

E Mapping from Emissions to Temperature

In this section, we present an alternative interpretation of the temperature process, where it is expressed as a function of emissions instead of the AR(1) process used earlier. To achieve this, we start with the system of equations as proposed by Bansal et al. (2021) and then proceed with a reformulation that leads to the temperature process as described in Section 3.This approach allows us to explore the relationship between emissions and temperature dynamics in our model framework.

The global temperature anomaly is driven by carbon emissions, which themselves are a function of consumption growth:

$$T_{t+1} = \chi \varepsilon_{t+1}, \tag{33}$$

$$\varepsilon_{t+1} = \nu \varepsilon_t + \Theta(\mu_c + \sigma_\eta \eta_{t+1}) + \sigma_\zeta \zeta_{t+1}, \tag{34}$$

where ν determines the persistence of carbon emissions in the atmosphere and, consequently, also the persistence of temperature. Θ measures carbon intensity of consumption. The parameter $\chi > 0$ reflects the climate sensitivity to emissions, indicating how anthropogenic carbon emissions influence global temperature in this model. The exogenous innovation to emissions and temperature is represented by ζ, assumed to follow a normal distribution with a mean of zero and a standard deviation of σ_ζ.

By inserting equation 34 into equation 33, temperature dynamics in this model are given by:

$$T_{t+1} = \chi\nu\varepsilon_t + \chi\Theta(\mu_c + \sigma_\eta \eta_{t+1}) + \chi\sigma_\zeta \zeta_{t+1}. \tag{35}$$

We know that the unconditional (long-run) mean of temperature is given by:

$$\mu_T = \frac{\chi\Theta\mu_c}{1-\nu}. \tag{36}$$

For simplicity, we ignore the i.i.d. consumption shock in the following and use $\chi\varepsilon_t = T_t$, following equation 33, and $\chi\Theta\mu_c = (1-\nu)\mu_T$, following equation 36. Inserting in equation 35 yields:

$$T_{t+1} = (1-\nu)\mu_T + \nu T_t + \chi\sigma_\zeta \zeta_{t+1}.$$

By defining ζ_{t+1} as a temperature instead of an emission shock, we arrive at equation 6 from the main part:

$$T_{t+1} = (1-\nu)\mu_T + \nu T_t + \sigma_\zeta \zeta_{t+1}.$$